NTNU – Trondheim
Norwegian University of
Science and Technology

# Fatigue Analysis of Column-Pontoon Connection in a Semi-submersible Floating Wind Turbine

Øyvind Tvare

Marine Technology
Submission date: July 2014
Supervisor: Torgeir Moan, IMT

Norwegian University of Science and Technology
Department of Marine Technology

**NTNU Trondheim**
**Norwegian University of Science and Technology**
*Department of Marine Technology – Group of Marine Structures*

# MSC THESIS IN MARINE TECHNOLOGY

## SPRING 2014

## FOR

## STUD.TECHN. Øyvind Tvare

## Fatigue Analysis of the Column-Pontoon Connection in a Semi-submersible Floating Wind Turbine

Utmattingsanalyse av søyle-pontoon forbindelse i en halvt-nedsenkbar flytende vindturbin

**Background:**
Semi-submersible floating wind turbines have been proposed for deep water offshore wind energy application. A conventional semi-submersible consists of three or four columns interconnected by braces. A novel pontoon-type semi-submersible floating wind turbine has been developed at CeSOS, NTNU. It consists of four cylindrical columns with one central column supporting the 5MW NREL wind turbine. Each side column is spaced at a 120-degree interval and connected at the bottom to the central column by a rectangular pontoon.

The column-pontoon connection presents a challenge for structural design (in particular fatigue design) when the floating wind turbine is subjected to combined wind and wave loads. A smooth structural transition from cylindrical column to rectangular pontoon should be designed to avoid sharp corners and to reduce stress concentration. Internal stiffeners, girders and bulkheads should be considered for both columns and pontoons. The central column, which supports the wind turbine, is directly subjected to the wind turbine aerodynamic loads and the wave loads. The joint between the central column and the pontoons needs to be strengthened considering both wind- and wave-induced load effects. While, the fatigue loads in the other three side columns are mainly induced by wave loads and rigid-body motions (i.e. inertial load effects).

In a project work from the MSc student Traian I. Marin, two alternative structural designs for the column-pontoon connection have been proposed. In this thesis work, the MSc student should focus on and improve the design with a transition hull from the cylindrical column to the rectangular pontoon. The candidate should carry out a detailed FE analysis of that design to determine the stress distribution at various hot-spots under different cross-sectional loading conditions and estimate the fatigue damage due to combined load effects.

Global response analysis results for representative wind and wave conditions will be provided by the PhD candidate Chenyu Luan.

**Assignment:**
The following tasks should be addressed in the thesis work:

1. Literature review on finite element analysis to determine stress concentration, the SN-curve approach for fatigue analysis and multiaxial fatigue.

2. Use the developed FE model in GeniE to identify the area with high stress concentration and improve the design of local structural parts with respect to fatigue. Necessary internal structural components such as stiffeners, bulkheads, etc. should be arranged. Refine the mesh in these areas and

perform a FE analysis using the submodeling technique to determine the stress distribution under various cross-sectional loading conditions.

3. Assume a linear structural behaviour and estimate the stress distribution due to actual combined loading conditions. Important cross-sectional loads, such as vertical bending moment, axial force, as well as torsional moment in misaligned wind and wave conditions should be considered.

4. Develop a method that, in some circumstances, can be used to include the effect of multiaxial fatigue, when calculating fatigue damage in accordance with DNV-RP-C203.

5. Estimate fatigue damage for selected environmental conditions according to DNV-RP-C203. If time allows, perform long-term fatigue analysis considering various environmental conditions. If possible, include the effect of all stress components (share, parallel and normal stress) when calculating fatigue life, and estimate the effect of neglecting share and parallel stress.

6. Conclude the work and give recommendations for future work.

7. Write the MSc thesis report.

In the thesis the candidate shall present his personal contribution to the resolution of problem within the scope of the thesis work.

Theories and conclusions should be based on mathematical derivations and/or logic reasoning identifying the various steps in the deduction.

The candidate should utilize the existing possibilities for obtaining relevant literature.

The thesis should be organized in a rational manner to give a clear exposition of results, assessments, and conclusions. The text should be brief and to the point, with a clear language. Telegraphic language should be avoided.

The thesis shall contain the following elements: A text defining the scope, preface, list of contents, summary, main body of thesis, conclusions with recommendations for further work, list of symbols and acronyms, reference and (optional) appendices. All figures, tables and equations shall be numerated.

The supervisor may require that the candidate, in an early stage of the work, present a written plan for the completion of the work. The plan should include a budget for the use of computer and laboratory resources that will be charged to the department. Overruns shall be reported to the supervisor.

The original contribution of the candidate and material taken from other sources shall be clearly defined. Work from other sources shall be properly referenced using an acknowledged referencing system.

The thesis shall be submitted in two copies as well as an electronic copy on a CD:

- Signed by the candidate
- The text defining the scope included
- In bound volume(s)

- Drawings and/or computer prints which cannot be bound should be organized in a separate folder.

Supervisors:
Torgeir Moan
Zhen Gao

Zhen Gao (on behalf of Prof. Torgeir Moan)

Deadline for master thesis: 01.07.2014

# Preface

This report is the result of the work for the Master Thesis in the Discipline of Marine Structural Enginneering at Norwegian University of Science and Technology (NTNU). The work with this thesis was carried out in the Spring of 2014.

This report deals with fatigue related challenges for a semi submersible floating wind turbine developed by CeSOS, NTNU.

I would like to thank Professor Torgeir Moan for making this thesis possible and Adjunct Associate Professor Zhen Gao and Chenyu Luan for their quality answers and willingness to help. I would also like to thank my fellow students at my office for their support.

Oslo, July 2, 2014

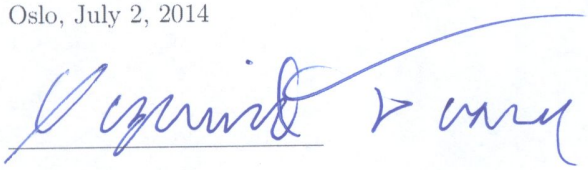

Øyvind Tvare

# Abstract

In a world with ever increasing energy demands, there is a need to find new ways to harvest renewable energy. Floating offshore wind turbines could be an important energy source in the future. To make this possible a better understanding of offshore wind turbines is essential. This thesis has dealt with fatigue associated challenges related to a column-pontoon connection in a semi-submersible floating wind turbine developed at CeSOS, NTNU.

The specific design investigated in this report has a transition hull from the cylindrical column to the rectangular pontoon. A finite element model of the connection was available and revealed very high stress concentration at some areas. The sub-modeling technique was applied at two crucial areas for a detailed stress analysis. The design of the connection was changed in order to reduce the stress concentration.

Fatigue analysis were carried out at the intersection between the midpoint at the upper hull of the pontoon and the transition piece. The same was done at 13 points along the weld between the hull of the transition piece and the hull of the column. Load time series from global dynamic response analysis from 13 sea states, representing wave and wind conditions at deep water in the North Sea with 0°, 30° and 60° wave heading, were available and used in fatigue calculations. Load time series from -30° and -60° heading were created assuming symmetry around the vertical midplane of the structure. 10 one hour simulations of every sea state were used.

Cumulative fatigue damage at all sea states and wave headings were calculated and compared using rainflow counting, an appropriate S-N curve and Miner's rule. Estimated time to failure is calculated assuming a constant wave heading over the lifetime of the structure. The estimated fatigue life is also determined for a combined wave heading. The combined wave heading corresponds to the column-pontoon connection where 0° heading is dominating.

There will be a multiaxial stress state at the different hot spots. A simplified method for including the fatigue damage contribution from all the different stress components (stress parallel with the weld, stress normal to the weld and shear stress) is proposed. The method has large limitations, but is intended to be used when there is a close to linear relationship between the different stress components. This method has been used when predicting fatigue life at all hot spots and the results have been evaluated.

Estimated fatigue life at the most critical hot spot is 1.9 years under a combined wave heading. Multiple hot spots have a fatigue life under 10 years. More design changes is needed to achieve acceptable fatigue life. The method proposed for including multiaxial fatigue effects show promising results at some hot spots. The accuracy depends on which hot spot is analyzed and wave heading.

# Sammendrag

I en verden med stadig økende energibehov, er det viktig å finne nye måter å utvinne energi. Flytende vindmøller til havs kan bli en viktig energikilde i fremtiden. For at dette skal skje er det viktig å få en bedre forståelse av påkjenningen slike strukturer blir utsatt for. Denne masteroppgaven tar for seg utmattings relaterte utfordringer knyttet til en pongtong-søyle-forbindelse i en halvt nedsenkbar flyttende vindmølle utviklet av CeSOS, NTNU.

Det spesielle designet undersøkt i arbeidet med denne rapporten har et overgangselement mellom søylen og pongtongen. En elementmetodemodell av søyle-pongtong-forbindelsen var tilgjengelig og viste veldig høye spenningskonsentrasjoner i noen områder. Submodelleringsteknikk ble brukt på to forskjellige steder for å kunne utføre en detaljert spenningsanalyse. Konstruksjonsdesignet av forbindelsen ble forbedret for å redusere spenningskonsentrasjonen.

En utmattingsanalyse ble utført ved skjæringspunktet mellom midtpunktet til det øvre pongtongskroget og overgangselementet. The samme ble gjort for 13 punkter langs sveisen mellom skroget til overgangselementet og søylen. Tidsserier av laster fra global dynamisk responsanalyse var tilgjengelig for 13 sjøtilstander, som representerer bølge- og vindforhold på dypt vann i Nordsjøen, med 0° 30° og 60° bølgeretning. Disse ble brukt i utmattingsberegningene. Tidsserier av laster for -30° og -60° bølgeretning ble laget ved å anta symmetri rundt det vertikale midtplanet til strukturen. 10 en times simuleringer av hver sjøtilstand ble brukt.

Akkumulert utmattingsskade fra alle sjøtilstander og bølgeretninger ble beregnet og sammenlignet ved å bruke rainflow-telling , en egnet S-N kurve og Miners regel. Tid til brudd ble estimert ved å anta konstant bølgeretning over levetiden til strukturen. Tid til brudd ble også estimert for en kombinert bølgeretning. Den kombinerte bølgeretningen svarer til den ene av de tre søyle-pongtong forbindelsene som er dominert av 0° bølgeretning.

Det vil være en multiaksial spenningstilstand ved de forskjellige punktene med spenningskonsentrasjon analysert. En metode for å inkludere bidraget til utmattingsskade fra de ulike spenningskomponentene (spenning parallelt med sveisen, spenning normal på sveisen og skjærspenning) er utviklet. Metoden har store begrensninger, men er tenkt å brukes når det er store tendenser til en lineær relasjon mellom de ulike spenningskomponentene. Denne metoden har blitt brukt under utmattingsanalysen av de forskjellige punktene på konstruksjonen og resultatene har blitt evaluert.

Estimert utmattingslevetid for det mest kritiske punktet undersøkt var 1.9 år ved kombinert bølgeretning. Mange punkt har utmattingslevetid under 10 år. For å oppnå akseptabel utmattingslevetid er det nødvendig med flere designendringer for å minke spenningskonsentrasjonen. Metoden som ble foreslått for å inkludere de multiaksiale utmattingseffektene viser lovende resultater for noen punkter. Nøyaktigheten av metoden avhenger av hvilket punkt som er analysert og bølgeretning.

# Contents

# List of Figures

# List of Tables

# Nomenclature

$\alpha$ Fatigue parameter depending on classification of structural detail

$\alpha_{1,med}$ Negative slope of the curve describing the relationship between simplified shear stress and real perpendicular stress

$\alpha_{2,med}$ Negative slope of the curve describing the relationship between simplified parallel stress and real perpendicular stress

$\bar{\lambda}$ Weighted average of $\lambda$ for all simulations with a specific heading

$\bar{\lambda}_{parallel\,stress}$ Weighted average of ratio between the standard deviation of constructed and real parallel stress for all simulations with a specific heading

$\bar{\lambda}_{shear\,stress}$ Weighted average of ratio between the standard deviation of constructed and real shear stress for all simulations with a specific heading

$\bar{\sigma}_{std}$ Weighted average of the stress standard deviation for all simulations with a specific heading

$\beta$ Material dependent parameter related to multiaxial fatigue

$\Delta\sigma$ Stress range

$\Delta\sigma_0$ Stress range value when S-N curve changes slope

$\Delta K$ Stress intensity range

$\Delta S$ Stress range

$\Delta\sigma_1$ The first principal stress range

$\Delta\sigma_2$ The second principal stress range

$\Delta\sigma_\perp$ Perpendicular stress range

$\Delta\sigma_{a,hot\,spot}$ Membrane stress at hot spot

$\Delta\sigma_{b,hot\,spot}$ Bending stress at hot spot

$\Delta\sigma_{e,hot\,spot}$ Effective hot spot stress

$\Delta\tau_\parallel$ Parallel shear stress range

$\frac{da}{dn}$ Crack growth rate per cycle

$\lambda$ ratio between the standard deviation of constructed and real stress for a specific simulation

$\overline{a}$ Intercept of the design S-N curve with the log N axis

$\overline{y}_{0,1}$ Simplified shear stress value when the perpendicular stress is zero

$\overline{y}_{0,2}$ Simplified parallel stress value when the perpendicular stress is zero

$\overline{y}_{1,1}$ The mean value of the shear stress when the perpendicular stress crosses its mean

$\sigma_{0,hs,i}$ The hot spot stress from a unit stress loading

$\sigma_{\parallel,b}$ Bending component of the parallel stress

$\sigma_{\parallel,m}$ Membrane component of the parallel stress

$\sigma_{\parallel,s}$ Simplified parallel stress found by the linear simplification method

$\sigma_{\parallel}$ Stress in plate parallel with weld toe

$\sigma_{\perp,b}$ Bending component of the normal stress

$\sigma_{\perp,m}$ Membrane component of the normal stress

$\sigma_{\perp}$ Stress in plate perpendicular to weld toe

$\sigma_{Eff}$ Effective stress range

$\sigma_{F_{ij}}$ Load standard deviationn for sea state i and seed j

$\sigma_{hs,i}$ Hot spot stress from wave cross sectional loading in i direction

$\sigma_{hs}$ Hot spot stress from wave cross sectional loading in all direction

$\sigma_{ij}^{(I)}$ Stress at crack tip in the i-j direction due to loading in mode III

$\sigma_{ij}^{(I)}$ Stress at crack tip in the i-j direction due to loading in mode I

$\sigma_{ij}^{(II)}$ Stress at crack tip in the i-j direction due to loading in mode II

$\sigma_{ij}^{(total)}$ Total stress in the i-j direction at crack tip

$\sigma_{nd,i}$ Stress from a cross sectional unit stress loading in i direction

$\sigma_{r,i}$ The stress from cross sectional wave loading in i direction

$\sigma_{xx}$ Normal plate element stress in x-direction

$\sigma_{xx}$ Stress in the global x direction

$\sigma_{yy}$ Normal plate element stress in y-direction

$\tau_{\parallel,constructed}$ Constructed shear stress

$\tau_{\parallel,real}$ Real shear stress

$\tau_{\parallel,s}$ Simplified shear stress found by the linear simplification method

$\tau_{\parallel}$ Shear stress in plate parallel with weld toe

$\tau_{xy}$ In plane share stress in xy-direction in a plate element

$\theta$ Wave heading angle

$A$ A constant

$bar\sigma_{std,combined}$ Weighted average of stress standard deviation for all simulations with all heading angles

$C$ Material dependent parameter related to fatigue

$D$ Accumulated fatigue damage

$d_{avr,combined}$ The average damage for a combined heading

$d_{avr,i}$ The average damage for wave heading i

$f$ PDF wave heading

$F_{0,i}$ Applied cross sectional loading in the FE-model

$F_{r,i}$ Wave cross sectional loading in i direction

$H_s$ Significant wave height

$k$ Parameter used to define the wave spreading function

$m$ Crack growth parameter

$N$ Number of cycles to failure

$n$ Parameter used to define the wave spreading function

$N_i$ Number of cycles to failure at a given streess range

$n_i$ Number of cycles at a given streess range

$n_{headings}$ Number of different heading angles analyzed

$n_{Sea}$ Number of sea states analyzed

$n_{sees}$ Number of analysis in each sea state

$overline\sigma_{\perp}$ The mean value of the perpendicular stress

$p_i$ The probability of sea state i

$p_k$ Probability of heading k

$r$ The ratio between fatigue life when using only normal stress and when also using simplified shear and parallel stress

$std$ standard deviation

$t$ Plate thickness

$t$ Thickness through which a crack will most likely grow

$t$ Time

$T_s$ Spectral peak period

$t_{f,all}$ Time to failure when including real normal stress and simplified shear and parallel stress

$t_{f,combined}$ Time to failure for a combined wave heading

$t_{f,normal}$ Time to failure when only including normal stress

$t_{ref}$ Reference thickness

CeSOS Center for Ships and Ocean Structures

DNV Det Norske Veritas

DOF Degrees of freedom

FE Finite element

NTNU Norwegian University of Science and Technology

PDF Probability density function

PDMR Path-dependent maximum range

SCF Stress concentration factor

WAFO Wave Analysis for Fatigue and Oceanography

# Chapter 1

# Introduction

In recent years extensive research have been done on floating wind turbines. In a world with ever increasing energy demands, the potential of floating wind turbines as a sustainable energy source in the future is huge. Typically, wind is both stronger and more consistent at sea. Also, much of the required technology can be taken from the oil industry, which have a lot of experience developing safe and cost effective floating structures. These are some of the factors making floating wind turbines attractive [25].

Today most offshore wind turbines are installed in shallow waters with bottom fixed support structures. The economic feasibility of floating wind turbines as of today is uncertain. More research and full scale testing is needed to reduce cost and demonstrate economic feasibility.

CeSOS at NTNU has developed a semi-submersible floating wind turbine [16]. This thesis has dealt with fatigue associated challenges related to a column-pontoon connection in this structure.

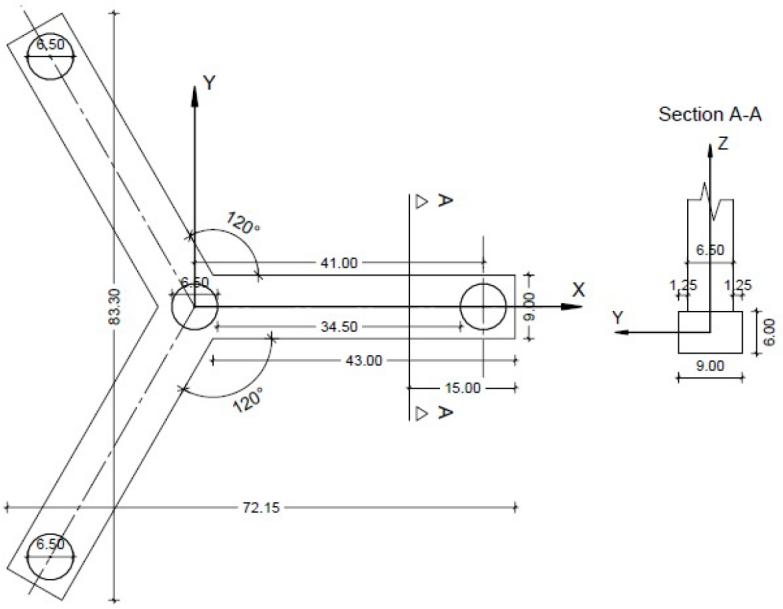


Figure 1.1: Design of semi-submersible floating wind turbine [18]

## 1.1 Objectives

The main objectives of this Master project are listed here:

1. Use the developed FE model of the column-pontoon connection with a transition hull to identify the areas with stress concentration and improve the design of local structural parts with respect to fatigue.

2. Estimate the stress distribution due to actual combined loading conditions assuming linear structural behavior.

3. Develop a method, that under some circumstances, can be used to include the effect of multiaxial fatigue, when calculating fatigue damage.

4. Estimate fatigue damage for selected environmental conditions at various hot spots according to DNV-RP-C203. Perform long-term fatigue analysis considering various environmental conditions. If the developed method for including multiaxial fatigue is applicable, include the effect of all stress components (shear, parallel and normal stress) when calculating fatigue life, and estimate the effect of neglecting shear and parallel stress.

## 1.2 Method

The SESAM software package has been used to perform the FE analysis. Relevant stresses at various points on the structure for a constant cross sectional loading in every DOF is saved to .txt files from Xtract. Real cross sectional loading from global response analysis at various environmental conditions are provided by PhD candidate Chenyu Luan. A MATLAB script is created with the purpose of doing the following:

1. Import the relevant stresses from Xtract at various points and calculate hot spot stresses based on constant cross sectional loading in all directions (refered to as the nondimensional hot spot stresses).

2. Import actual cross sectional loading at various environmental conditions and couple them with the nondimensional hot spot stresses, in order to calculate the real effective hot spot stresses as a function of time.

3. Calculate stress ranges based on rainflow counting

4. Estimate cumulative damage from each sea state based on a chosen S-N curve and Miner's rule.

5. Estimate fatigue life for all the points analyzed based on the cross sectional loading under all available environmental conditions.

6. Create and saving plots displaying important parameters.

In addition to this the script also intends to include the fatigue damage from all the different stress components ($\tau_{\parallel}$, $\sigma_{\parallel}$ and $\sigma_{\perp}$) in the multiaxial stress state, in accordance with the proposed simplified method.

## 1.3 Report Structure

The rest of the report is structured as follows:

**Chapter 2** An introduction to some of the theory relevant for the fatigue analysis

**Chapter 3** A presentation of the FE-model of the column-pontoon connection and design changes that have been made

**Chapter 4** A short introduction to the computer programs used and flowchart of MATLAB script.

**Chapter 5** A description of sea state characteristics and global loads on the structure

**Chapter 6** Fatigue analysis results from the submodel of the intersection between the midpoint at the upper hull of the pontoon and the transition piece

**Chapter 7** Fatigue analysis results from a number of hot spots along the weld between the hull of the transition piece and the hull of the column

**Chapter 7-8** Concluding remarks and recommendations for further work

**Note:** The reader is expected to read Chapter 6 before Chapter 7. Some of the terms used in Chapter 7 is introduced and explained in Chapter 6. The approach used to find the results is also described in more detail in the Chapter 6.

# Chapter 2

# Theory

## 2.1 Fatigue

Under cyclic loading below yield strength cracks may occur. If the loading continues the crack will propagate, and the construction weakens because of the crack propagation. This phenomenon is called fatigue. Under the cyclic loading the crack will continue to grow until it becomes unstable and fracture occurs.

Fatigue has become increasingly important in design of offshore structure in later years. The strength of materials used in construction has improved. The utilization of the materials is typically higher now due to better methods for determining stresses. Both these factors have led to a general increased stress levels in constructions, which leads to higher risk of fatigue Damage [5].

Moan and Næss argues that fatigue is a challenging failure mode to deal with due to the following reasons[24]:

- The fatigue process, especially initiation, is by nature unpredictable
- It is difficult to translate laboratory test to in-service conditions
- It is difficult to model the load environment and the complex stress states

## 2.2 Stress intensity factor

The stress and strain fields around a crack can be uniquely defined by a stress intensity factor [4]. There are three types of loading that can be applied to a crack as indicated in figure 2.1. The stress intensity factor depends on loading type. Mode I corresponds to tensile loading, mode II corresponds to in-plane-shear and mode III corresponds to out-of-plane shear stress. Mode I is by far the most common case in practical problems [4][27]. When more than one loading mode is present the total stress can be calculated from the principle of linear superposition [1]:

$$\sigma_{ij}^{(total)} = \sigma_{ij}^{(I)} + \sigma_{ij}^{(II)} + \sigma_{ij}^{(III)} \tag{2.1}$$

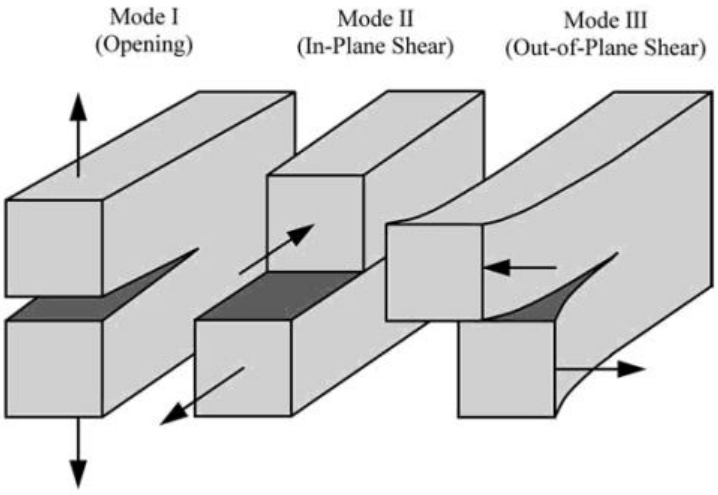


Figure 2.1: The basic modes of loading that can be applied to a crack [1]

## 2.3 S-N curve

The most used form of expressing fatigue capacity is S-N curves [15] [24]. DNVs recommended practice for offshore steel structure is to base fatigue design on such curves, which are obtained from fatigue tests. [12].

S-N curves are based on the assumption that linear elastic fracture mechanics can be applied. The crack growth curve can be split into three stages as shown in Figure 2.2. In stage two the crack growth rate is approximately linear. Fatigue of welded joints is dominated by the crack growth in stage two [5]. For steel the crack growth rate will be approximately the same for different steel grades, assuming normal temperatures. The relation between the crack growth and the stress intensity range in this region can be defined by Paris law.

$$\frac{da}{dn} = C(\Delta K)^m \tag{2.2}$$

$\frac{da}{dn}$ is the crack growth rate per cycle, $C$ and $m$ are material dependent parameters and $\Delta K$ is the stress intensity range.

from Paris law one can derive the following relationship between stress range and number of cycles to failure (The stress range is the same for all cycles):

$$N(\Delta S)^m = A \tag{2.3}$$

$N$ is cycles to failure, $\Delta S$ is the stress range, $A$ is a constant and $m$ is the same material parameter as in equation 2.2.

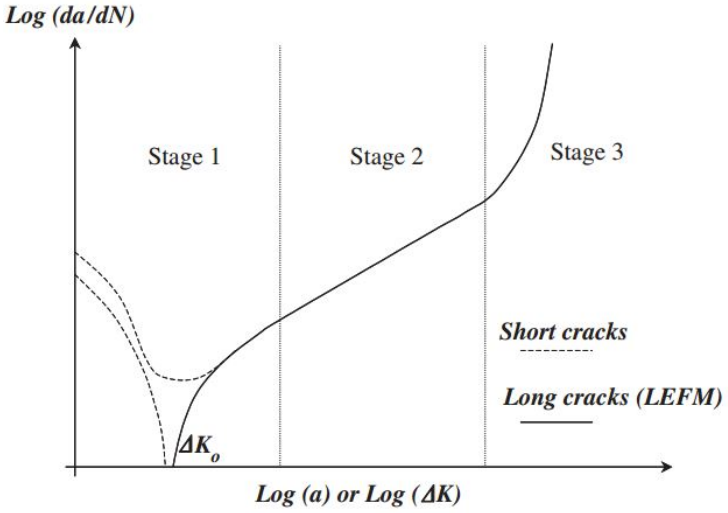


Figure 2.2: Crack growth rate curve [21]

DNV guidelines provides multiple S-N curves which should be chosen according to the nature of the fatigue problem (see figure 2.3). The choice of S-N curve should be based on the following criteria [12]:

- The geometrical arrangement of the detail
- The direction of the fluctuating stress relative to the detail
- The method of fabrication and inspection of the detail

The S-N curves can be defined by the equation:

$$\log N = log\overline{a} - m \log \left( \Delta\sigma \left( \frac{t}{t_{ref}} \right)^k \right) \tag{2.4}$$

$\overline{a}$, $m$ and $k$ are defined parameters depending on chosen S-N curve. $\overline{a}$ is defined so that the S-N curve can be associated with a 97.7% probability of survival.
$t_{ref} = 25$ mm for welded connections other than tubular joints.
$t$ is the thickness through which a crack will most likely grow (equal to $t_{ref}$ if the thickness is smaller than $t_{ref}$).

The slope change in the S-N curves in figure 2.3 at 10 million cycles can be explained this way. A structure that experience variable loading over time will initially have some loads under the threshold region. After the crack has grown the stress intensity factor will increase, and some loadings that were previously under the threshold region will now contribute to crack growth. The S-N curve can be written as shown in equation 2.5 if $t \leq t_{ref}$.

$$\log N = \begin{cases} \log \overline{a}_1 - m_1 \log \Delta\sigma & \text{if } \Delta\sigma \geq \Delta\sigma_0 \\ \log \overline{a}_2 - m_2 \log \Delta\sigma & \text{if } \Delta\sigma < \Delta\sigma_0 \end{cases} \tag{2.5}$$

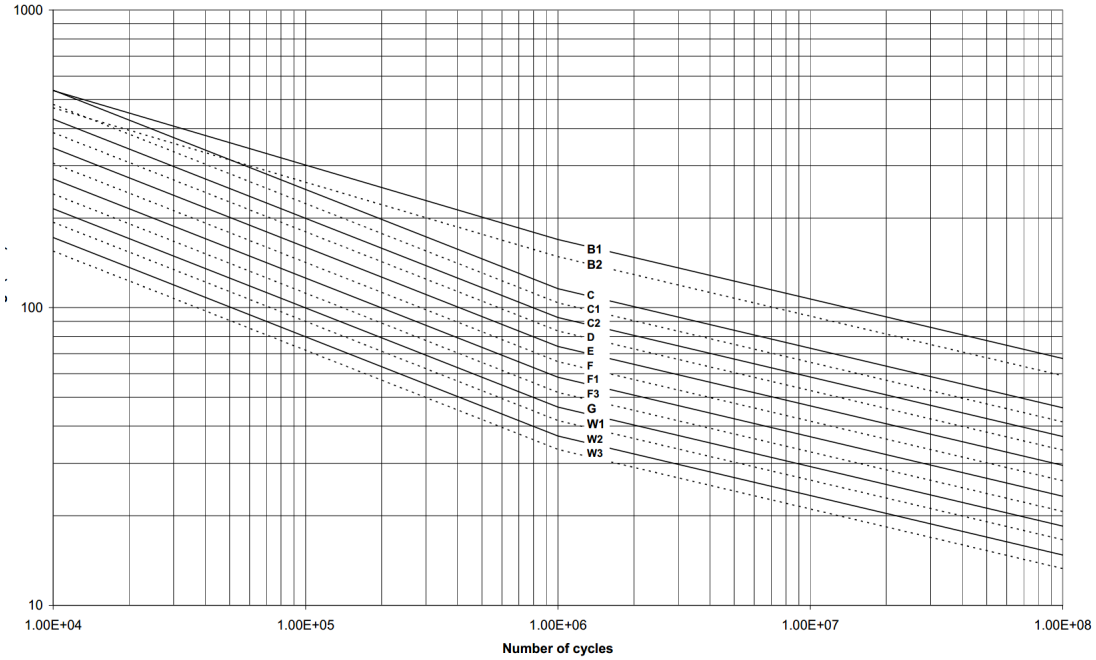


Figure 2.3: S-N curves in seawater with cathodic protection from DNV-RP-C203 [12]

## 2.4 Cumulative damage

There exist various methods for calculating cumulative damage under stochastic loading. One such method is the Miner summation. Berge [5] argue that the Miner summation method has proved to be no worse than any other method, but much simpler. The basic assumption is that the fatigue damage per cycle is constant at a given stress range and equal to

$$D = \frac{1}{N} \tag{2.6}$$

N is a the number of cycles to failure at a given stress range. The total damage can be written

$$D = \sum_i \frac{n_i}{N_i} \tag{2.7}$$

where $n_i$ is the number of cycles and $N_i$ is the number of cycles to failure for a given stress range. $D \geq 1$ indicates failure. It can be shown that for a SN curve written on the DNV form indicated in equation 2.5 the total miner damage can be written as in equation 2.8

$$D = \sum_{\Delta\sigma \geq \Delta\sigma_0} \frac{n_i}{\bar{a}_1} {\Delta\sigma_i}^{m_1} + \sum_{\Delta\sigma < \Delta\sigma_0} \frac{n_i}{\bar{a}_2} {\Delta\sigma_i}^{m_2} \tag{2.8}$$

$\Delta\sigma_0$ is the fatigue limit at 10 million cycles.

To estimate the cumulative damage for a structure subjected to wave loads one should estimate the damage for a representative set of sea states. To reduce the effect of short term variability multiple time domain simulations per sea state are normally required [24]. The total damage over the lifetime of the structure will be the combined damage of each sea state multiplied with the expected number of each sea state.

damage per time at a given sea state of length $t_{sea}$ is

$$d_{sea} = \frac{D_{sea}}{t_{sea}} \tag{2.9}$$

$D_{sea}$ is damage for the given sea state and $d_{sea}$ is damage per second.

The average damage per time for a distribution of $n$ different sea state, each with a probability $p_i$ and $m$ different time domain simulations becomes

$$d_{avr} = \sum_{i=1}^{n} \sum_{j=1}^{m} \frac{d_{sea,ij}}{m} \cdot p_i \tag{2.10}$$

Estimated time to failure, $t_f$ will then be

$$t_f = \frac{1}{d_{avr}} \tag{2.11}$$

## 2.5 Fatigue design factor

Because of the difficulty associated with predicting fatigue life with accuracy offshore codes such as NORSOK includes a safety factor. The fatigue design check can be written on the form

$$D_c = \frac{1}{FDF} \tag{2.12}$$

where $D_c$ is the estimated cumulative fatigue damage and $FDF$ is the fatigue design factor.

In the NORSOK standard the FDF varies between 1 and 10, depending on the consequence of failure and the accessibility for inspection and repair.

Table 2.1: Fatigue design factors from NORSOK [23]

| **Classification of structural components based on damage consequence** | **Not accessible for inspection and repair or in the splash** | **Accessible for inspection, change or repair and where inspection or change is assumed** | |
|---|---|---|---|
| | | Below splash zone | Above splash zone or internal |
| Substantial consequences | 10 | 3 | 2 |
| Without substantial consequences | 3 | 2 | 1 |

## 2.6 Hot spot method

The hot spot method is probably the most frequently used method for calculating stresses used in fatigue life prediction. How to find the hot spot stress by finite element analysis is

described in DNVs classification note 30.7, Fatigue Assessments of Ship Structures. For a finite element model with shell elements the following procedure can be used. The hot spot stresses are found by linear extrapolation over reference points with a distance from the hot spot equal to 0.5 and 1.5 times the plate thickness. The stress to be used with the S-N curve is calculated from the extrapolated component values [7]. The hot spot stress does not take into account the stress intensity facttor from the weld itself. This effect is to be included later in the S-N Curve.

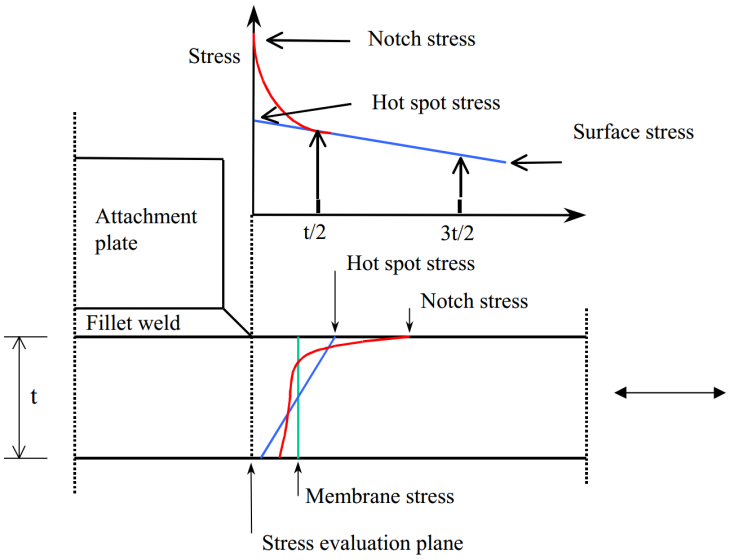


Figure 2.4: Schematic stress distribution at hot spot [7]

DNV has proposed the following formula for calculating the effective hot spot stress range when fatigue cracking can occur along a weld toe, and when the principal stress direction is more parallel with the weld [12]:

$$\sigma_{Eff} = \max \begin{cases} \sqrt{{\Delta\sigma_{\perp}}^2 + 0.81{\Delta\tau_{\parallel}}^2} \\ \alpha|\Delta\sigma_1| \\ \alpha|\Delta\sigma_2| \end{cases} \tag{2.13}$$

$$\Delta\sigma_1 = \frac{\Delta\sigma_{\perp} + \Delta\sigma_{\parallel}}{2} + \frac{1}{2}\sqrt{(\Delta\sigma_{\perp} - \Delta\sigma_{\parallel})^2 + 4\Delta\tau_{\parallel}^2} \tag{2.14}$$

$$\Delta\sigma_1 = \frac{\Delta\sigma_{\perp} + \Delta\sigma_{\parallel}}{2} - \frac{1}{2}\sqrt{(\Delta\sigma_{\perp} - \Delta\sigma_{\parallel})^2 + 4\Delta\tau_{\parallel}^2} \tag{2.15}$$

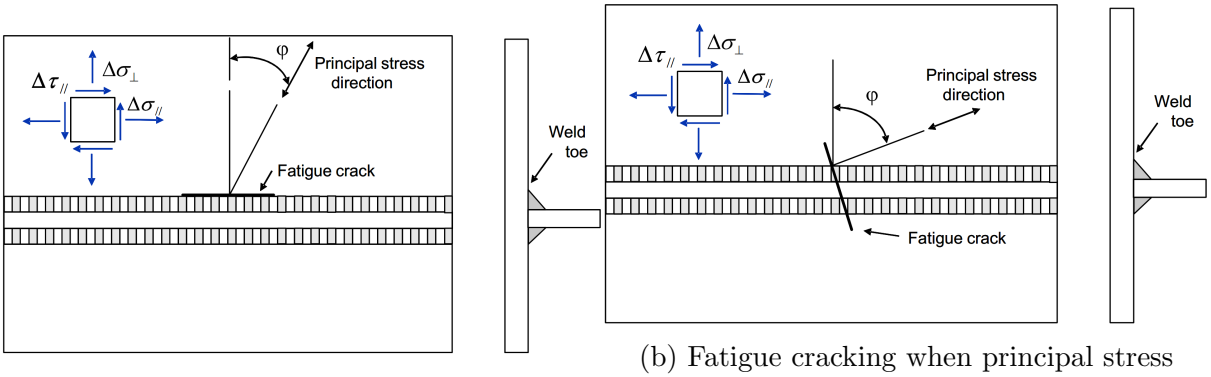


(a) Fatigue cracking along weld toe

(b) Fatigue cracking when principal stress direction is more parallel with weld toe

Figure 2.5: Cracking pattern equation 2.13 is made to account for [12]

The following equation is recommended by DNV to derive the effective hot spot stress at hot spots with significant plate bending [12]:

$$\Delta\sigma_{e,hot\ spot} = \Delta\sigma_{a,hot\ spot} + 0.60\Delta\sigma_{b,hot\ spot} \tag{2.16}$$

The equation can be explained by the fact that the crack tip will grow into regions with reduced stress. It is not generally correct to reduce the stress concentration of the bending component to 60%, as the effect is limited to areas with a localized stress concentration (for example at a hopper corner) [12].

## 2.7 Rainflow counting

'For cumulative damage analysis, the stress-time history is broken down into individual cycles which are summed up to a distribution of stress ranges' [5]. There exist various methods for breaking the stress-time history into individual cycles, and the estimated fatigue damage may differ depending on method. There seems to be a common consensus that the rainflow method is superior to other cycle counting methods for fatigue damage estimation [5][24].

The principle the rainflow method is based on is illustrated in figure 2.6. Every closed loop in the strss-strain plane corresponds to one cycle. The algorithm for finding the stress ranges with the rainflow method can be described by these steps [24].

1. Imagine that the time history of the stress is turned 90°with the start of the time series at the top. As illustrated in figure 2.7.

2. Each rainflow begins at the beginning of the time series and at the inside of every peak and valley.

3. Rainflow initiating at a peak (or a valley) drops down until it reaches an opposite peak with a higher amplitude than the peak from which it started.

4. Rainflow also stops when it meets the rainflow from a roof above.

5. Rainflow must terminate at the end of the time series.

6. The horisontal length of each rainflow is counted as a half-cycle with that stress range.

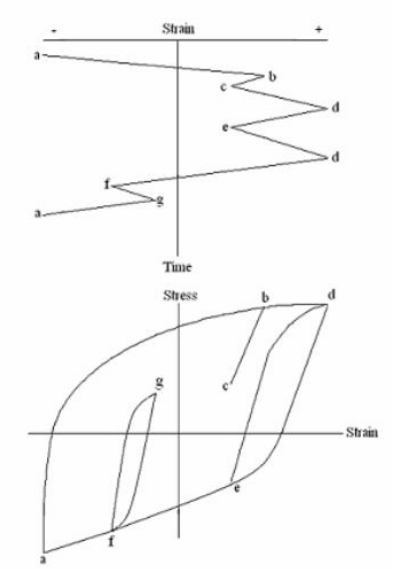


Figure 2.6: Part of a strain history and corresponding stress-strain response [2]

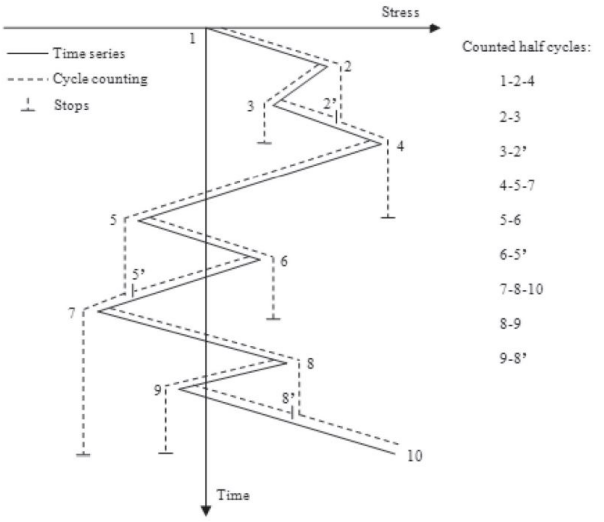


Figure 2.7: Illustration of the rainflow cycle counting algorithm [24]

The rainflow method can be applied for both narrow and broad banded stress responses. The method is based on the assumption that the load sequence does not matter.

## 2.8 Multiaxial fatigue

Multiaxial fatigue can be defined as fatigue due to mixed-mode loading where the crack will experience mixed-mode growth. The authors of the book Multiaxial Fatigue gives the following introduction to mulitiaxial fatigue today [27]:

'Fatigue evaluation of components and structures has become and integral part of the design process in many industries. However, multiaxial fatigue continues to be largely the domain of a limited number of specialists. During the analysis of components subject to multiaxial loading, the problem often is reduced to an "equivalent" uniaxial fatigue case without thought as to whether the simplifying assumtions are valid for the specific load sequence or component being considered.'

Plate and shell structures will have a combination of Mode I and Mode II loading. Mode III is unusual for these kind of structures [27]. When the loading is non-proportional different problems arise. Socie and Marquis argue that at least three potential problems are associated with non-proportional load histories.

1. Additional strain hardening may occur.

2. For uniaxial loading the rainflow method is well established. For complex multiaxial load histories there exist no well accepted cycle counting procedure.

3. The interpretation of multiaxial damage parameters. For complex loading the maximum shear strain amplitude and maximum of the damage parameter is not necessarily on the same plane.

### 2.8.1 Path-dependent maximum range cycle counting method

In recent years extensive research has been done on multiaxial fatigue. One of the most recent methods proposed for multiaxial fatigue life assessment is the Path-Dependent Maximum Range cycle counting method (PDMR), developed by Battelle researchers. PDMR is a cycle counting and fatigue life evaluation procedure. When applied to uniaxial loading the PDMR cycle counting procedure give the same results as the rainflow method.

The PDMR method can be described as a procedure seeking the maximum possible distance between any two points in the stress space over a given time history [6], as illustrated in figure 2.8 for a time history from P to Q. R is a turning point and $R^*$ is a projected turning point. The parameter $\beta$ is a material parameter normaly between 2 and 4 for steel. A more detailed description of the method can be found in reference [6].

The PDMR method has proved effective for some of the well-documented test data available in the literature [6][29]. Forte and Wei showed that the PDMR method was capable of predicting fatigue life for unidirectional composites tested at different fiber/load angles with reasonable accuracy [29].

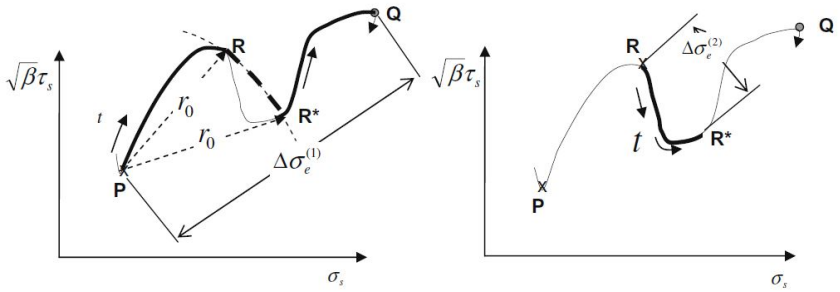


Figure 2.8: Illustration of PDMR cycle counting procedure [6]

## 2.9 Linear simplification for calculating effective stress ranges under multi-axial loading

When dealing with multi-axial fatigue life prediction in which more than one stress or strain components are operative and out-of-phase with each other, there exists no well-accepted cycle counting procedure [6]. Rainflow counting can be used to count the stress ranges for each of the stress components separately, but they can not be compared with each other due to the fact that they are not in phase. A turning point from the perpendicular stress time series will not necessarily occur at the same time as the turning points

of the parallel shear stress and parallel stress. The number of turning points for each stress component is also likely to differ, and thus the number of stress ranges.

In an out-of-phase multi-axial stress state it is not possible to calculate the effective stress ranges from equation 2.13. The author of this paper has proposed the following method for estimating the effective stress ranges for a multi-axial stress state when the different stress components are nearly in-phase or nearly in-opposite-phase:

1. Map the time histories of the stresses onto a transformed stress space on the form $\sigma_{\perp} - \sqrt{\beta}\tau_{\parallel}$ and $\sigma_{\perp} - \sigma_{\parallel}$. If the plot resembles a line it means that the stresses are nearly in-phase or in-opposite-phase with each other. The mapped time historie of the hot spot stress for a given hot spot and loading condition is given in Figure 2.9. $\beta$ is a material parameter not relevant for the calculations and is set equal 3.

2. Estimate which stress components is likely to contribute the most to fatigue damage. Construct time series of the other stresses based on the assumption that they can be expressed as a linear function of the most important stress component. If $\sigma_{\perp}$ is deemed to be the most important stress, the simplified stress time histories of the other stress components should be expressed on the form:

$$\tau_{\parallel,s}(t) = \overline{y}_{0,1} + \alpha_{1,med}\sigma_{\perp}(t) \tag{2.17}$$

$$\sigma_{\parallel,s}(t) = \overline{y}_{0,2} + \alpha_{2,med}\sigma_{\perp}(t) \tag{2.18}$$

   $\overline{y}_{0,1}$ and $\alpha_{1,med}$ can be calculated the following way:

   - Calculate the mean of $\sigma_{\perp}(t)$, $\overline{\sigma}_{\perp}$, and find the corresponding shear stress values when $\sigma_{\perp}$ crosses its mean value. Calculate the mean of this shear stress values, $\overline{y}_{1,1}$.
   - At any time, $t$, $\alpha_1$ can be calculated as

$$\alpha_1 = \frac{\overline{y}_{1,1} - \tau_{\parallel}(t)}{\overline{\sigma}_{\perp} - \sigma_{\perp}(t)} \tag{2.19}$$

     Note that the median value of $\alpha_1$ should be used to define the simplified shear stress, not the mean value. The reason for this is to avoid the influence of singularities when $\overline{\sigma}_{\perp} - \sigma_{\perp}$ is close to zero.

   - $\overline{y}_{0,1}$ can now be calculated as

$$\overline{y}_{0,1} = \overline{y}_{1,1} - \alpha_{1,med} \cdot \overline{\sigma}_{\perp} \tag{2.20}$$

   The parameters $\overline{y}_{0,2}$ and $\alpha_2$ can be found in a similar manner.

3. Plot the constructed stresses versus the real stresses as a function of time to get an idea of how good the linear simplification is. See figure 2.10 and 2.11.

4. The turning points from the chosen real stress and the two corresponding constructed stress components will now occur at exactly the same time. That means that a rainflow cycle counting procedure now will produce the same number of stress

ranges for all the stress components. Each stress cycle in the chosen real stress components time history will also be comparable to corresponding stress cycles in the constructed stress components time histories. As a result the stress ranges from the time histories of the linearized stresses will be proportional to the stress ranges from the chosen real stress time history. If $\sigma_{\perp}$ is chosen as the real stress component the stress ranges of the other stress components will be on the form

$$\Delta\tau_{\parallel}(t) = \alpha_{1,med}\Delta\sigma_{\perp}(t) \tag{2.21}$$

$$\Delta\sigma_{\parallel}(t) = \alpha_{2,med}\Delta\sigma_{\perp}(t) \tag{2.22}$$

As a result of this the stress ranges of the chosen real stress component and the two linearized stress components can be compared with equation 2.13, and effective stress ranges can be calculated.

5. The total fatigue damage can now be calculated with the Miner summation procedure using the effective stress ranges found above.

The accuracy of the method depends on how strong the linear correlation between the stresses are. Their are several ways one can measure the accuracy. One way is to also calculate fatigue damage with one (or both) of the other stress components chosen as the real stress. The total fatigue damage should be roughly the same no matter what stress component was chosen as real.

Another way to measure accuracy is to calculate the standard deviation in time domain of the simplified stress component and compare it to the standard deviation of the actual stress. As long as the linear correlation is not perfect, the standard deviation of the simplified stress should be lower than of the real stress. That being said, the difference should be very small if fatigue damage effects are to be captured properly by the simplified stress. In this thesis both these methods have been used to evaluate the accuracy of the simplified linear stress method.

When the linear correlation between the chosen real stress component and one of the other stress components approaches zero, the standard deviation of the simplified stress will also approach zero. As a result of this the simplified stress will not give any contribution to the effective stress ranges. The effective stress ranges from this method when the linear correlation between the stresses are low will converge towards the stress ranges found when only evaluating the chosen real stress component.

The method is easy to implement in a program, which purpose is to estimate fatigue life and is likely to give a good estimation of effective stress ranges as long as the constructed time histories of the stresses are close to the real time histories. The method will always be somewhat non-conservative, due to the lower standard deviation of the simplified stresses. The PDMR-method is likely to estimate a shorter fatigue life. The reason is that the PDMR-method seeks to find the maximum possible distance between any two points in the stress space over a given time history [6]. If one were to compress a time history in the stress space to a line the maximum distance will decrease between the two points. The total number of stress cycles is also likely to be lower than for the PDMR-method, as the turning points will occur at exactly the same time for all stress components.

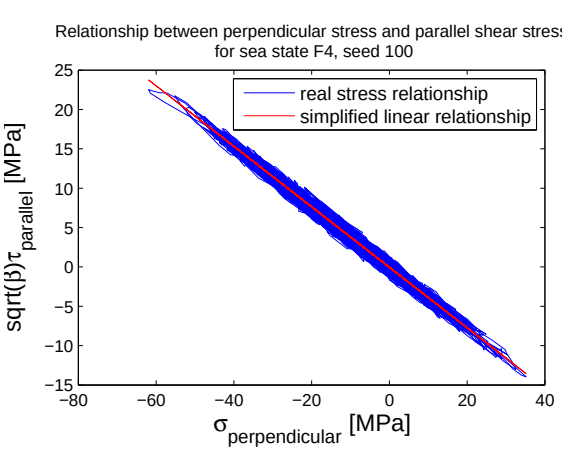


(a) $\sigma_{\perp} - \sqrt{\beta}\tau_{\parallel}$ plane

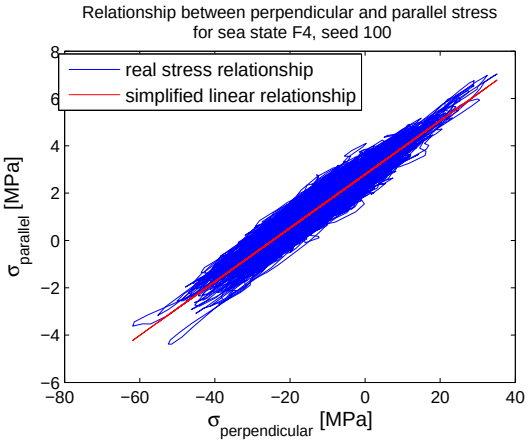


(b) $\sigma_{\perp} - \sigma_{\parallel}$ plane

Figure 2.9: Stresses plotted in the stress space

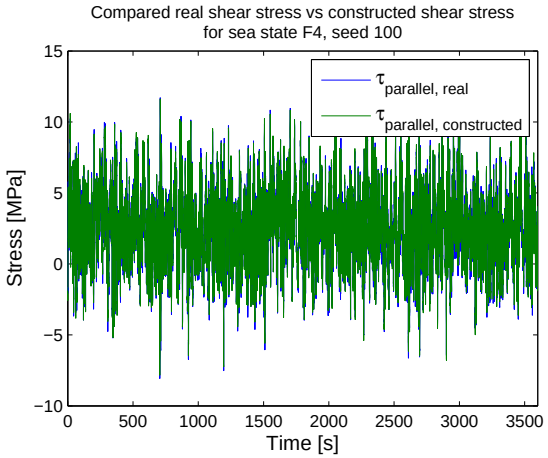


(a) real and constructed shear stress

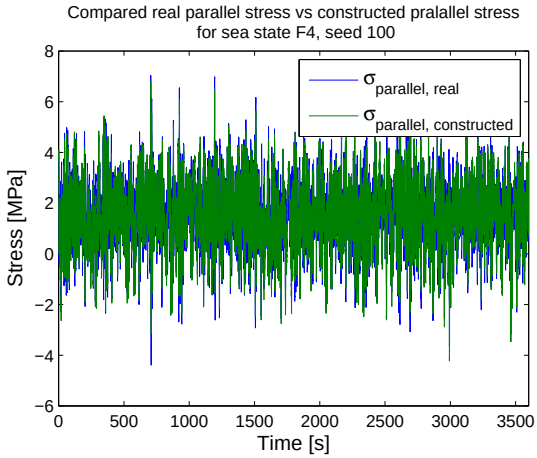


(b) real and constructed parallel stress

Figure 2.10: Compared real stress and constructed stress

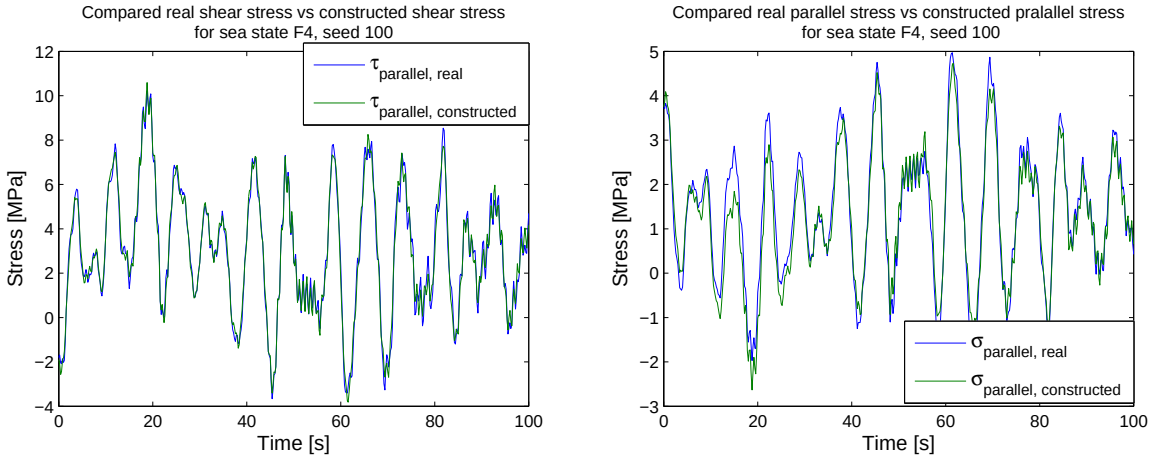


(a) real and constructed shear stress

(b) real and constructed parallel stress

Figure 2.11: Compared real stress and constructed stress in a short time span

# Chapter 3

# Design and Finite Element Model

The finite element model of the column-pontoon connection have been based on the work done be MSc student Traian I. Marin [18]. This model has been further developed by the author of this report. The structural design has been improved in order to reduce stress concentration at hot spots.

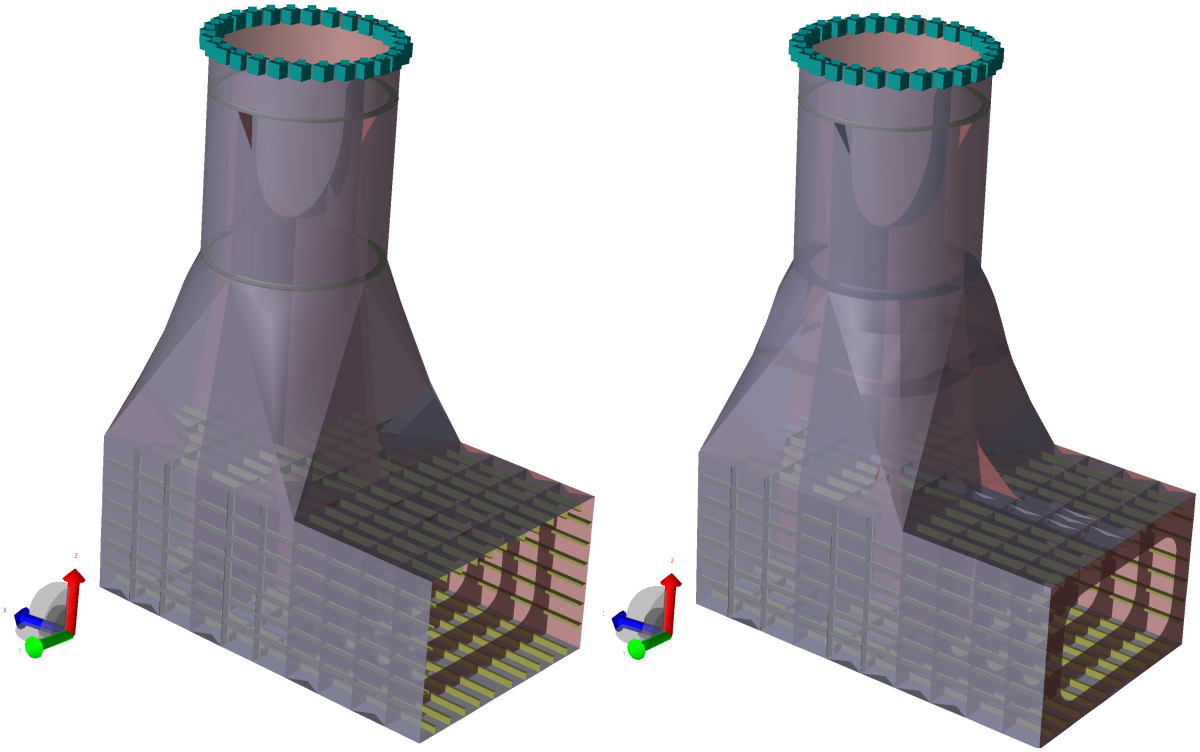

(a) Original FE-model (b) Improved FE-model

Figure 3.1: Finite element model before and after improvements

## 3.1 Element type

The model consist of shell and beam elements. Most beams are modeled with beam elements, but in areas close to hot spots analyzed plate elements have been used for increased accuracy. Second order quadratic thick shell elements are used, although there are some

triangular elements in order to create a smooth mesh.

Thick shell elements are based on Mindlin's thick plate theory. Thick plate theory, as opposed to thin plate theory, accounts for shear deformation. This implies that a straight line normal to the midsurface of the plate before loading is still straight, but not normal to the midsurface after deformation [19].

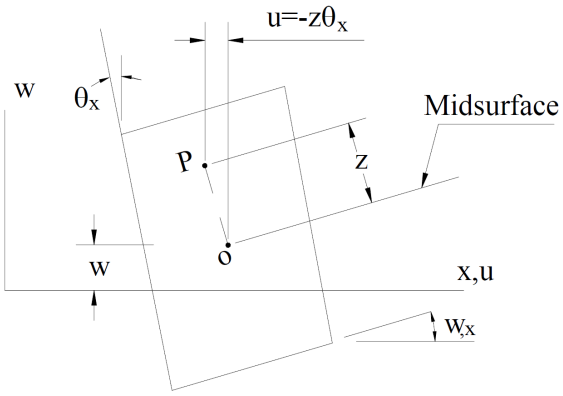


Figure 3.2: Thick plate element after loading [20]

### 3.1.1 Stress distribution over the plate thickness

The different stress types will vary in magnitude over the thickness of the plate. $\sigma_{xx}$, $\sigma_{yy}$ and $\tau_{xy}$ will have one constant stress component over the plate (membrane stress) and one component with opposite values on each plate surface (bending stress). The stress distribution over the thickness for $\sigma_{xx}$ and $\sigma_{yy}$ is given in Figure 3.3. The $\tau_{xy}$ distribution is given in Figure 3.4. Because the elements are based on Mindlin's thick plate theory there will also be transverse shear stress (given in Figure 3.5).

The distribution of the transverse shear is different than the distribution for the other stress types. The transverse shear will be very small, due to the thin plate thickness and has been disregarded in fatigue calculations. For both normal stresses and in plane shear the decomposed membrane and bending stresses have been used in fatigue calculations.

Note that in Figure 3.4 the in plane shear stress component with opposite values on each surface side is defined as twisting shear. Although this name is a better description of how this shear stress component acts, in this report it is always referred to as the "bending shear component".

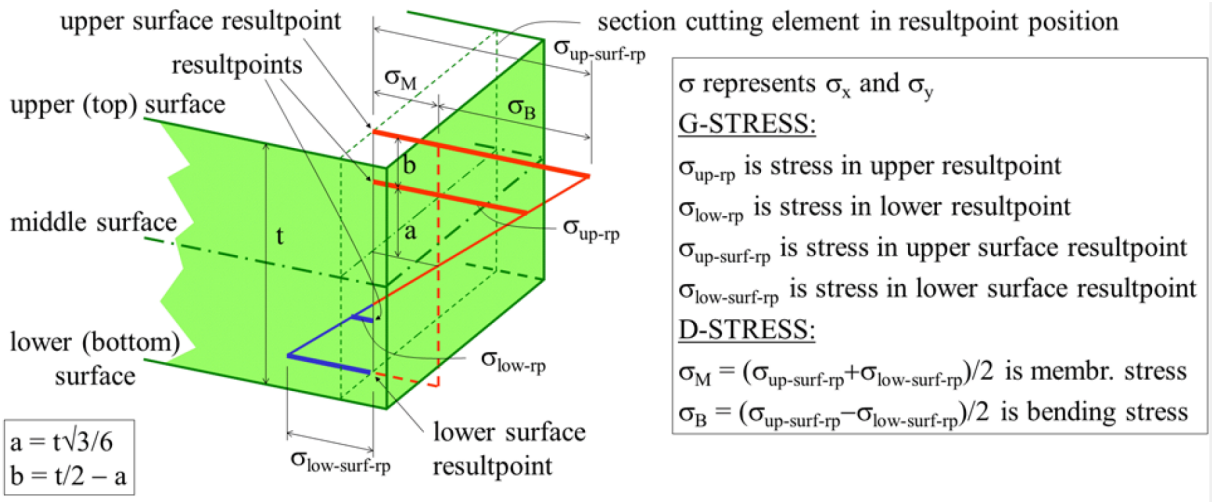


Figure 3.3: Decomposed normal stress for 8 node shell element [10]

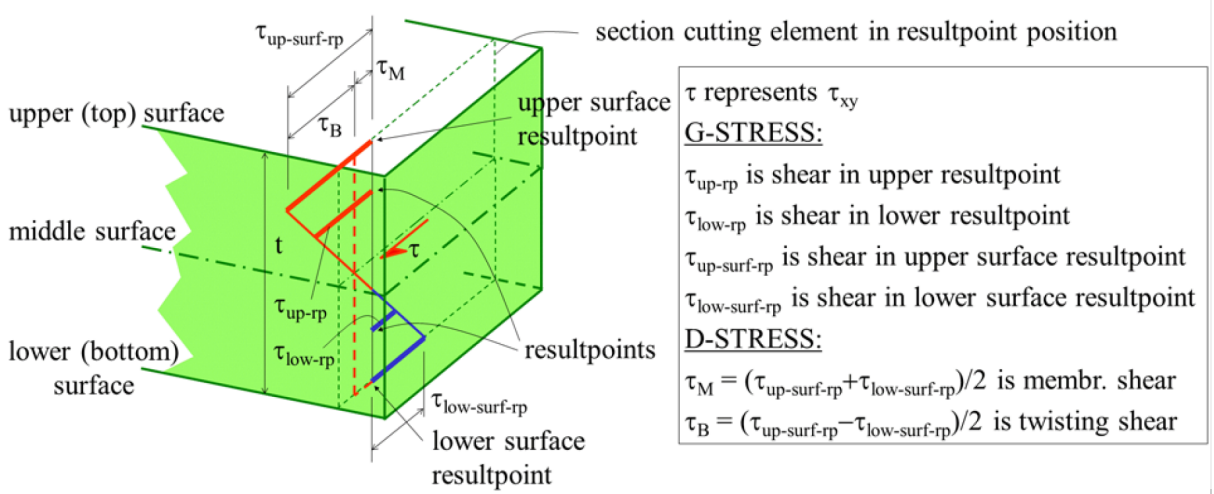


Figure 3.4: Decomposed in plane shear stress for 8 node shell element [10]

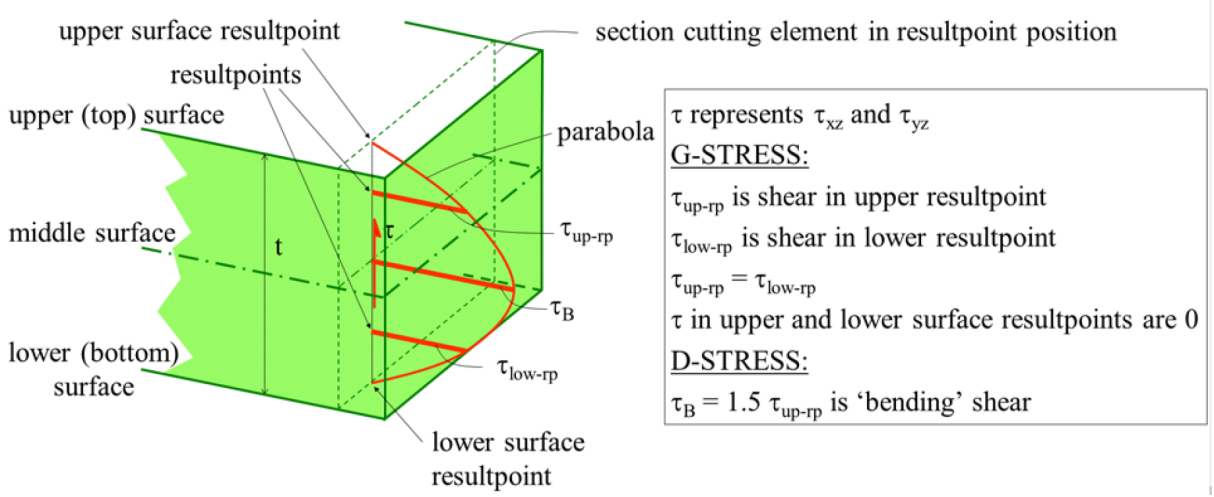


Figure 3.5: Decomposed transverse shear stress for 8 node shell element [10]

## 3.2 Meshing

In the global model the element length is set to 0.5 m. As the submodelling technique will be applied in hot spot areas a relatively coarse mesh is acceptable in the global model. In the submodels a t x t element size are used, where t is the plate thickness. GeniE is capable of generating a satisfactory mesh solely based on the concept model [8].

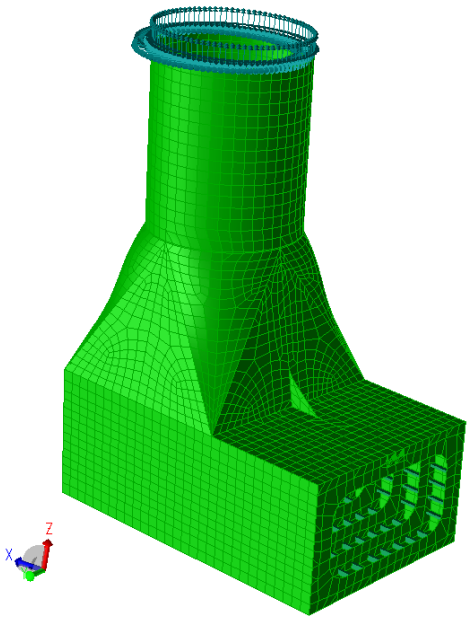


Figure 3.6: Global mesh

In the submodels "advancing front quad mesher" is used on some of the plates. This has been done to achieve a good quality mesh with only quadratic elements in the hot spot area where stresses are to be extrapolated. The advancing front mesher generates the mesh along the edges first before filling the rest of the surface. This results in a significant better quality mesh along the outer boundaries of the surfaces [9].

Table 3.1: Finite element model information

| | Global model |
|---|---|
| Number of elements | 9302 |
| Number of nodes | 23 263 |
| Element size | 500mmx500mm |

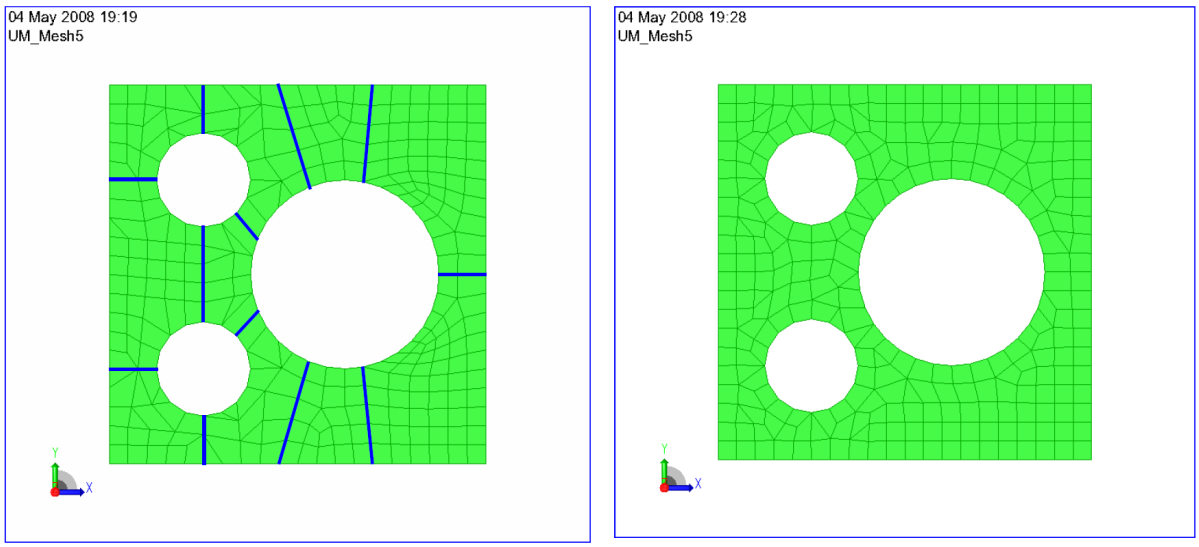


*Sesam quad mesher* Advancing *front quad mesher*

Figure 3.7: Difference between regular Sesam quad mesher and advancing front quad mesher [9]

## 3.3 Boundary conditions

The boundary condition has not been changed from the original model. All 6 DOF are constrained at the cross section where the column is cut. This is conservative. In reality one can expect some movements in this area. In reality the column continues further upwards. MSc student Traian showed that the stresses in the region of interest are almost independent of the choice of boundary condition [18].

## 3.4 Loading

Each cross sectional loading condition is defined as described in [18]. There are applied loads in every degree of freedom at the cross section where the pontoon is cut. The loads applied are not unit loads, but loads that will produce a input stress equal 100 MPa in the area where they are applied.

$F_x$ loading result in $\sigma_{xx} = 100$ MPa, $F_y$ and $F_z$ result in shear stresses equal 100 MPa in the horizontal and vertical walls respectively. The moment $M_x$ will produce a shear stress in the walls equal 100 MPa and $M_y$ and $M_z$ will produce bending stresses with the same magnitude in the horisontal and vertical walls respectively. Defining the loading conditions this way make it easier to compare hot spot stresses from different load direction.

Table 3.2: Total cross sectional load applied on the cross section in different loading conditions

| Load case | Total load [MN] | Load case | Total moment [MNm] |
|---|---|---|---|
| $F_x$ | 74.7 | $M_x$ | 268 |
| $F_y$ | 74.7 | $M_y$ | 215 |
| $F_z$ | 74.7 | $M_z$ | 251 |

All loads are applied in the positive direction. The real stress, $\sigma_{r,i}$, at an arbitrary point in the structure from a real load $F_{r,i}$ in the $i$ direction can be calculated as

$$\sigma_{r,i} = \frac{F_{r,i}}{F_{0,i}} \cdot \sigma_{nd,i} \tag{3.1}$$

$F_{0,i}$ is the cross sectional loading applied in the FE-model in direction $i$ to achieve a input stress equal 100 MPa, given in Table 3.2.
$\sigma_{nd,i}$ is the nondimenional stress at the arbitrary point corresponding to a "unit stress" on the cross section where loads are applied. That means the stress from the FE-model with one of the load cases above divided by $10^8$ MPa. When later it will be refereed to the nondimensional hot spot stress, it is defined the same way.

## 3.5 Improvements

There were done several changes in the FE-model. The ring stiffener 5 cm above the intersection between the cylindrical column and the transition hull (marked in blue in Figure 3.8) has been made larger. It has also been modeled with shell, elements, to increase stress accuracy in the sub model. Web length and flange width are doubled, but thickness remain the same. This has been done to increase the stiffness in this area. Second order elements are chosen because there are steep stress gradients at some areas in the model.

The transition hull deformations are quite large. To reduce the deformations a ring stiffer is added 4 meters above the the top of the rectangular pontoon. The geometry of this part is somewhat complex, due to the curvature of the hull at this location. The stiffener has a T-cross section with length of the web around 1 meter and flange width 0.24 meters. The thickness of both flange and web is set to 25 mm.

To increase the stiffness 4 longitudinal stiffeners have also been inserted, from each corner at the bottom to the ring stiffener at the cylinder. The stiffener is a plate with thickness 25 mm, where the edge turning inwards is parallel with the z-axis.

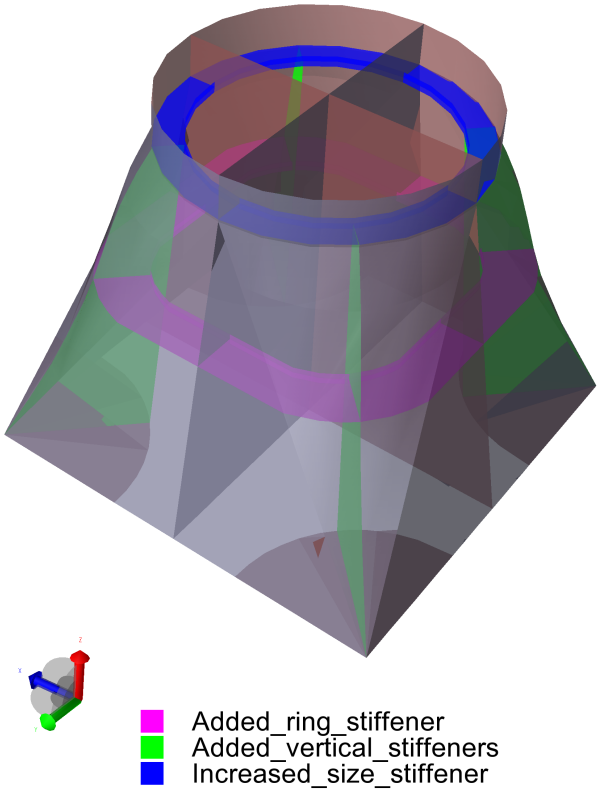


Figure 3.8: Highlighted changes made at the transition piece

At the point where the upper hull of the pontoon intersects with the bulkhead in the x-z plane inside the transition piece, there was very large stress concentration. This is the point where the highlighted parts in Figure 3.9 intersect. The reason for the very large stress concentration, is that all the stresses at the upper hull of the pontoon will be transferred to the bulkhead in the transition piece through one single point. To reduce the stress concentration several changes were made.

To increase the direct contact surface between the bulkhead and the pontoon part another longitudinal stiffener was added under the pontoon hull. It has the same dimensions as the other longitudinal stiffeners at the pontoon. It ends where the bulkhead begins. As other beams close to areas where hot spots are analyzed plate elements have been used to model it, not beam elements.

To further increase the contact surface the upper hull of the pontoon was extended with another plate (makred in blue). This reduced the hot spot stresses significantly, but not enough. It was estimated that fatigue failure would occur after 27 days. Especially the stress concentration due to cross sectional loading in pitch was too high. Therefore, it was decided to insert a kneeplate outside the hull between the pontoon and transition hull. This is effective in reducing stress concentration caused by bending in the xz-plane. The area of the plate is a bit over 1 $m^2$ with rounded edges to reduce stress concentration here.

Using a kneeplate outside the hull is controversial and is not necessarily the best option. The kneeplate will be exposed to the environment. Hydrodynamic forces acting on the plate surface may be a problem as well as damage from accidents. there are alternative

ways to reducing the stress concentration. For example, the two plates the kneeplate is welded on can be curved so that there will not be any sharp corners. For this to be done it would be necessary to redesign much of the FE-model. Therefore, the author chose to use a kneeplate.

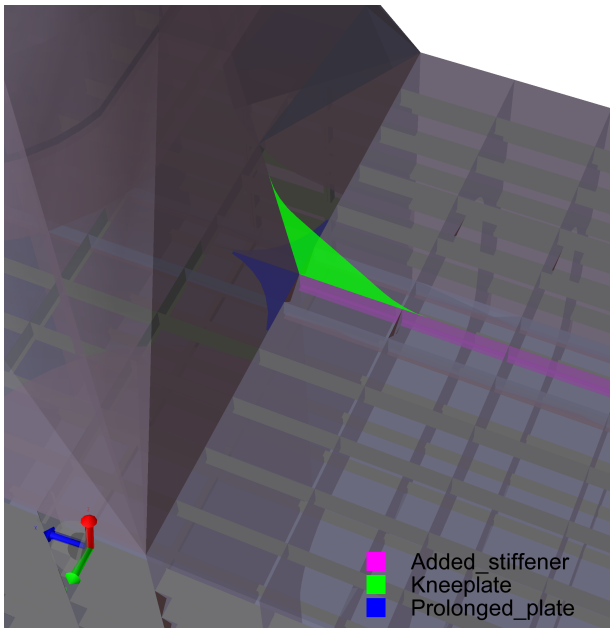


Figure 3.9: Highlighted changes made at the intersection between the pontoon and the transition piece

In Figure 2.2 the nondimenional hot spot stresses for all cross sectional loading conditions are given after every structural improvement. The stresses are split into perpendicular, parallel and shear stress. Both membrane and bending part are displayed for each stress component. The hot spot stresses are found by extrapolating the stresses at the upper hull of the pontoon 1.5t and 0.5t away from the intersection.

The perpendicular hot spot stresses is most important to reduce. Especially the stresses due to $M_y$ loading. One can see significant improvements after every structural change. The bending stress component has not been reduced that much. It actually increases when inserting a longitudinal stiffener, before it is reduced after the adding of the prolonged plate and kneeplate. That being said, reducing the membrane stress was much more important because of its large magnitude.

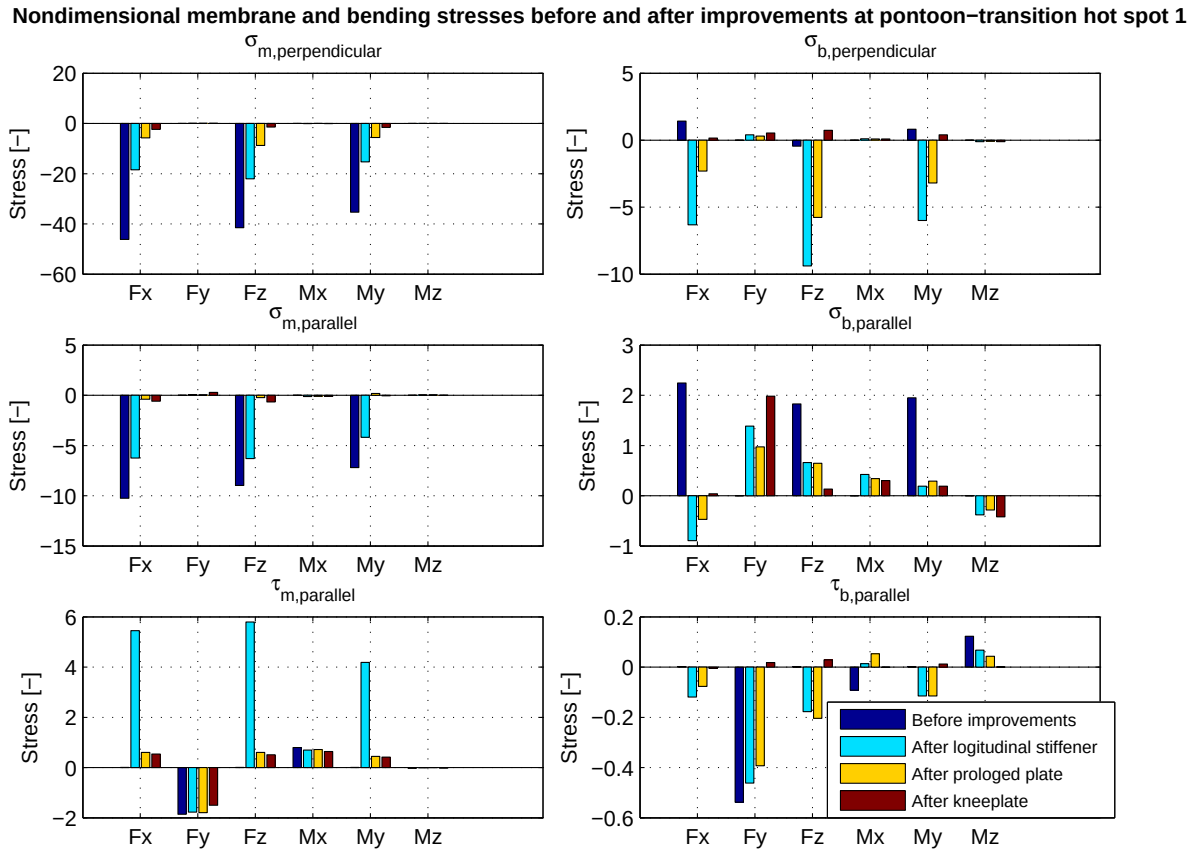


Figure 3.10: Highlighted changes made at the transition piece

The downside with the changes proposed here is increased structural complexity and higher steel weight. More welding is required. The added ring stiffener and vertical stiffener have to be tailor made for this structure because of the special transition hull curvature. These are all factors increasing the cost of building the wind turbine. The structural changes made here are not necessarily the most optimal improvements from an economic perspective, but stress concentration will be reduced. It may prove that further changes are needed to reduce hot spot stresses, but this has not been done in this work. All further discussion in this report is based on the model with all the improvements mentioned here.

## 3.6 Submodeling

For fatigue limit state analysis a very fine mesh is needed close to the hot spot in the finite element model. The submodeling technique is a method for studying a specific area of a finite element model with refined mesh, using the displacement of the global model in the border area as boundary condition [26]. To obtain accurate results the global model has to define the displacement at the boundary with sufficient accuracy.
The Submod program in the SESAM package can be used for submodeling. The procedure can be described as follows:

1. Create a global finite element model and cut the structure at the boundary of the

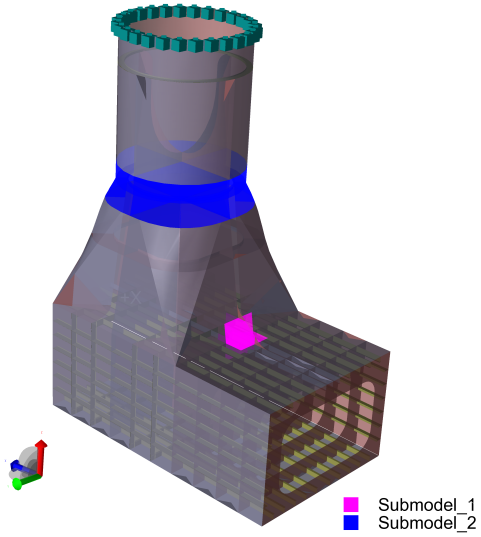


Figure 3.11: Sections analyzed with the submodeling technique

area that will have a refined mesh.

2. Export the structure inside the chosen area to a separate finite element model. This will be the local model. Define the boundary conditions as "prescribed" where the structure connects with the global model. Mesh the local structure with a refined mesh to create a .fem file

3. Solve the equations in the global model using Sestra. This will produce a .sin result file.

4. Use the two files as input in Submod. The output will be a .fem file with the displacement from the global model as boundary condition.

5. Run the resulting .fem file in Sestra. The output file contains the results for the local model and can be investigated further in Xtract.

Two regions in the global model were analyzed with refined mesh using the submodeling technique (see figure 3.11 and 3.12). The first region is located where the middle of the upper plate of the pontoon intersect with the transition piece, as indicated in the figure. The other region is where the cylinder at the top intersects with the transition piece. It was difficult to assess what point on the intersection line would be the worst in regard to fatigue. Therefore, the submodel is defined large enough to enclose all points at the intersection between the cylinder and transition piece.

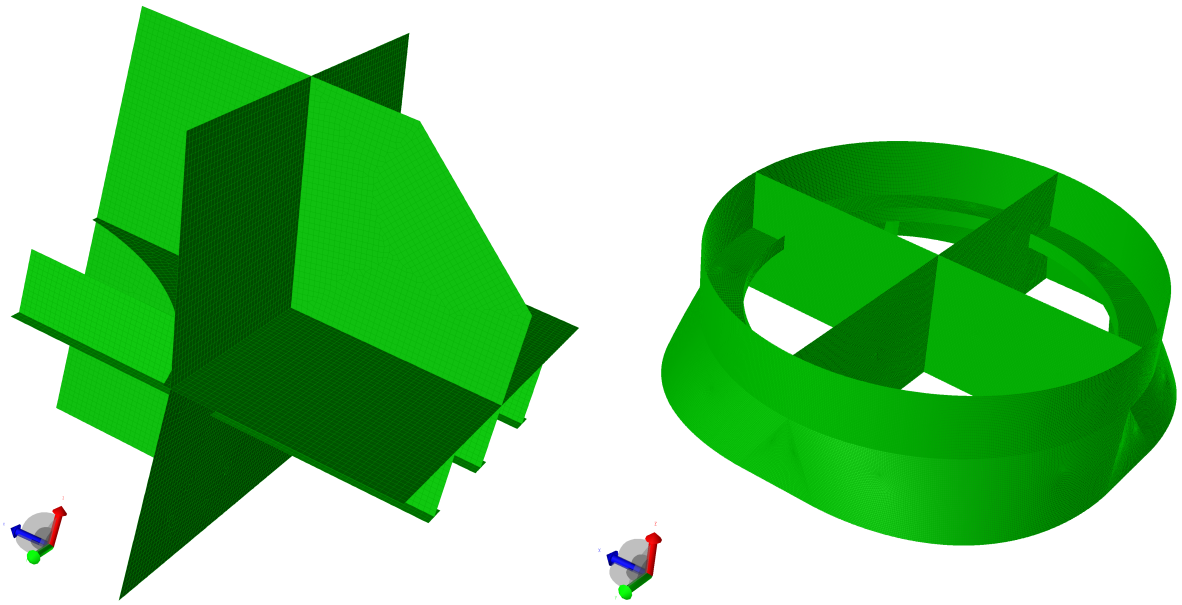

(a) Submodel 1 (b) Submodel 2

Figure 3.12: Sections with refined mesh

Table 3.3: Finite element model information

| | Submodel 1 | Submodel 2 |
|---|---|---|
| Number of elements | 19 584 | 150 000 |
| Number of nodes | 59 585 | 451 901 |
| Element size | 25mmx25mm | 25mmx25mm |

# Chapter 4

# Software

Several different software have been used in the thesis work. Several programs from DNVs SESAM package has been used for the modeling of the structure and calculating unit load stresses. The SESAM package consist of several different programs to be a complete strength assessment system for engineering of ships and structures offshore.

- GeniE V6.6.8 has been used for the modeling of the structure. It is a software tool for designing and analyzing maritime structures made of beams and plates, using the finite element procedure. The original finite element model from Traian was made in GeniE. The improvements of the structural design by this author has also been done with this program.
- Sestra V6.8.1 has been used to solve the finite element equations.
- SesamManger V8.6.1 has been used to create and execute the sub-modeling analysis workflow.
- Submod V.3.2.2 has been used for the sub-modeling analysis. It is a program that can set the displacements from a global model as boundary conditions in a local model with refined mesh.
- Xtract V4.1.2 has been used for post processing. Relevant stresses are exported from Xtract and used as input in fatigue life calculations.

MATLAB R2013b has been used for post-processing of results and estimating fatigue life. MATLAB is a coding language for numerical calculation, programming and data visualization. Rainflow counting was performed with the help of the WAFO 2.5 scripts dat2tp.m and tp2rfc.m. WAFO is a free MATLAB toolbox for statistical analysis and simulation of random waves and random loads [28]. The function intersections.m, created by Douglas Scwarz and freely available from MathWorks, has been used for estimating the locations where two curves intersect [26]. Two other functions have also been taken from MathWorks, subplot_tight [22] and subplotplus [13]. These functions have been used to generate easy to read result figures, when the figure consist of more than one plot. The rest of the MATLAB functions has been created by the author of this paper.

## 4.1 Scripting

The script calculating fatigue life import stresses at read out point at all points of interest in either Submodel 1 or Submodel 2 from .txt files created in Xtract. It returns fatigue life at both upper and lower side of the plate surface, as well as other relevant fatigue parameters. It also creates multiple figures displaying a range of relevant parameters. All plots are saved and arranged orderly in an output folder.

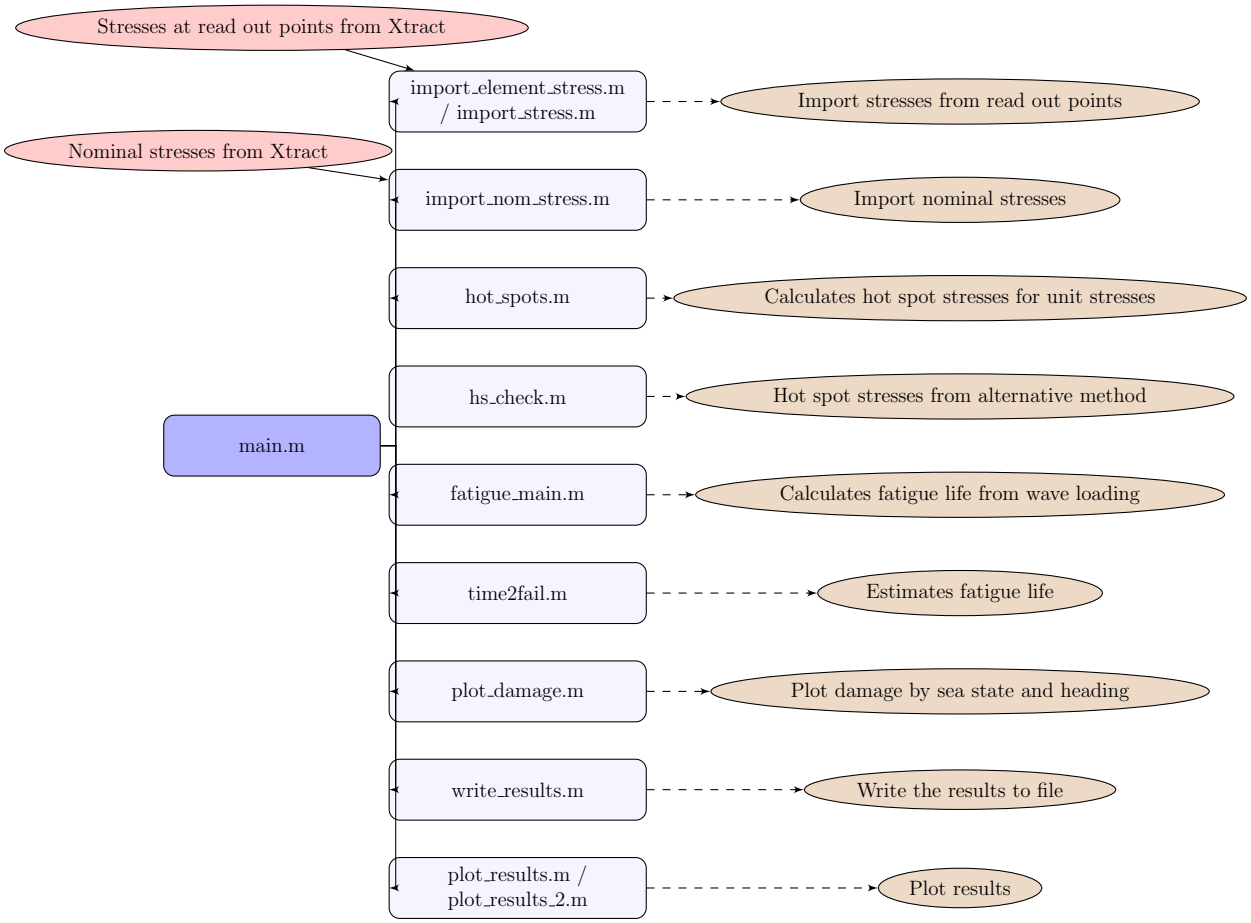


Figure 4.1: General flowchart for MATLAB program calculating hot spot stresses and fatigue life

- Xtract has been used to create files with decomposed stresses at the read out points of each hot spot investigated. When possible the average nodal stresses at the nodes 0.5t and 1.5t away from the hot spot have been exported. When multiple plates are connected to the same node, Xtract can not calculate average nodal stresses. When this is the case the decomposed stresses at the Gaussian points of elements connected to the nodes at the read out points are exported. The local node of the element corresponding to the read out point is then identified. The stresses at these points is used later in the fatigue calculation. Nominal stresses approximately 1 meter away from the hot spot are also exported.

- main.m is the main script. Loops in main.m runs through both plate surfaces of every hot spot and every wave direction. Important parameters from other functions

are sent back to this script.

- The function import_element_stress.m or import_stress import the stresses at the read out points, deepening on whether the stress file consist of average nodal stresses or element stresses. Nominal stresses are imported from import_nom_stress.m.
- hot_spots.m calculates hot spot stresses from unit stresses by interpolating stresses from the read out points. hs_check.m calculates the hot spot as 1.12 times the stress 0.5t away from the hot spot for comparison.
- The function fatigue_main.m consist of several sub functions and is described more detailed below.
- time2fail.m calculates time to failure for a given surface side of hot spot.
- plot_damage.m plots cumulative fatigue damage distributed between sea state and wave heading for a a given surface side of a hot spot.
- The function write_results.m write important result parameters to a .txt file. plot_results.m / plot_results_2.m produces plots of the same result parameters.

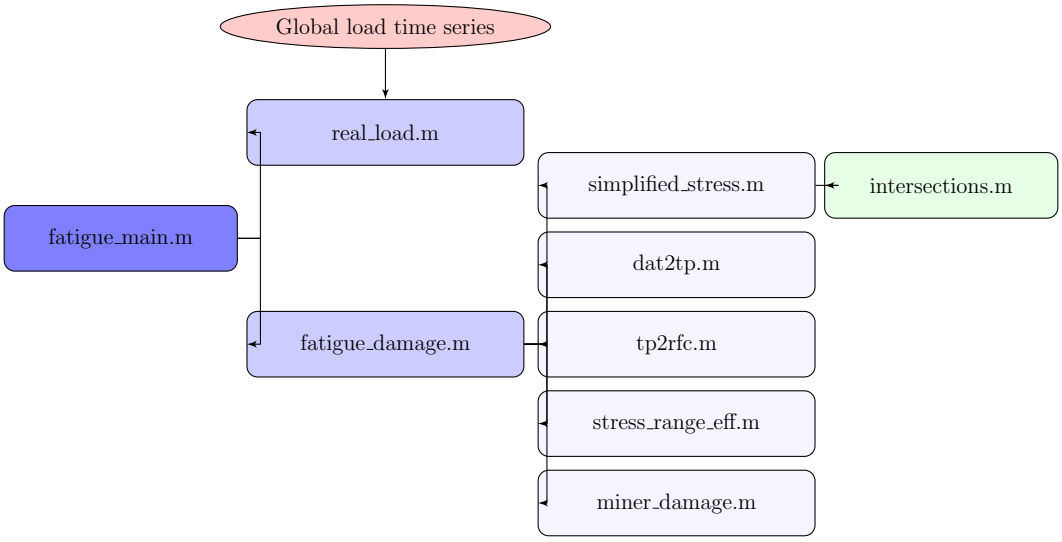


Figure 4.2: Detailed flowchart for MATLAB functions calculating fatigue life

- The purpose of fatigue_main.m is to calculate fatigue damage for all loading conditions given the hot spot and wave direction.
- real_load.m imports real global loading time series and combine it with non dimensional hot spot stresses and produces time series of actual hot spot stresses.
- fatigue_damage. calculates fatigue damage for given time series of global loads. It consist of several sub functions.
- the sub function simplified_stress.m has time series of two different stress components as input. It returns a simplified stress time history of one of the stress

components. The simplified stress will have a linear relationship with the other stress component, in accordance with the method described in section 2.9. In this function intersection.m is used to find the values of the stress component that will be simplified when the other stress component crosses its mean value.

- The WAFO functions dat2tp.m and tp2rfc.m have been used to calculate the rainflow cycles from the time history of a given stress component. dat2tp.m estimates the value and location of all turning points and tp2rfc.m calculates the rainflow cycles from the series of turning points.

- stress_range_eff calculates the effective stress ranges from time series of $\sigma_{\perp}$, $\sigma_{\parallel}$ and $\tau_{\parallel}$ from equation 2.13. The different stress components can not be compared directly with each other, as the turning points not necessarily occur at the same time. Therefore one real stress component is compared with two simplified stress components found by the sub function simplified_stress.m.

- miner_damage.m calculates the Miner damage for a given stress range distribution in accordance with DNV guidlines.

In addition to the functions connected to the main.m script listed above, several other functions have been used for plotting purposes. They are not included here. In order to save space some of the minor functions connected to the main.m script are not included in the flow chart.

# Chapter 5

# Sea State Characteristics

To be able to estimate fatigue life, fatigue damage has been calculated from a representative number of sea states. To reduce the effect of short term variability the damage from 10 different time domain simulations of each sea state have been calculated. All time series of the loading on the cross section of the pontoon have been provided by Ph.D Candidate Chenyu Luan. The duration of each time domain simulation was one hour.

Table 5.1: Sea states used in time domain simulations [16]

| Analysis case number | Case name | North Sea probability [-] | Mean wind speed [m/s] | Turbulence intensity [%] | $H_s$ [m] | $T_p$ [s] | Wave direction (towards) [deg] | Power production |
|---|---|---|---|---|---|---|---|---|
| 1 | F1 | 0.2062 | 4.9 | 23 | 1.0 | 7.8 | 0 | Yes |
| 2 | F2 | 0.3040 | 8.0 | 17 | 2.0 | 8.5 | 0 | Yes |
| 3 | F3 | 0.2207 | 11.0 | 15 | 3.0 | 9.4 | 0 | Yes |
| 4 | F4 | 0.1313 | 13.8 | 14 | 4.0 | 10.2 | 0 | Yes |
| 5 | F5 | 0.0751 | 16.5 | 13 | 5.0 | 10.7 | 0 | Yes |
| 6 | F6 | 0.0353 | 18.9 | 12.6 | 6.0 | 11.1 | 0 | Yes |
| 7 | F7 | 0.0163 | 21.3 | 12 | 7.0 | 11.5 | 0 | Yes |
| 8 | F8 | 0.0070 | 23.4 | 11.9 | 8.0 | 12.1 | 0 | Yes |
| 9 | F9 | 0.0027 | 25.4 | 11.7 | 9.0 | 12.6 | 0 | Yes |
| 10 | F10 | 0.0010 | 27.1 | 11.5 | 10.0 | 13.1 | 0 | No |
| 11 | F11 | 0.00002 | 28.8 | 11.3 | 11.0 | 13.7 | 0 | No |
| 12 | F12 | 0.000008 | 30.0 | 11.2 | 12.0 | 14.0 | 0 | No |
| 13 | F13 | 0.000012 | 31.3 | 11.1 | 13.0 | 14.4 | 0 | No |

To be able to estimate fatigue life realistically one should account for the fact that not all wave will propagate in the same direction. According to DNV Classification Note No. 30.7 [7] the wave spreading function may be expressed on the form

$$f(\theta) = k\cos^n(\theta) \tag{5.1}$$

where k is selected such that

$$\sum_{\theta-90\,\mathrm{deg}}^{\theta+90\,\mathrm{deg}} f(\theta) = 1 \tag{5.2}$$

The exponent $n$ is set equal 4 in all sea sea states in accordance with what is proposed in [11]. The spreading function is thus obtained as

$$f(\theta) = \frac{8}{3\pi}\cos^4(\theta) \tag{5.3}$$

Cross sectional loads for 0°, 30°and 60°heading was provided by Ph.D Candidate Chenyu Luan. Loads for -30°and -60°heading were found by taking the loads from 30°and 60°heading, but multiplying the forces in sway, roll and yaw by -1. This can be because of symmetry in the structure. The wind turbine is not absolutely symmetric around the xz-plane because of the torque on the rotor, but multiplying the loads with -1 will be adequate, according to Luan [17]. The wave spreading functions and the simplified wave heading distribution, based on the heading angles analyzed, are plotted in Figure 5.1. The probability of each heading is given in table 5.2.

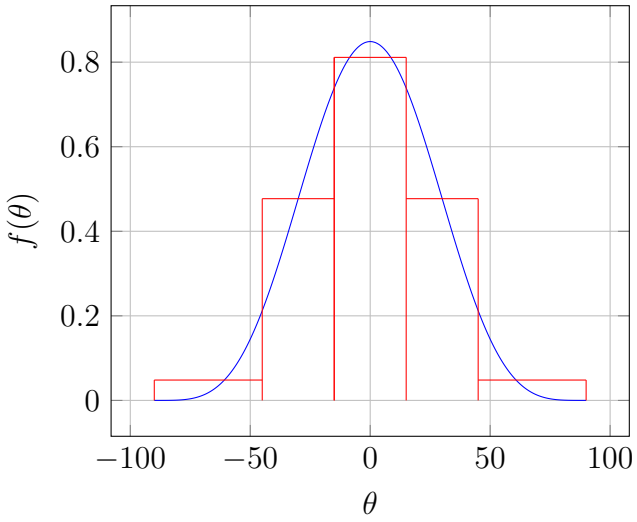


Figure 5.1: Wave spreading function

Table 5.2: Probability of different headings

| Heading [°] | Probability [-] |
|---|---|
| -60 | 0.04 |
| -30 | 0.25 |
| -0 | 0.42 |
| 30 | 0.25 |
| 60 | 0.04 |

## 5.1 Loading

It was found that the sea state generally contributing most to fatigue damage had a significant wave height equal 4 meter. This was true for all wave headings. Therefore, special attention is given to the loading and stresses from this sea state. Global cross sectional loads for this sea state for different wave headings are given in Figure 5.2. Wawes with -30°and -60°headings are not included, as the only difference from 30°and 60°headings is to multiply sway, roll and yaw loads with -1.

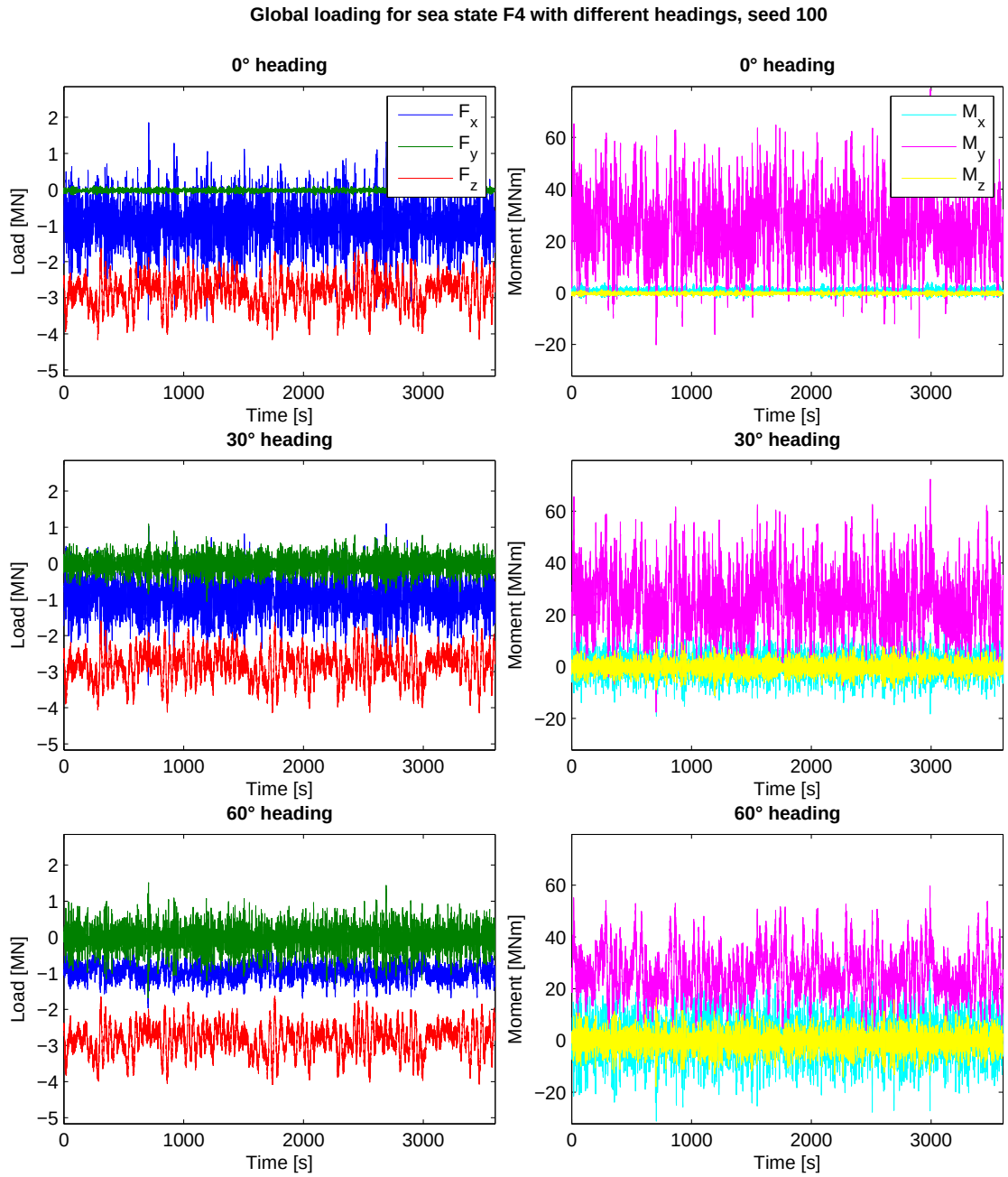


Figure 5.2: Time series of cross sectional loads with $h_s$=4m for different wave headings

At 0°heading the forces acting in the x-z plane are dominating. The forces in sway, roll and yaw is close to zero. This is as expected, due to structural symmetry around the x-z plane. Waves propagating parallel to the symmetry plane can not generate out of plane forces. The structure is not 100% symmetric due to the torque on the rotor. This may be the reason the forces are not completely zero.

The yaw, roll and sway become increasingly important for large heading angles. As it is the variation in loading that causes fatigue damage, the load standard deviation in time domain for a given sea state can be a good indication of how important it is in regard to fatigue. To include the effect of all the sea states one could calculate the weighted average of the standard deviation in each sea state (found in table 5.3). The weighted average should be used, instead of the total standard deviation of the stresses during the lifetime of the structure, as the later will include the effect of long term variability. This is not relevant for fatigue damage. The weighted load standard deviation have been calculated with the following equation:

$$\bar{\sigma}_{_F} = \sum_{i=1}^{n_{sea}} \sum_{j=1}^{n_{seed}} \frac{\sigma_{_{F_{ij}}}}{n_{seed}} p_i \tag{5.4}$$

$n_{sea}$ is the number of sea states analyzed.
$n_{seed}$ is the number analyses in each sea state.
$\sigma_{_{F_{ij}}}$ is the load standard deviation for sea state $i$ with seed $j$.
$p_i$ is the probability of sea state $i$.

Table 5.3: Weighted average of load standard deviation

| | $\bar{\sigma}_{F_x}$ [MN] | $\bar{\sigma}_{F_y}$ [MN] | $\bar{\sigma}_{F_z}$ [MN] | $\bar{\sigma}_{M_x}$ [MNm] | $\bar{\sigma}_{M_y}$ [MNm] | $\bar{\sigma}_{M_z}$ [MNm] |
|---|---|---|---|---|---|---|
| 0° | 0.48 | 0.03 | 0.28 | 0.64 | 8.96 | 0.29 |
| -30°and30° | 0.40 | 0.18 | 0.28 | 3.53 | 8.09 | 1.95 |
| -60°and 60° | 0.18 | 0.28 | 0.27 | 6.08 | 5.75 | 3.07 |

The weighted average of the load standard deviation in 5.3 give the same picture as the Figure of load time histories for the sea state with significant wave height 4m. The conclusions drawn from Figure 5.2 seems to be valid not only for that specific sea state.

It is important to note that the weighted average of the load standard deviation fails to capture the effect of frequency differences between different sea states and heading angles. The difference in frequency have been investigated for each load type in all sea states and for all heading angles. The difference between the frequency of each load component, given the sea state, is significant. The frequency of surge and pitch loads increases with larger heading angles, while the frequency of sway, roll and yaw loads decreases. The load frequency for waves with 60°heading can be twice as big or half as big, depending on the load direction, as the frequency with 0°heading. The heave load frequency increase a bit (under 5%) with 60°heading compared to 0°heading. The load frequencies also change with sea state. Generally the load frequencies decreases with increasing significant wave height. This is natural as the wave frequency also decreases with increasing significant wave height, because the wave period increases too.

# Chapter 6

# Results Submodel 1

The hot spot where all the colored plates in Figure 6.1 intersect was investigated in regard to fatigue. The geometry at this point is rather complex. The node at the intersection is connected to elements from seven different pates. There exist no useful analytical solution as the geometry of the structural detail is too complex. The complexity also makes it hard to use the nominal stress method as it will be difficult to to choose a representative S-N curve for the detail. Therefore, the hot spot method has been used to find the stresses to be used in fatigue calculation. The hot spot stresses have been defined as the interpolated stresses from the read out points at 0.5t and 1.5t from the intersection.

It is difficult to estimate from which side of the weld toe a potential crack will cause failure. Therefore the hot spot stresses at the intersection point has been evaluated for all the plates connected at the intersection. The different plates analyzed are colorized in Figure 6.1. The stress read out points are chosen as nodes 0.5t and 1.5t away from the intersection point, as the maximum stresses generally occur here. For the horizontal plates the read out points are chosen as nodes 0.5t and 1.5t from the intersection along weld line 3 and the stresses are extrapolated to weld line 2. For the plates in the xz-plane the read out points are chosen along weld line 1 and extrapolated to weld line 3. Plate 4 and 5 have read out points along weld line 1 and the stresses are extrapolated to weld line 2.

A crack may initiate at both the upper and lower surface of a plate. The condition for crack growth is not the same on each side due to the bending stress. It is difficult to estimate which side of the plate a crack is most likely to grow, based solely on the hot spot stresses from unit loads, without having a good knowledge about the real loading on the structure. Initially it was thought that the bending stress could be simplified, in a conservative way, by setting the direction of the bending stress equal the direction of the membrane stress, from a unit loading in any direction. This is conservative if one were to estimate fatigue life from loading in that specific direction. When there is loading in multiple directions at the same time this approach will become non-conservative. Therefore, fatigue life have been calculated for both sides of the plates. Unless specifically stated otherwise the figures and comments in this section refer to the side of the plate with lowest estimated fatigue life from a combined heading.

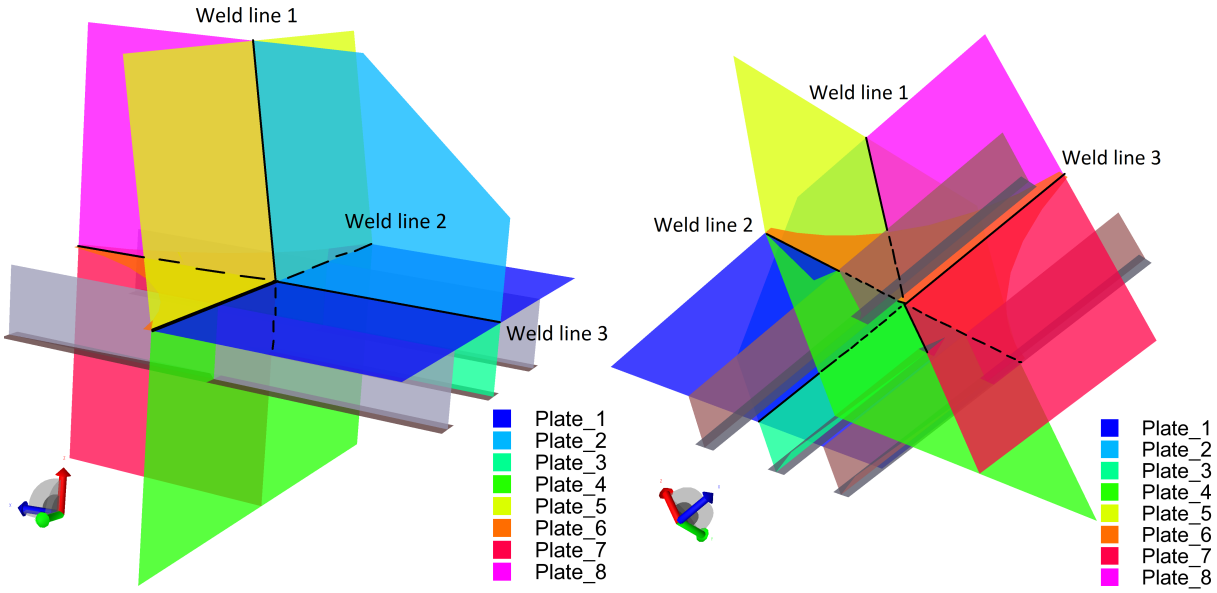


(a) Viewpoint 1 (b) Viewpoint 2

Figure 6.1: Plates investigated at hot spot at pontoon-transition piece connection

## 6.1 Hot spot stresses

Nondimensional hot spot stresses for all the plates are listed in Figure 6.4. The stresses are defined as the ratio between the actual stress and the normalized stress, which is 100 [MPa]. $\sigma_{\perp}$, $\sigma_{\parallel}$ and $\tau_{\parallel}$ are evaluated separately. The effective hot spot stresses has been calculated as the sum of membrane and bending stress. The membrane stress will have a constant stress distribution over the surface, while the bending stress will be in compression at one side of the plate and in tension on the other side. The bending stress has been reduced to 60% by equation 2.16 as the the bending stress gradients along weld line 1,2 and 3 are large.

To check if the results make physical sense simple mechanic principles are used. A (very) simplified physical representation of the structure could be the frame shown in Figure 6.2. How this frame structure will bend at different load cases will give a relatively good indication on how the real structure will behave.

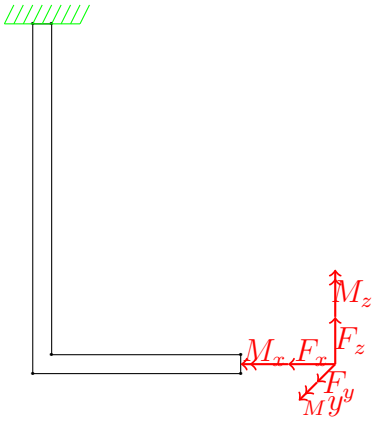


Figure 6.2: Simplified frame structure

Plate 1 will be in compression for load case $F_x$, $M_y$ and $F_z$ and dominated by stress in the global x-direction. The shear force should be more dominant for load case Fy and Mx due to torsion moment. This agrees well with the Plate 1 hot spot stresses in Figure 6.4.

Plate 2 should have large stresses for load case $F_x$, $M_y$ and $F_z$ as the function of the kneeplate is to reduce the bending in the x-z plane. The high stresses in came as a surprise, but it may occur because the torsion moment causes part of the kneeplate connected to the pontoon to rotate with the pontoon, while the transition piece will stop the part of the kneeplate it is connected to from rotating. If that is the case the plate should experience significant plate bending and no membrane stress. The hot spot stresses have been further decomposed to membrane and bending stresses, shown in Figure 6.5. Looking at the bending stresses at Plate 2 in this figure one can clearly see that this is the case. The plate will also encounter significant plate bending in the $M_x$ load case.

Plate 3 is a part of the horizontal stiffener that start where the load is applied and ends at the intersection with the transition piece. It should have a similar stress distribution as Plate 2. Negative stresses for load case $F_x$, $M_y$ and $F_z$ as the upper part of the pontoon will be in compression and only bending stress for load case $F_y$ and $M_x$ as the plate can not take up membrane stresses in this direction. This corresponds well with the displayed hot spot stresses.

Plate 4 and 5 should have lower membrane stresses for load case $F_x$ as plate 4 can not take up membrane stresses in this direction, as it is located in the y-z plane and plate 5 can take up very little. The normal to plate 5 ha a 10° angular offset from the y-z plane. For load case $F_y$ these plates are the only one able to take up the shear force in the pontoon, so the shear stress should be high.

As plate 6 is a continuation of plate 1 they should have a similar stress distribution. One can clearly see that this is the case. The difference in shear stress for load case $F_y$ can be explained by the fact that plate 4 and 5 will take up a lot of the shear force from plate 1.

Plate 7 and 8 should be in compression for loading condition $F_x$, $F_z$ and $M_y$. For loading condition $F_x$ the stress component in the global x direction should dominate and the stress

in the global y direction should be negligible. The stresses are much higher for plate 8 under load case $F_y$. The explanation for this is believed to be that the high stresses from plate 2 in this condition will be transferred to plate 8. Nonetheless, the magnitude of the difference is surprising. The stress distribution for this loading condition have therefore been investigated further in Xtract. The gradient of the bending stress perpendicular to weld line 3 is very large along the interpolation line. This is believed to be the explanation of the large difference. Another noticeable difference between plate 7 and plate 8 is the difference in shear stress for loading condition $F_z$ and $M_y$. This is a result of the same difference between plate 2 and plate 3. The large shear stresses in plate 3 will be transferred to plate 7.

Concluding, the stresses at the different plates connected to the hot spot at the intersection between the pontoon and transition piece matches well with what was expected based on simple mechanics. No indication of gross errors in the finite element model or the MATLAB program calculating the hot spot stresses have been found.

Plots of the stress concentration factor have been created, but not included in this report, as fatigue life is estimated from the effective hot spot stresses, not the stress concentration factor. The author found it hard to obtain any real information about the stress distribution based on SCF as the complexity of the structure makes it hard to define the nominal stress. The SCFs found are in some cases very large because the nominal stress is close to zero. The nondimensional hot spot stresses are deemed sufficient for understanding the stress concentration at different areas of the structure.

The effective hot spot stresses found by interpolation have been compared with an alternative method of finding the hot spot stresses. Here the hot spot stresses are taken to be the stresses at the read out point 0.5t away from the intersection multiplied with 1.12. The results from this method gives relatively similar results as the interpolation method, but is generally more conservative. In most cases the slope of the stress from interpolation is lower than the stress slope from the alternative method. An exception is the bending stress, where the stress gradient can be very high close to the intersection. The hot spot stresses from the interpolation method is usually more conservative for load case $F_y$, where the bending stress is much larger than the membrane stress. The hot spot stresses at plate 1 obtained from the alternative method is included in Figure 6.3.

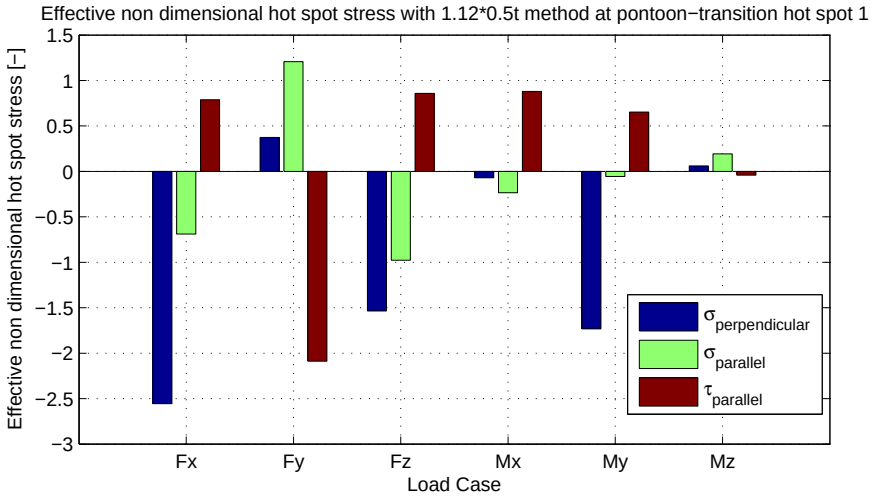


Figure 6.3: Effective hot spot stresses at plate 1 from alternative method

From comparing Figure 6.3 and Plate 1 in Figure 6.4 one can see that the results are very similar. The two different ways of calculating hot spot stresses at the other plates have also been compared. The results are similar enough that the author believes that no gross errors have been done when calculating hot spot stresses from interpolation. Figures of hot spot stresses from the alternative method at the other plates are not included in this report.

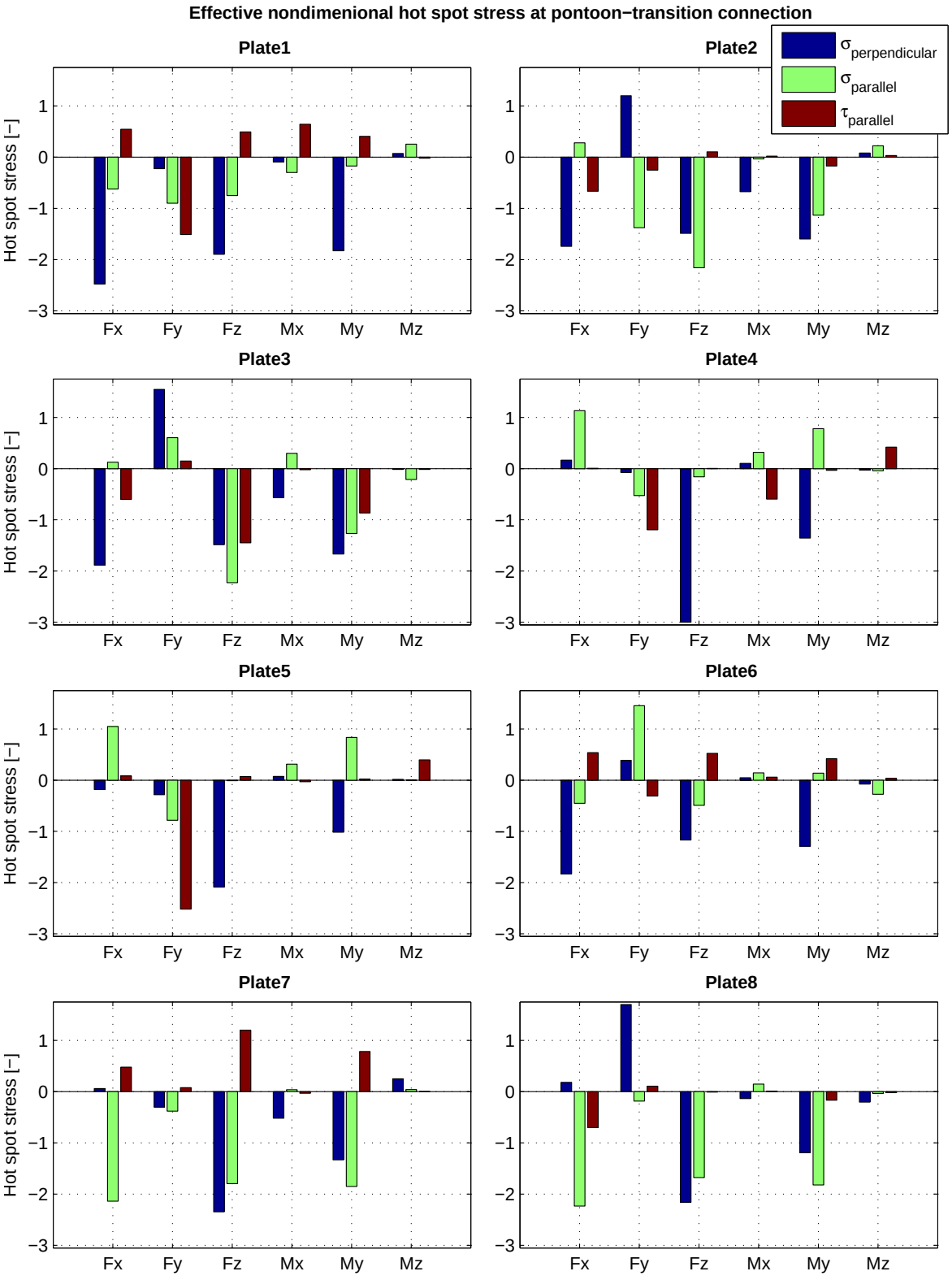


Figure 6.4: Effective nondimenional hot spot stress at pontoon-transition connection

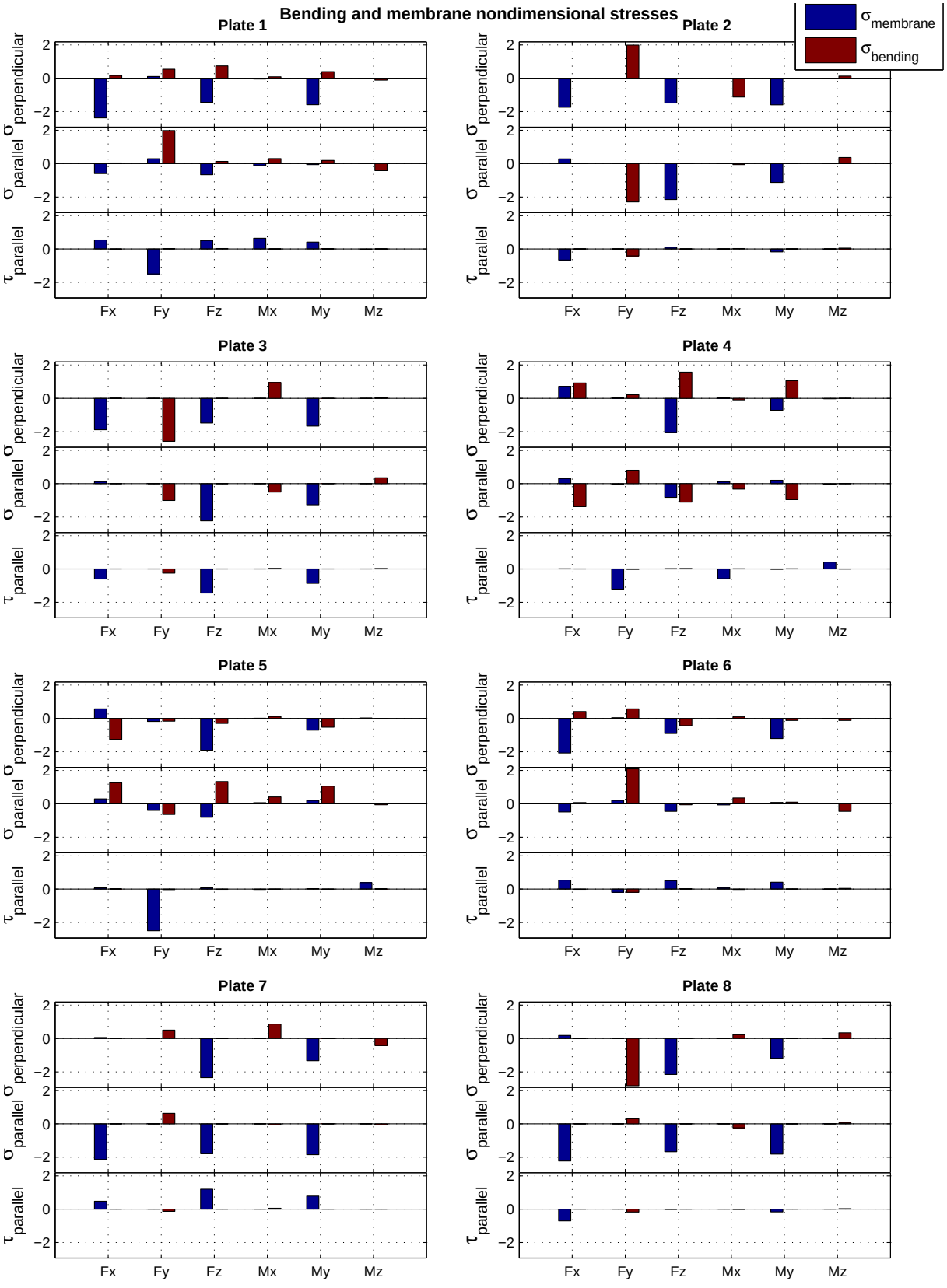


Figure 6.5: Nondimenional bending and membrane hot spot stresses at pontoon-transition connection

## 6.2 Real stresses from time domain simulation

The hot spot stresses from the real loading, determined by time domain simulations, can be expressed with the equation:

$$\sigma_{hs,i}(t) = \frac{F_{r,i}(t)}{F_{0,i}}\sigma_{0,hs,i} \tag{6.1}$$

$F_{r,i}(t)$ is the total load in the i-direction on the cross section as a function of time from time domain simulations.
$\sigma_{hs,i}$ is the real hot spot stress from the loading $F_{r,i}$
$\sigma_{0,hs,i}$ is the nondimensional hot spot stress found in the previous section.
$F_{0,i}$ is the force applied in the i direction at the cross section in the FE-model. It is necessary to divide by $F_{0,i}$ because a "unit stress" rather than a unit load was applied to the model in each loading condition.

As the structure is assumed to behave linearly the hot spot stress from each loading condition can be superpositioned. The total hot spot stress at the time $t$ can therefore be expressed as:

$$\sigma_{hs}(t) = \sum_{i}^{6} \sigma_{hs,i}(t) \tag{6.2}$$

It is hard to estimate from which side of the welds at the intersection point a crack will cause failure first, based on the nondimensional hot spot stresses in Section 6.1. A high nondimenional hot spot stress in one loading condition will not necessarily result in a high real hot spot stress as the loading in that direction may be small. That being said, the perpendicular stress is usually the biggest contributor to crack growth and waves with a heading around 0° will be dominating. $F_x$, $F_z$ and $M_y$ will be the dominant forces in this heading. As the waves will propagate in the xz-plane and the structure is symmetric around this plane, the wave forces in sway, heave and yaw should be zero. From this knowledge one can predict that the plates with large nondimensional hot spot stresses perpendicular to the weld in surge, heave and pitch should have lower fatigue life. However, this is just a calculated guess surrounded by uncertainties. Therefore, all of the hot spot stresses extrapolated from the different plates connected to the hot spot have been analyzed further. Plate 1 is used for illustration purposes.

Hot spot stress as function of time for different headings can be found in Figure 6.6. As the sea state with significant wave height equal 4 meters contributes the most to fatigue damage, the author has chosen to illustrate the hot spot stress in this sea state. To the left in the figure is the resulting hot spot stress from each loading component and to the right is the added total hot spot stress. The hot spot stress is decomposed to stress normal to the weld, stress parallel to the weld, and shear stress parallel to the weld.

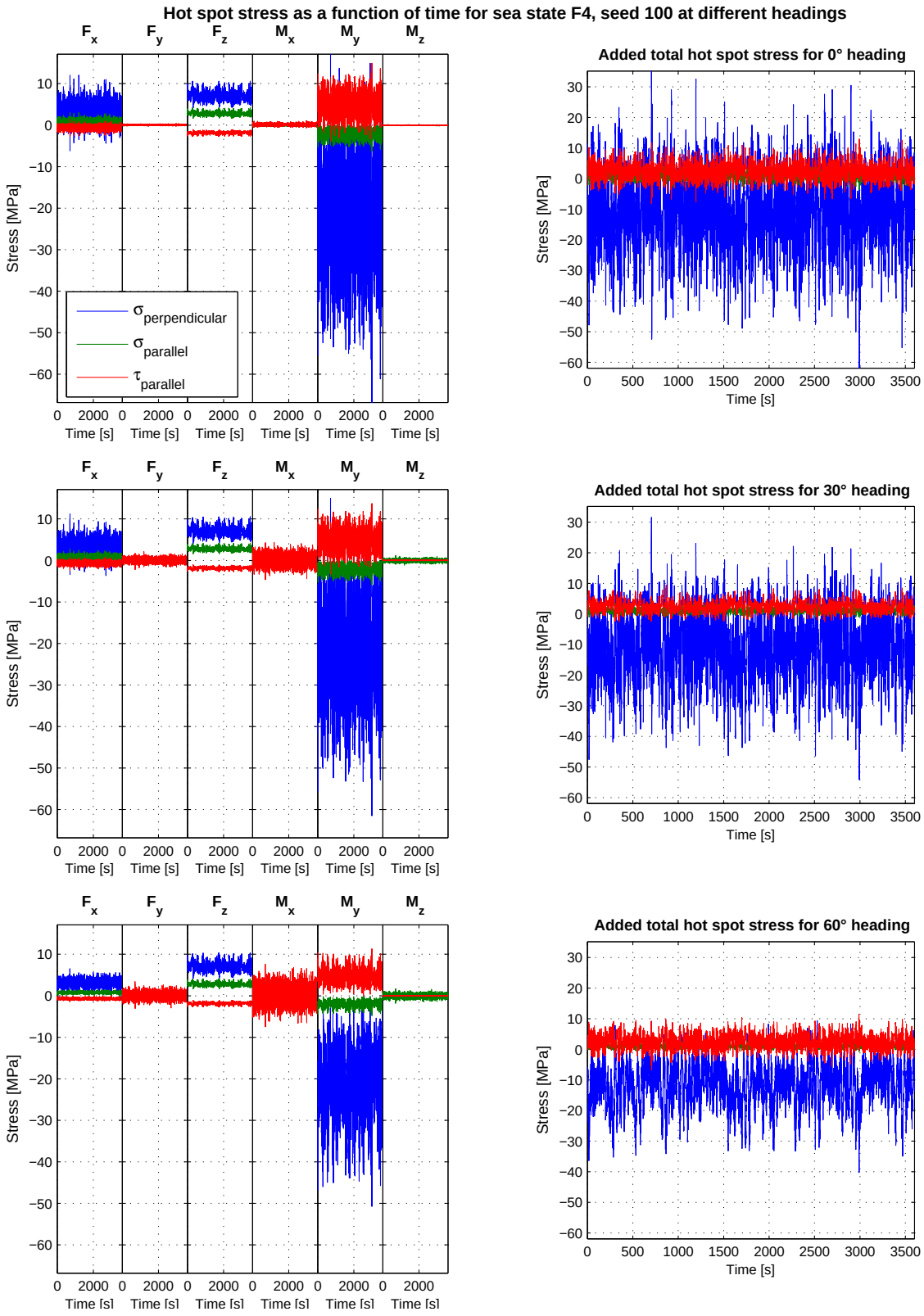


Figure 6.6: Hot spot stresses in plate 1 by each loading component and added total hot spot stresses for different headings (0° on top, 30° in the middle, 60° at the bottom)

It is clear from Figure 6.6 that pitch loading causes highest hot spot stresses by a large margin for all wave directions. $\sigma_{\perp}$ is the dominant stress component. The normal stress

component due to wave loading in surge and have cancel out some of the normal stress due to wave loading in pitch. A 0° heading angle causes largest hot spot stress. Waves with 60° heading are least critical. There seems to be some difference frequency forces on the structure. These forces become more dominant with larger heading angles. For sea state with significant wave height less than 4 meters the difference frequency forces are easier to spot. The conclusions drawn from Figure 6.6 are valid for the other sea states as well.

It is easy to think that the total hot spot stress should be the same for -30° and 30° and -60° and 60 ° heading due to symmetry, but this is not completely true. For Plate 1 the stresses from elements on the positive y-axis side of the kneeplate in the middle have been used in the calculation. The shear stress and stress in the global y-direction will be opposite, not zero, on each side of the kneeplate. Added total hot spot stress for -30° and -60° heading are given in Figure 6.7.

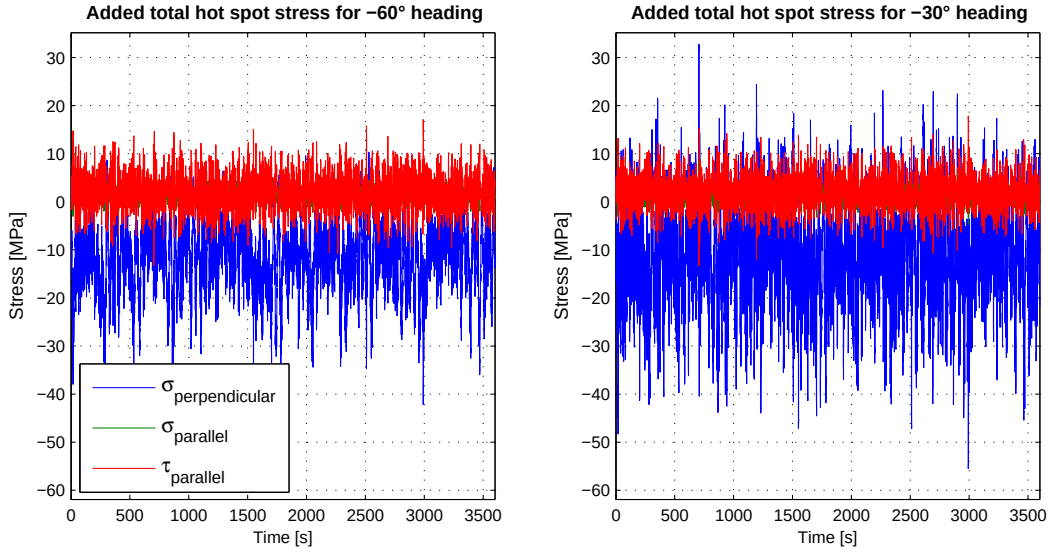


Figure 6.7: Hot spot stresses in plate 1 for negative headings with significant wave height equal 4 m

The normal stress component with negative headings is more or less identical with positive headings, but comparing Figure 6.7 and 6.6 one can clearly sea that the shear stress have a significant larger deviation with negative headings. It is not easy to sea from the figure but the same tendency is true for the parallel stress component.

## 6.3 Stress simplifications

From Figure 6.6 and 6.7 it is evident that the normal stress component will be most important. The easiest way to calculate fatigue damage would be to neglect shear and parallel stress in fatigue calculation, but this may underpredict fatigue damage. In reality the stress state at the hot spot is multiaxial. As $\tau_{\parallel}(t)$ and$\sigma_{\parallel}(t)$ is not completely proportional to $\sigma_{\perp}(t)$ there exist, as far as the author knows, no well accepted easy method of

including the effect of these stress components when calculating fatigue.

The author of this article has tried to include the effect of the $\tau_{\parallel}(t)$ and $\sigma_{\parallel}(t)$ with the proposed method described in Section 2.9. It is important to note that this method is only expected to give accurate results when there is a clear linear tendency between the perpendicular stress and the other two stress components. When this is not the case the method will underestimate fatigue damage, but will still be more conservative than neglecting the secondary stress components completely.

The shear and parallel stress are simplified so that they can be described as linear functions of the normal stress. The objective is to construct simplified stresses with turning points at exactly the same place as the normal stress, so that the effective hot spot stress can be calculated by equation 2.13.

In Figure 6.8 plots over the real and constructed shear stress for sea state F4, seed 100, at different wave headings are given. $\sigma_{\perp} - \sqrt{\beta}\tau_{\parallel}$ plane ($\beta$=3) with plotted real stress time history together with the calculated simplified linear relationship between the stress components to the left. Real and constructed shear stress as a function of time is plotted for a short time interval to the right.

At 0° wave heading the shear stress is almost completely in opposite phase with the shear stress. The constructed shear stress is almost identical to the real shear stress. Therefore, using the constructed shear stress instead of the real shear stress in fatigue calculation, should give very realistic results.

For -30° wave heading there will be some errors, but the constructed shear stress is overall a good fit. The shear stress still has a clear in opposite phase tendency with the normal stress. For 30° and -60° wave heading the constructed shear stress will be an increasingly bad representation of the real stress, as the in-opposite-phase tendency become less clear. At 60° heading the shear stress is completely out of phase (and not in opposite phase) with the normal stress. The linear simplification completely fails to resemble the real stress. Using the simplified stress for fatigue calculations in this case would be meaningless.

To obtain a measurement of how good the approximation is the following parameter is introduced:

$$\lambda = \frac{std(\tau_{\parallel,constructed}(t))}{std(\tau_{\parallel,real}(t))} \tag{6.3}$$

$std(\tau_{\parallel,constructed}(t))$ is the standard deviation of the constructed shear stress time series. $std(\tau_{\parallel,real}(t))$ is the standard deviation of the real shear stress time series.

The linear simplification is likely to have a lower standard deviation because the scatter in the $\sigma_{\perp} - \sqrt{\beta}\tau_{\parallel}$ plane is reduced. How much the standard deviation is reduced depends on how large the original scatter was. $\lambda$ close to 1 means that the linear simplification should lead to accurate results. A $\lambda$ much lower than one signify that the linear simplification is a bad representation of reality. Although $\lambda$ is a measurement of correlation it should not

be confused with Pearson product-moment correlation coefficient. $\lambda$ is used throughout this report because it is easier to relate this value to actual differences between the real and constructed stress component. The ratio between the standard deviation of the real and constructed shear stress for the different headings in Figure 6.8 are given in Table 6.1.

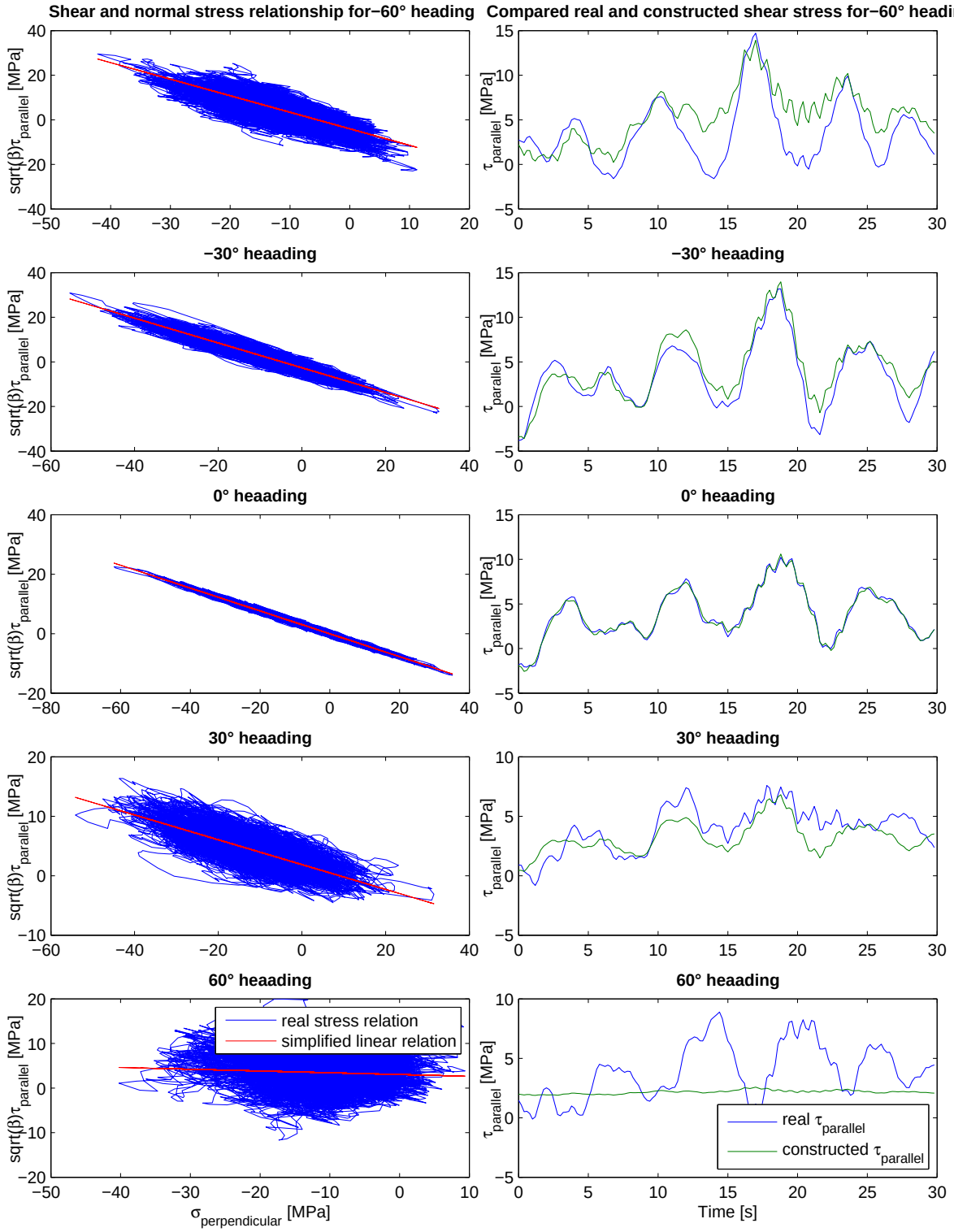


Figure 6.8: Real and constructed shear stress for sea state F4, seed 100 at different wave headings

Table 6.1: Ratio between standard deviation of constructed and real shear stress given in Figure 6.8

| Heading | -60° | -30° | 0° | 30° | 60° |
|---|---|---|---|---|---|
| $\lambda$ [-] | 0.830 | 0.950 | 0.996 | 0.748 | 0.069 |

The $\lambda$ values in Table 6.1 correspond well with the conclusions drawn from Figure 6.8. For 0° heading $\lambda$ is approximately 1 and decreases when the difference between the real and constructed shear gets bigger. Based on the figure the difference between the real and constructed shear stress seems to be acceptable for -30° heading with $\lambda = 0.956$, but unacceptable for -60° heading with $\lambda = 0.854$. On this basis $\lambda = 0.95$ is defined as the lower limit where linear simplification can be used. Using the method when $\lambda < 0.95$ will give a too low estimation of fatigue damage.

One could argue that the lower limit should be defined a bit lower or higher. The value is chosen solely on the authors visual perception of what seems to be a good fit in the figure above. It is worth noticing that reducing the equivalent stress range to 95% of its original value will increase fatigue life with a factor of $\frac{1}{0.95^m}$ For a stress higher than the kneepoint $m = 3$. Then the a equivalent stress range reduction will cause fatigue life estimation to be 17% higher. With other words are fatigue life estimation very sensitive to changes in the stress range. However, reducing the standard deviation of the shear or parallel stress with a factor of 0.95 is not equivalent with increasing fatigue life with $\frac{1}{0.95^m}$. The shear and parallel stress are of secondary importance (at least in the load cases discussed in this section) and the increase in estimated fatigue life should be much lower. Performing a rainflow counting on the constructed and real shear stress will likely result in some differences in the "high frequency" low amplitude stress ranges, but the stress ranges with large amplitude will stay similar.

The parallel stress have been simplified the same way as the shear stress. Figure 6.9 show real and constructed parallel stress for sea state F4, seed 100, at different wave headings. The correlation for each wave heading is given in Table 6.2.

Overall the linear correlation between the parallel and the perpendicular stress is a bit higher than between the shear and perpendicular stress. Only 0° heading have an acceptable $\lambda > 0.95$, but -30 and 30° heading are very close to the limit. The parallel stress have an in phase tendency with the perpendicular stress for all wave headings, not an in opposite phase tendency as the shear stress have.

Table 6.2: Ratio between standard deviation of constructed and real parallel stress given in Figure 6.9

| Heading | -60° | -30° | 0° | 30° | 60° |
|---|---|---|---|---|---|
| $\lambda$ [-] | 0.756 | 0.935 | 0.967 | 0.941 | 0.182 |

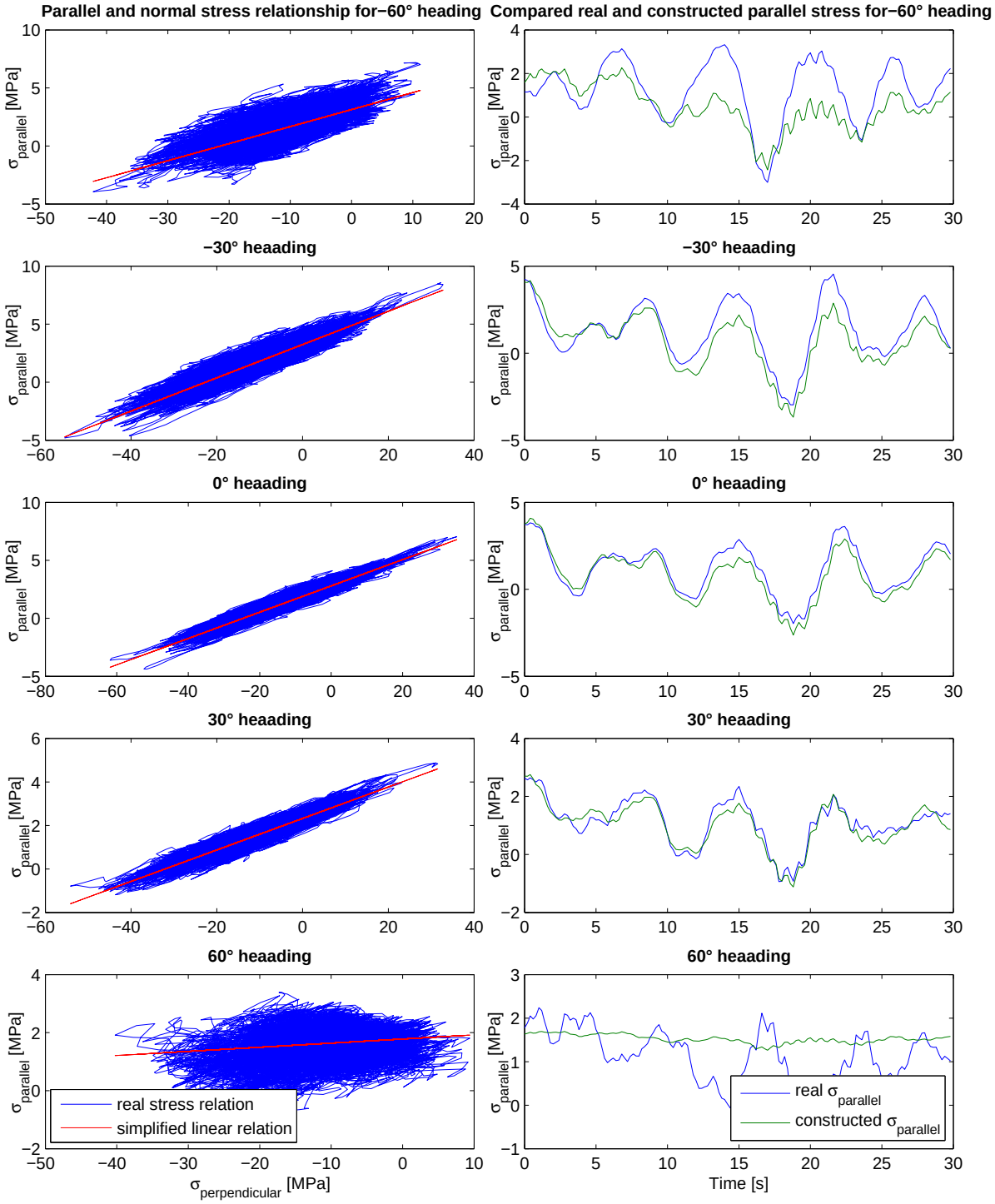


Figure 6.9: Real and constructed parallel stress for sea state F4, seed 100 at different wave headings

## 6.4 Weighted average of stress parameters

Until now only the stresses from five short term simulations, corresponding to five different wave headings, for one of the plates connected to the hot spot have been discussed. In

reality 10 simulations, for each of the 13 sea states, for 8 different plates connected to the hot spot have been analyzed. When taking in to account that 5 different headings have been examined, the total number of simulations analyzed is 5200 (for this specific area). Discussing all the simulations individually would be meaningless. To include the effects of all the sea states on different parameters important to fatigue the weighted average is used. The weighted average is defined the same way as the weighted load standard deviation in equation 5.4.

The standard deviation of the different hot spot components in time domain give a good indication of how important it is in regard to fatigue. The standard deviation is calculated for all simulations and weighted acording to the formula for the weighted average. The same is done for the parameter $\lambda$, showing the goodness of the linear simplification for given stress component.

The equations for the weighted average of the two different parameters are:

$$\bar{\lambda} = \sum_{i=1}^{n_{sea}} \sum_{j=1}^{n_{seed}} \frac{\lambda_{ij}}{n_{seed}} p_i \tag{6.4}$$

$$\bar{\sigma}_{std} = \sum_{i=1}^{n_{sea}} \sum_{j=1}^{n_{seed}} \frac{\sigma_{std,ij}}{n_{seed}} p_i \tag{6.5}$$

$n_{sea}$ is the number of sea states analyzed.
$n_{seed}$ is the number of analyses in each sea state.
$p_i$ is the probability of sea state $i$.
$\bar{\lambda}$ is the weighted average of the correlation parameter $\lambda$.
$\bar{\sigma}_{std}$ is the weighted average of the stress standard deviation. $\sigma$ can be the actual parallel stress, perpendicular stress or parallel shear stress.

The weighted average of the standard deviation of the different stress components for all plates and all wave headings are given in Figure 6.11. It seems like the highest stress variation perpendicular to the weld occurs at 0° wave heading for all plates. Plate 1 have the highest perpendicular stress variation. Here the perpendicular stress is very dominating. The combined stress standard deviation of plate 1 corresponds well with the results from the specific simulation discussed in Section 6.2.

To get a better picture of the stress variation with a combination of headings the weighted average of each heading is also calculated (see Figure 6.10). The weighted average of the stress standard deviation with combined heading is calculated with the formula:

$$\bar{\sigma}_{std,combined} = \sum_{k=1}^{n_{headings}} \sum_{i=1}^{n_{sea}} \sum_{j=1}^{n_{seed}} \frac{\sigma_{std,kij}}{n_{seed}} p_i p_k = \sum_{k=1}^{n_{headings}} \bar{\sigma}_{std} p_k \tag{6.6}$$

$n_{headings}$ is the number of different headings analyzed.
$p_k$ is the probability of heading $k$.

While the horizontal plates (Plate 1 and 6) are very dominated by stress variation perpendicular to the weld, the stress picture is more complicated at the other plates. The

plates in the x-z plane below the horizontal plate (plate 3 and 7) experience large shear stresses at all wave headings. Plate 5, 6 and 7 actually have the largest stresses parallel to the weld. For both plate 7 and 8 it was chosen to extrapolate stresses to weld line 3. If the stresses had been extrapolated to weld line 1 the perpendicular stress would have been the highest. Cracking from weld line 1 may be more critical. However, this has not been investigated in this report.

While neglecting the shear and parallel stress would probably not prolong estimated fatigue life very much for plate 1 and 6, doing the same for plate 7 and 8 could be fundamentally wrong. Here it is very important to include the parallel stress in fatigue calculations. This is also true for plate 5, but the low overall stress standard deviation suggests that this is not the plate that will fail first, and therefore not the most important important. The large shear stresses in plate 3 may also significantly reduce fatigue life, as the shear will cause a crack growing due to normal stress in tension to grow faster.

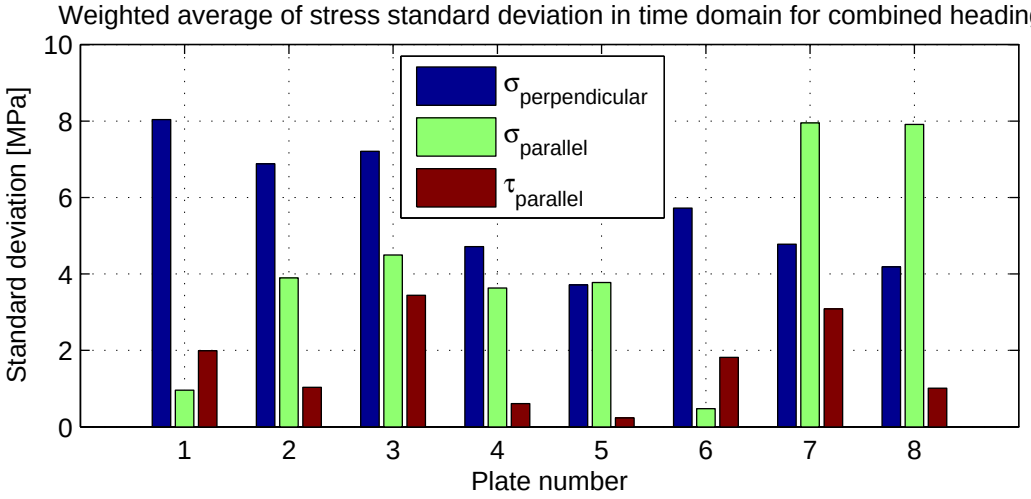


Figure 6.10: Weighted average of stress standard deviation in time domain for combined heading

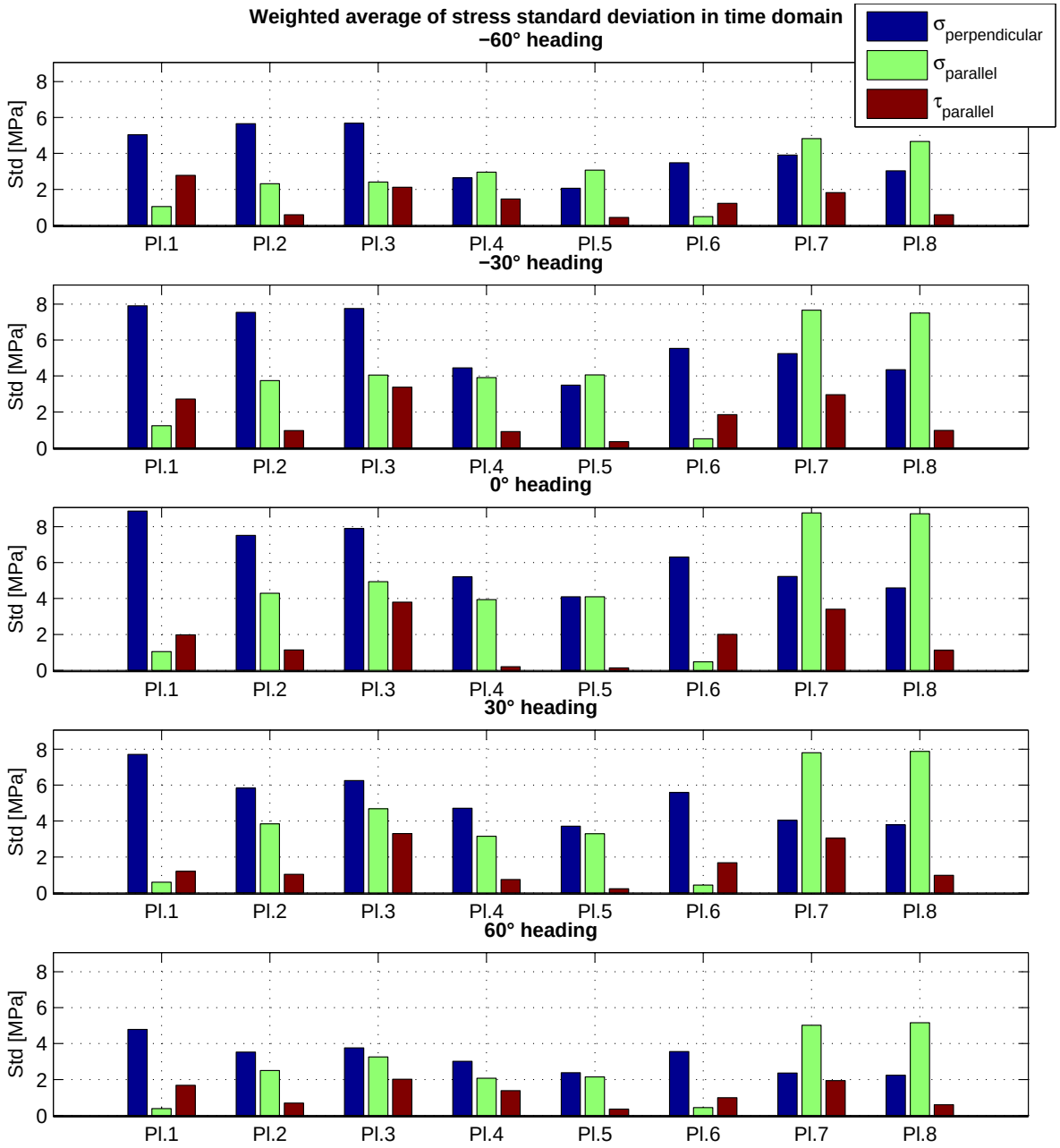


Figure 6.11: Weighted average of stress standard deviation in time domain for each heading individually

The weighted average of $\lambda$ for both shear and parallel stress at different plates and headings is given in Figure 6.12. From this figure one can see if the linear simplification method is expected to give accurate results. $\bar{\lambda} = 0.95$ is marked at the y-axis. If the correlation is lower than this, the method will result in too inaccurate stress time series. It is most important that $l\bar{\lambda} > 0.95$ at $0^\circ$ heading. Figure 6.11 show that generally the highest shear and parallel stress variations will occur at this heading, although that is not the case for plate 1 and 5. $0^\circ$ heading also have the highest probability of occurrence (42%).

The plates aligned in the x-z plane (plate 2, 3,7 and 8) have a very strong linear correlation

between both normal stress and shear stress, and normal stress and parallel stress. $\bar{\lambda} > 0.95$ for nearly all wave headings. There are some exceptions at -60° and 60° heading when $\bar{\lambda}_{shear\ stress}$ or $\bar{\lambda}_{parallel\ stress}$ is a bit under 0.95. At these headings the stress variation for all stress components are significantly lower than for other headings. The probability of -60° and 60° headings is just 4%. Therefore, the reduced correlation at these headings should not reduce the quality of the results from the linear simplification method much. The linear simplification method is expected to give very accurate results for this plate.

It is not entirely clear why the correlation between the normal stress and the other stress components are best for the plates aligned in the x-z plane. One explanation could be that theses plates can't take up much of the stress from forces in sway, roll and yaw. Stresses from forces in this direction are not in phase or in opposite phase with the largest stresses that come from loading in pitch.

For plate 1 it is acceptable to use the linear simplification at 0° heading and for the shear stress at -30° heading. Using the method in other situations would lead to too low stress variation, although $\bar{\lambda}_{shear\ stress}$ at -30 and 30° heading are very close to the defined limit. It seems like the shear and parallel stress become more critical for headings different than zero. This further suggests that using the method would result in too low fatigue damage estimation. That being said, at this plate the normal stress is much higher than the other two stress components. Whether the shear and parallel stress are included correctly or not are of minor importance since the normal stress will be the cause of most of the fatigue damage. It should still be noted that fatigue life estimation may be a bit lower than it should be.

At plate 4 and 5 the $\bar{\lambda}_{shear\ stress}$ values reveal that the linear simplification method should not be used on the shear stress component at any of the headings. The reason for the low linear correlation between normal stress and shear stress at these plates may be that wave loading in pitch, surge and heave will not result in shear stresses at these plates. The total shear stress only consist of shear stresses from sway, roll and yaw loads. These stresses will not be in phase or in opposite phase with the largest normal stresses from pitch loading. At these plates the shear stress variations will be significantly lower than for the other plates. Hence, including them correctly will not be as important here.

At plate 4 and 5 the parallel stress can be simplified with good accuracy for all headings except -60°. The parallel stress will be an important stress component in these plates. Not being able to include this stress correctly at -60° heading will probably cause the estimation of fatigue damage to be a bit low. Be that as it may, the overall stress variations at these plates are much lower than the other plates. Whether or not the parallel stress is included correctly will not alter the fact that these plates should have much longer fatigue life than the most critical plate. The probability of a -60° heading is also only 4%, so the difference between real and estimated fatigue damage should not be that great.

Plate 6 have $\bar{\lambda}_{shear\ stress} > 0.98$ for all wave headings. The reason for the good correlation between the shear and normal stress is probably because plate 4 and 5 will take up much of the shear stress in Plate 1, from loading in sway, roll and yaw, before it can reach Plate 6. $\bar{\lambda}_{parallel\ stress} < 0.95$ for all wave headings. Using the linear simplification method

on the parallel stress will not give acceptable results, but at this plate the parallel stress variation is so low compared to the normal stress that it should not matter.

The author has chosen to use the linear simplification method for all simulations, even when it is not expected to give accurate results. The reason for this is that the method is easy to implement, and that it always will be more conservative than neglecting the shear and parallel stress completely would be. Neither will it be too conservative. Fatigue life has also been estimated when only including the normal stress for comparison reasons.

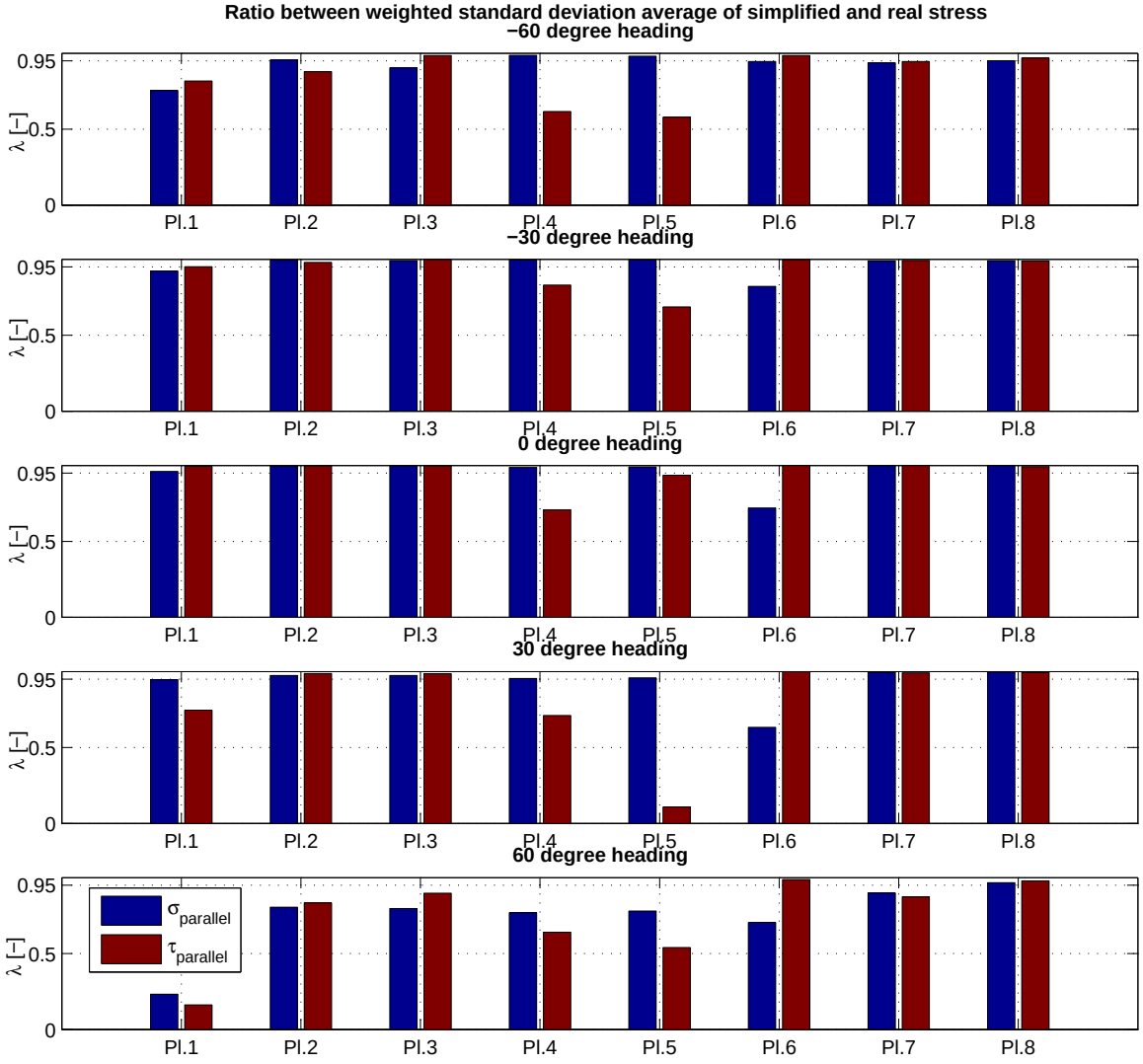


Figure 6.12: Weighted average of the ratio between the standard deviation of simplified and real stress for each plate connected to the hot spot at all wave headings

## 6.5 Fatigue damage

### 6.5.1 Stress ranges

The stress ranges have been calculated by performing rainflow counting on each perpendicular stress time series. Because the simplified shear and parallel stress have a perfectly linear relationship with the perpendicular stress the corresponding stress ranges of these stress components can be calculated with equation 2.17 and 2.22. This has been doubled checked by performing individual rainflow counting on the simplified stress components as well. The results are identical.

The stress ranges from each stress component have been compared by using equation 2.13 to find the effective stress ranges. Note that each stress range from the normal stress and the two corresponding simplified stress components will occur at exactly the same time. That is why they can be compared using equation 2.13. It should be noted that this equation does not distinguish between the normal stress in tension and compression. In reality the shear stress will only increase crack growth rate caused by stress normal to the weld when the normal stress is in tension. The plates at the hot spot area will mostly be in compression. Therefore, including the shear stress component in the equation may lead to somewhat lower fatigue life estimation than one can expect in reality. Regardless, the simplified shear stress component is always included in the equation.

The parameter $\alpha = 0.72$ is assumed for all plates. For this to be correct the detail must be classified as C from Table A-3 in DNV-RP-C203 [12]. C classification requires that automatic welds have been carried out from both sides. No start-stop position is permitted except when the repair is performed by a specialist and inspection have been carried out to verify the quality of the work. For a lower detail category the stress parallel to the weld will be increasingly important.

### 6.5.2 S-N curve to be used

The hot spot area is located under the sea surface. Therefore "Table 2-2 S-N curves in seawater with cathodic protection", from DNV-RP-C203 is used [12]. It is assumed that corrosion will not be a problem. The D-curve has been used to calculate fatigue damage because the hot spot method was used to derive the stress ranges. In some cases it is non-conservative to use the hot spot method with the D-curve for some simple connections, but as soon as there is a bracket behind the transverse plate the hot spot concept linked to the D-curve will give acceptable results [12]. That is the case in this area.

Table 6.3: S-N curve

| S-N curve | $N \leq 10^6$ cycles | | $N \geq 10^6$ cycles | | Fatigue limit at $10^7$ cycles | Thickness exponent k |
|---|---|---|---|---|---|---|
| | $m_1$ | $\log \bar{a}_1$ | $m_2$ | $\log \bar{a}_2$ | | |
| | 3 | 11.764 | 5 | 15.606 | 52.63 | 0.2 |

### 6.5.3 Damage

The damage was calculated as described in Section 2.4. Fatigue life was calculated assuming a constant heading over the lifetime. This was done for all available heading angles. The results were also combined to calculate fatigue life based on combined heading. The damage in each sea state was weighted with the formula:

$$d_{avr,combined} = \sum_{i=1}^{n} d_{avr,i} \cdot p_i \tag{6.7}$$

$d_{avr,combined}$ is the average damage for a combined heading
$d_{avr,i}$ is the average damage for wave heading i
$p_i$ is the probability of wave heading i

Time to failure for a combined wave heading can then be calculated as:

$$t_{f,combined} = \frac{1}{d_{avr,combined}} \tag{6.8}$$

In Figure 6.14-6.21 the Miner damage has been divided between sea states and wave headings for all plates connected to the hot spot. The sea state with significant wave height 4 meters contribute the most to fatigue damage at all the different plates and wave headings. Around 1/4 of the total damage comes from loads in this sea state. The reason for this have been investigated. The normal stress due to surge and heave loading have the same canceling effects on the normal stress due to pitch loading as the other load conditions. It seems like the only reason for the peak here is that this loading condition have the "best" combination between sea state probability and hot spot stress magnitude. Sea state F5 have a 25% increase in significant wave height and 20% increase in wind speed compared to sea state F4, but is nearly twice as unlikely.

The wave heading contributing the most to fatigue damage is 0° heading. The probability of that wave heading is 42% while the damage in this heading is, with one exception, between 60 and 70%. This is not surprising considering that the highest weighted standard deviation of the stresses generally occurred at this heading. Similarly the low damage at -60 and 60° heading is not surprising. The probability of those headings are only 4%, but the amount of damage is even lower.

The difference in damage between the -30 and 30° heading for the plates in the x-z plane is surprising. For plate 2 the difference is very large. -30° waves cause around 5 times more damage than 30° waves. The difference at the plates not in the x-z plane can be explained because consequently the element on the side of the symmetry line with positive y-coordinates have been used. As a result the hot spot stresses with positive and negative wave headings are not equal. For the plates in the x-z plane however, the elements used to extract the hot spot stresses lies exactly at the symmetry plane. Therefore, the difference in damage was not expected and the reason have been investigated.

While the element used are located at the symmetry plane, the stress read out points are located on the plate surface. The plate surface is not on the symmetry line and have

bending stress components with opposite values on each side of the plate. Plate 2 is used as an example here. At -30° heading the hot spot stress normal to the weld caused by roll loading on the cross section is in the same phase as the dominating hot spot stress from pitch loading. In other words will the total hot spot stress increase because of the roll loading. At 30° heading they are in opposite phase with each other. This means that the hot spot stress normal to the well, caused by cross sectional loading in roll, will cancel some of the dominating hot spot stress due to pitch loading. This is illustrated in Figure 6.13.

While the normal stress due to $M_x$ is much lower than the stress from $M_y$ the resulting total hot spot stress will differ significantly depending on whether the stress components are in same phase or in opposite phase. Notice the large differences between the resulting normal stress from -30° and 30° heading at around $t = 30$ seconds. At -30° the stress goes from around -5 MPa to -20 MPa. At 30° the stress goes from around -12 MPa to -17 MPa. The stress range from the negative heading is 3 times larger. Knowing how sensitive the fatigue life is to change in the stress range one can conclude that it is not unreasonable that -30° wave heading results in 5 times more damage at plate 2 compared to 30° wave heading. For plate 7 and 8 the opposite wave headings have much more similar percentage of the total damage, despite that hot spot stresses caused by sway, roll and heave loading will be in phase with the dominant hot spot stress for one heading and in opposite phase for the opposite heading. The reason for this is that the hot spot stress amplitude from roll loading will be significantly lower at these plates.
Based on the logic above one can predict the following for plates in the x-z plane: If the stresses were extracted from the surface on the other side of the plate, fatigue life due to combined heading should be the same, but the damage divided into wave headings should be opposite. The percentage of the total damage occurring from -30° wave heading when inspecting one side of the plate should be equal the damage from 30° heading when inspecting the other side of the plate. This has been investigated and found true.

Table 6.4: Time to failure for the plates in the x-z plane from hot spot stresses at each side of the plate

| | Plate 2 | Plate 3 | Plate 7 | Plate 8 |
|---|---|---|---|---|
| Time to failure upper surface [years] | 21.98 | 12.53 | 20.71 | 54.92 |
| Time to failure lower surface [years] | 22.09 | 12.46 | 20.59 | 54.54 |
| Ratio [-] | 0.995 | 1.005 | 1.006 | 1.007 |

As can be seen from the table above, estimated fatigue life is not completely identical at each side of the plate, but the largest difference is less than 0.7% Efforts have been done to find out why fatigue life is not 100% equal. It appears that even if the plates are aligned in the x-z plane there will be some membrane stresses in the plates due to cross sectional loading in sway,roll or yaw. The magnitude of hot spot bending stresses due to a unit loading in any of these directions is around 1000 times larger than the membrane stresses. So the effect is very limited and it does not affect the quality of the results

in this report. The membrane stresses are unphysical. The reason they are there may be because the meshing of the structure is not absolutely symmetric around the x-z plane.

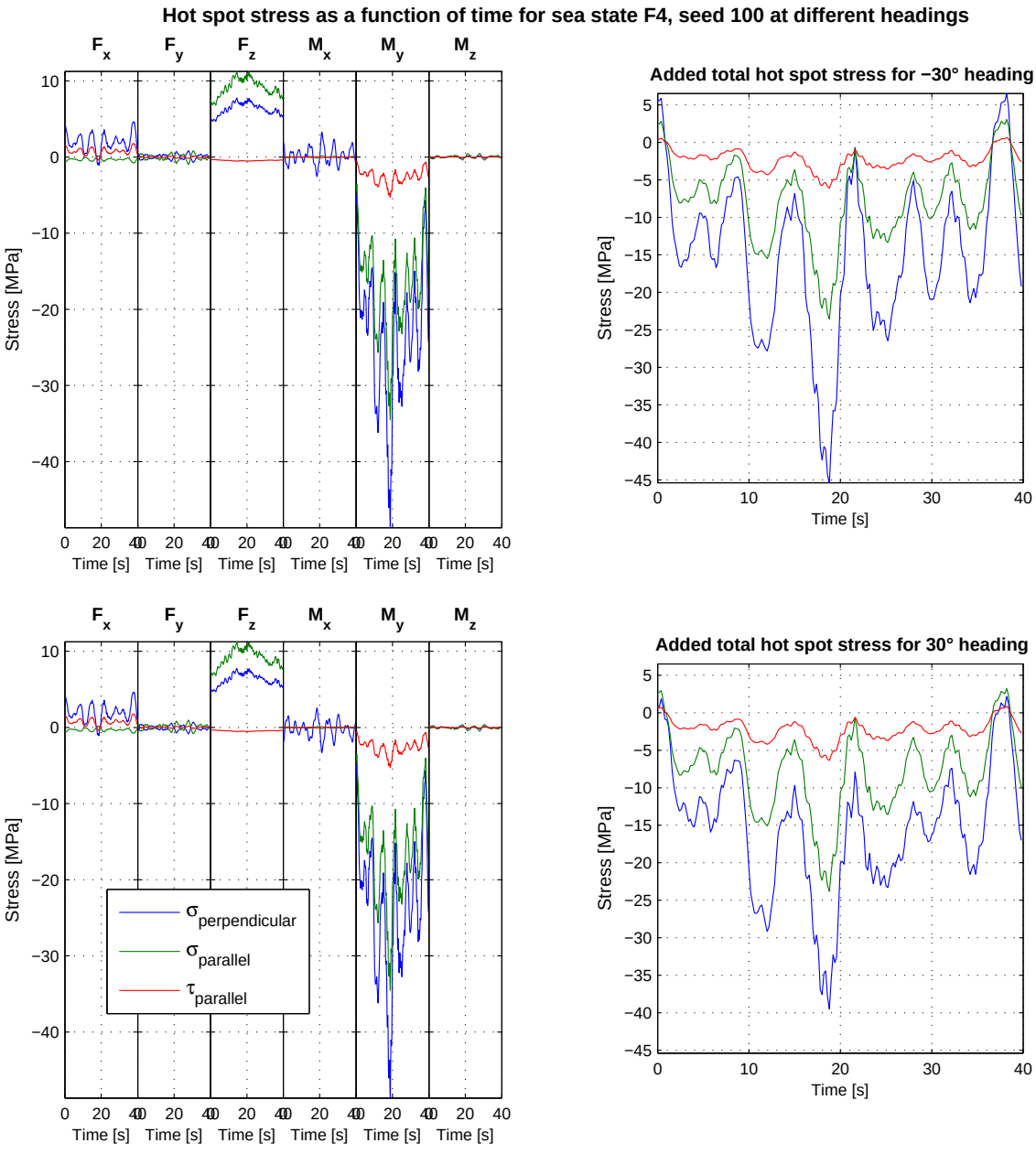


Figure 6.13: Compared hot spot stresses at plate 2 from -30°and 30°wave heading

Overall the damage distribution is very similar for the plates in Figure 6.14-6.21. The reason for this may be that the hot spots investigated for these plates lie in the same area. It will be interesting to sea how the damage distribution changes for hot spots at other locations.

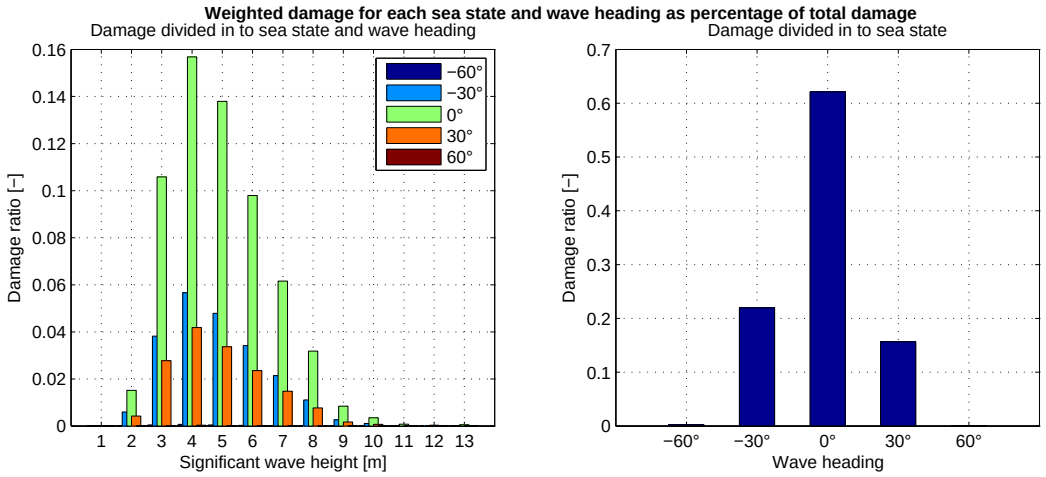


Figure 6.14: Damage distribution between sea states and wave headings for plate 1

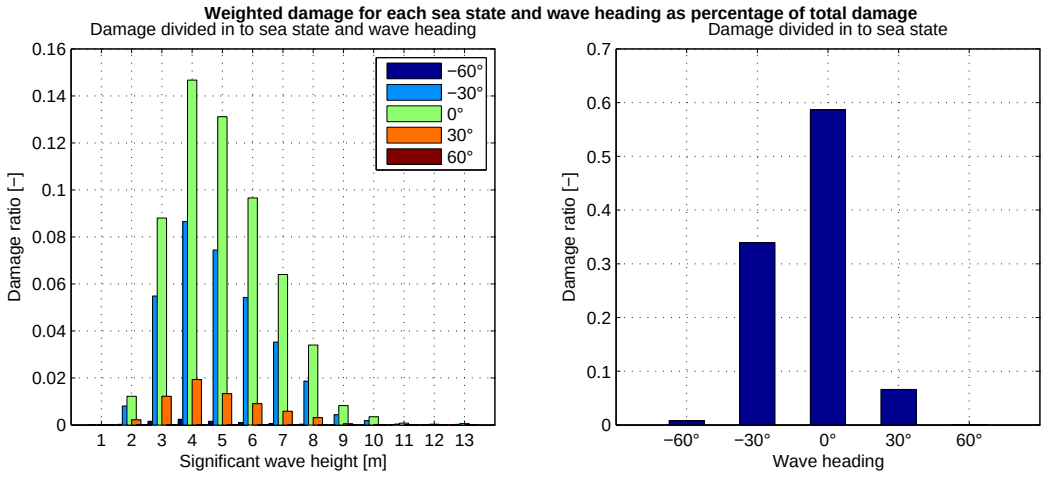


Figure 6.15: Damage distribution between sea states and wave headings for plate 2

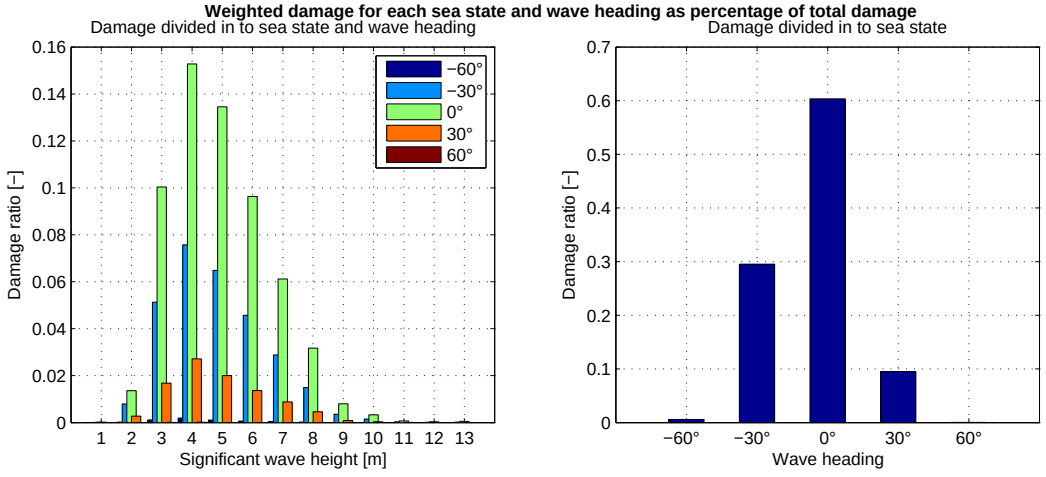


Figure 6.16: Damage distribution between sea states and wave headings for plate 3

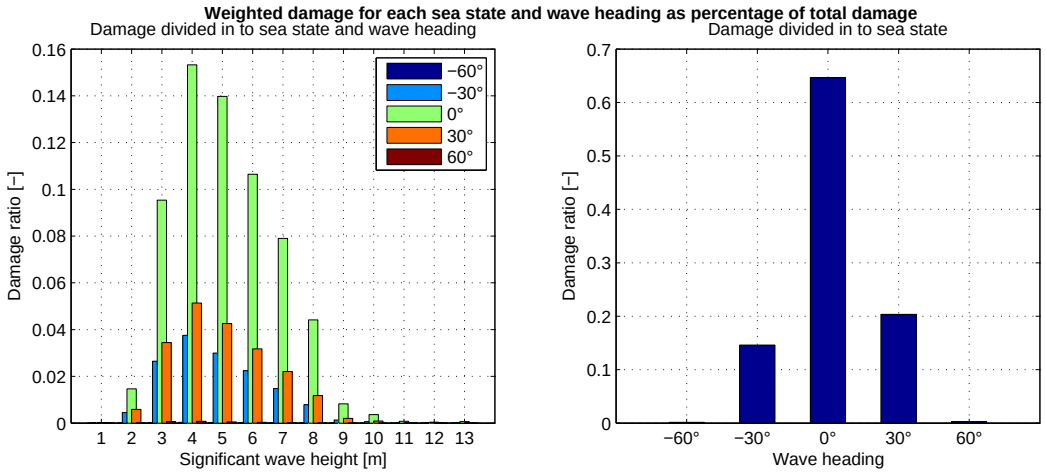


Figure 6.17: Damage distribution between sea states and wave headings for plate 4

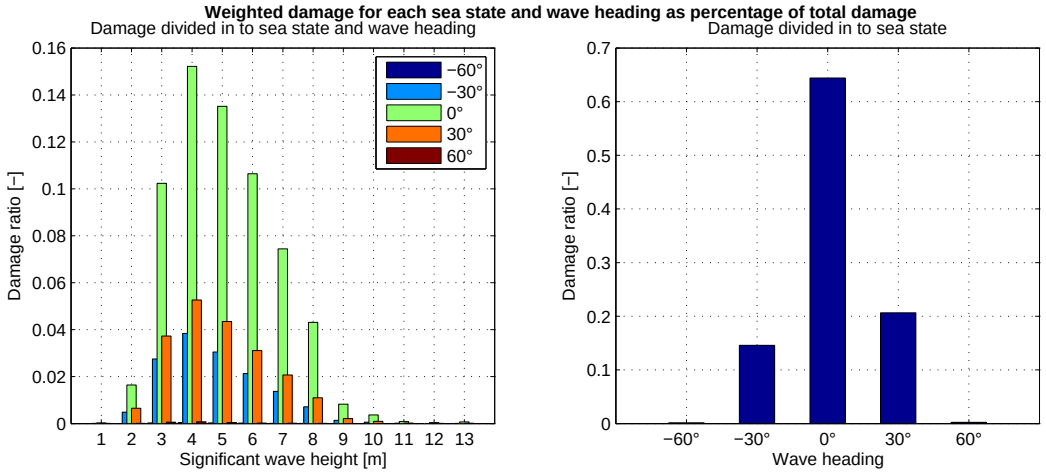


Figure 6.18: Damage distribution between sea states and wave headings for plate 5

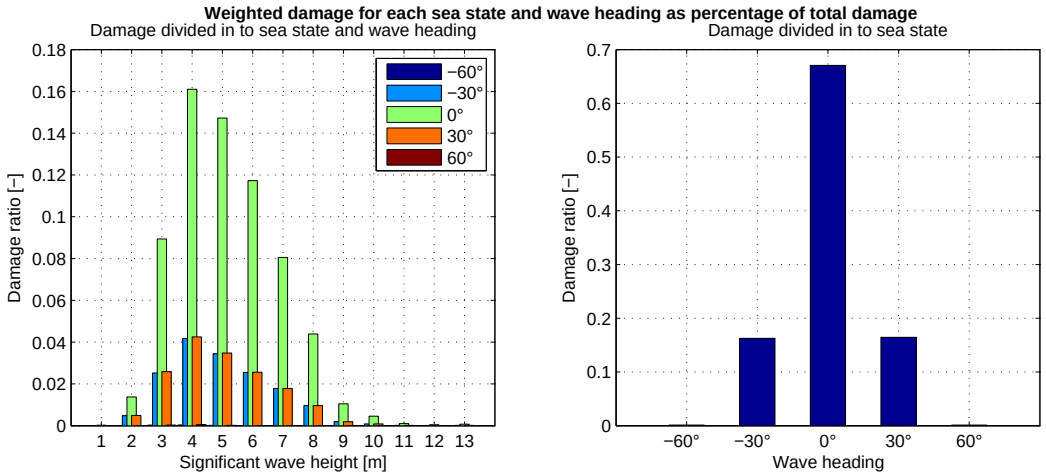


Figure 6.19: Damage distribution between sea states and wave headings for plate 6

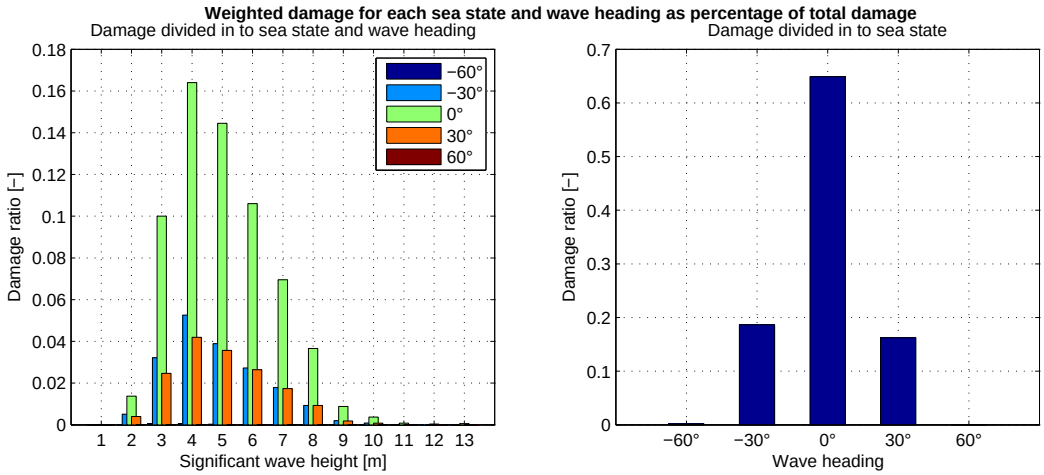


Figure 6.20: Damage distribution between sea states and wave headings for plate 7

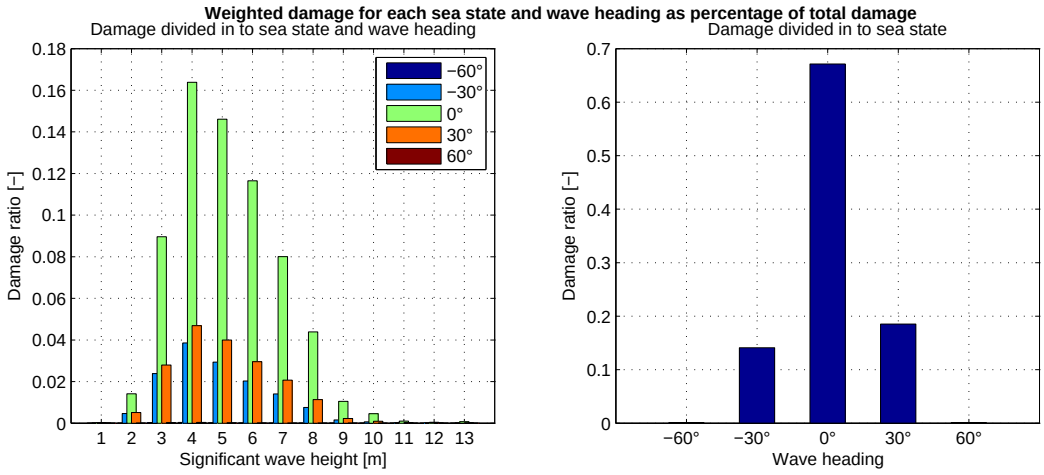


Figure 6.21: Damage distribution between sea states and wave headings for plate 8

### 6.5.4 Time to failure

Time to failure is presented in logarithmic scale in Figure 6.22. If one assumes a constant heading over the lifetime of the structure, a 0°heading will result in failure first at all the plates. At this heading Plate 1 has lowest fatigue life. For large headings Plate 3 is the most critical. This is true for negative headings also because the other side of Plate 3 (not included in the figure) will fail first. For a combined heading Plate 1 will be the most critical and will fail after 10 years. At this plate fatigue conditions are worse at the surface turning inside (not in touch with water).

To see the effect the simplified stress have on fatigue life, fatigue life has also been calculated by only using the normal stress. The ratio between the fatigue life is calculated as:

$$r = \frac{t_{f,normal}}{t_{f,all}} \tag{6.9}$$

$t_{f,normal}$ is time to failure including only nomrmal stress

$t_{f,all}$ is time to failure including simplified shear and parallel stress

The ratio $r$ is illustrated in Figure 6.23. As it will be hard to see the exact values from the figure when the ratio is close to 1, $r$ is also given in Table 6.5.

The effect of including simplified shear and parallel stress varies a lot. At the most critical plate, only including the normal stress result in 11% longer fatigue life estimation for combined heading. At Plate 7 and 8 however, it will result in 6 and 8 times longer fatigue life. That is not surprising considering how dominant the weighted standard deviation average of the perpendicular stress is in Plate 1 and how large the parallel stress variations are in Plate 7 and 8.

At Plate 2, 4 and 5, where the shear stress variation are small compared to the normal stress variations, the increase in fatigue life for a combined heading is lower than 5%. Note that not to much information can be drawn from Plate 4 and 5 because $\bar{\lambda}_{Shear\,stress} < 0.95$ for all headings. However that is not the case for the parallel stress, and the parallel stress variation is even av bit higher than the normal stress variation for some headings. The low effect the parallel stress has on fatigue life is unexpected. That being said, a low $\alpha$ was assumed in equation 2.13. A higher $\alpha$ would increase the effect of the parallel stress.

At Plate 6 where the shear stress variation is high compared to the normal stress, the increased fatigue life will be 25% if only normal stress is used.

Overall the *time to failure* and *time to failure ratio* are in good accordance with what could be expected from the weighted stress standard deviation average and $\bar{\lambda}$ values. There is not found any indication of calculation errors.

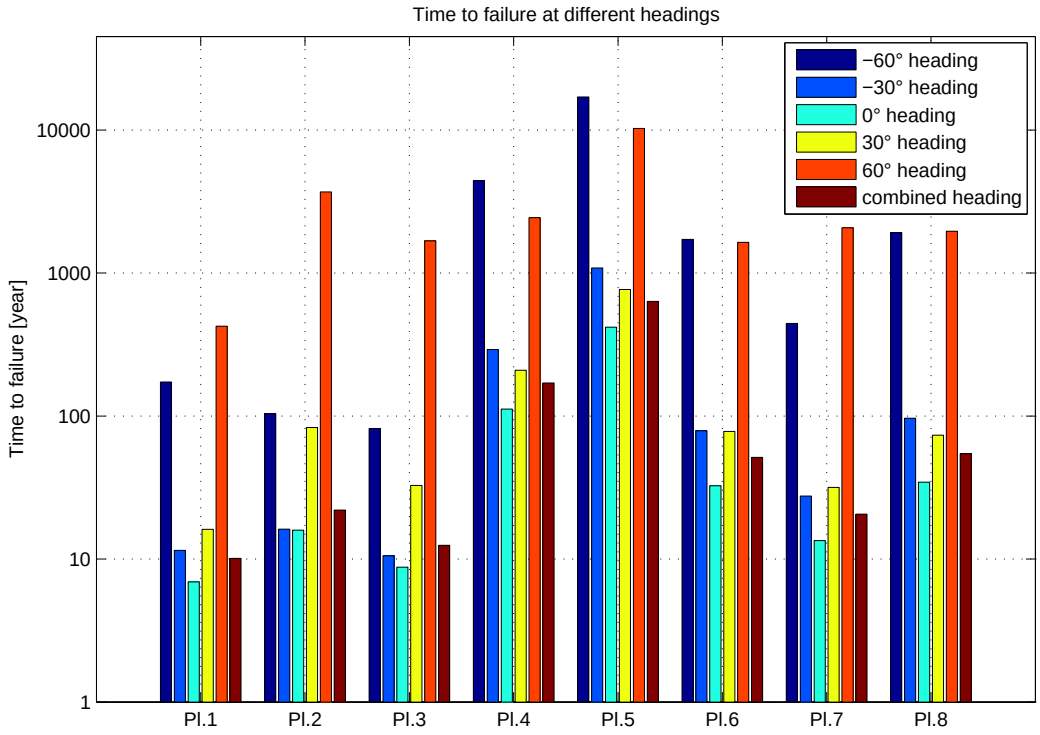


Figure 6.22: Time to failure for a constant heading over the lifetime, with real normal stress combined with simplified shear and parallel stress, and for a combined heading

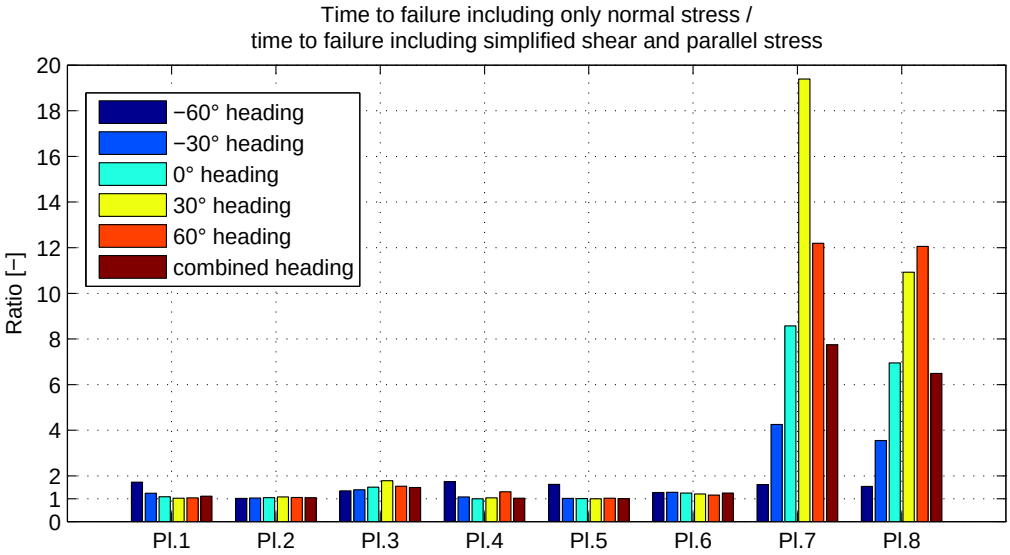


Figure 6.23: Ratio between time to failure when including only normal stress and when including simplified shear and parallel stress

Table 6.5: Ratio between time to failure when including only normal stress and when including simplified shear and parallel stress

| Heading | Plate 1 | Plate 2 | Plate 3 | Plate 4 | Plate 5 | Plate 6 | Plate 7 | Plate 8 |
|---|---|---|---|---|---|---|---|---|
| -60° | 1.72 | 1.02 | 1.34 | 1.75 | 1.63 | 1.28 | 1.62 | 1.54 |
| -30° | 1.24 | 1.03 | 1.39 | 1.08 | 1.01 | 1.28 | 4.25 | 3.55 |
| 0° | 1.09 | 1.05 | 1.50 | 1.00 | 1.00 | 1.25 | 8.57 | 6.95 |
| 30° | 1.02 | 1.08 | 1.79 | 1.04 | 1.00 | 1.21 | 19.39 | 10.92 |
| 60° | 1.04 | 1.05 | 1.54 | 1.31 | 1.02 | 1.16 | 12.19 | 12.06 |
| Combined | 1.11 | 1.04 | 1.49 | 1.02 | 1.00 | 1.25 | 7.75 | 6.49 |

An alternative way to get an indication of how accurate the simplified linear stress method is could be to estimate fatigue life with another real stress component. Instead of estimating a simplified shear and parallel stress from the actual normal stress component, one can estimate a simplified normal and parallel stress based on the actual shear stress. Of course one can also use the parallel stress as the real component. The author of this report has also calculated fatigue life using the shear stress as the real stress component. The resulting fatigue life is divided by fatigue life found using the real normal stress component. The results are found in Figure 6.24

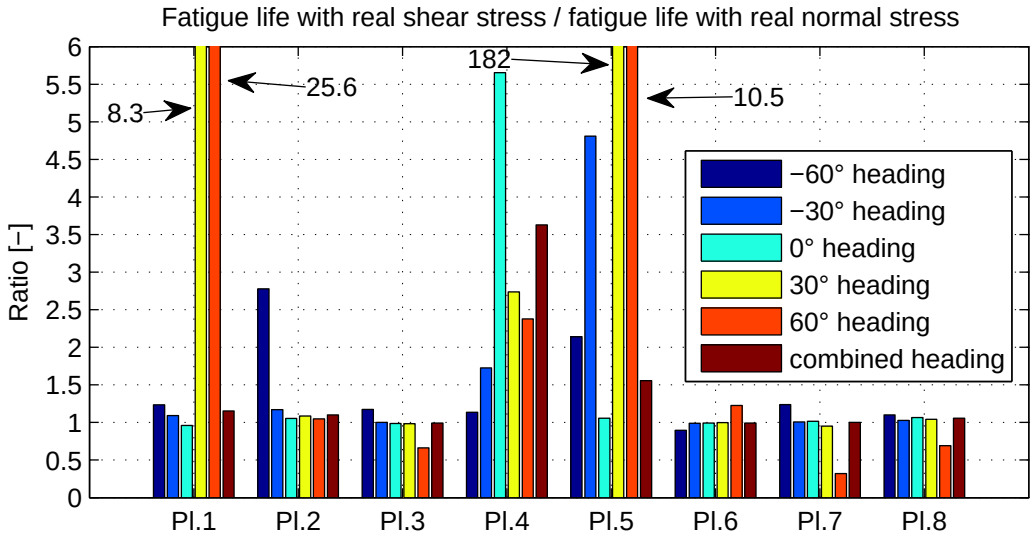


Figure 6.24: Ratio between time to failure when using the normal stress as the real component and when using the shear stress as the real component

A value close to 1 indicates that the error associated with simplifying the shear stress component is small. The figure gives a very similar picture as the $\bar{\lambda}_{shear\,stress}$ values illustrated earlier. When the correlation between normal and shear stress is low the value is far from 1. It is easy to think that ratio always should be above 1, because the simplified perpendicular stress should have a lower weighted standard deviation than the real. At 60°heading this is not always the case. At Plate 7 at 60°heading for example the ratio is only 0.32. The reason for this is that the real normal stress consist of one part with high frequency and another part with a much lower frequency. When simplifying the

normal stress as a linear function of the shear stress, the amplitude of the low frequency part decreases, while the amplitude of the high frequency part increases. This is worse in regard to fatigue, but the sample standard deviation should still be a bit lower than 1. This is shown in Figure 6.25, where the real and normal stress at Plate 7 with 60°heading are plotted together.

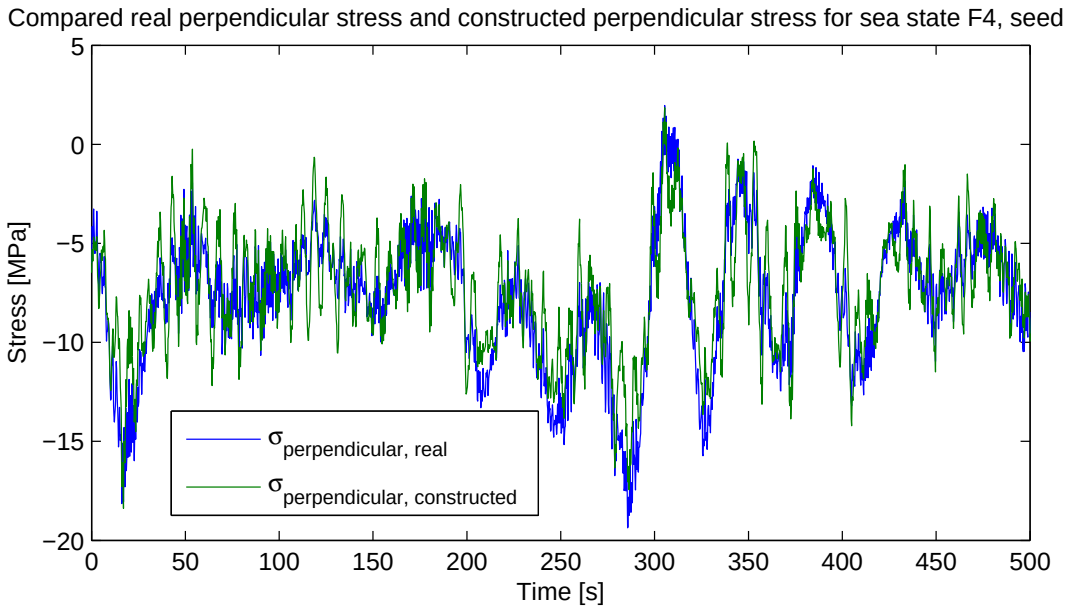


Figure 6.25: Comparison between real and constructed parallel stress at Plate 7 with 60°heading

At plate 7 and 8 the parallel stress is obviously the biggest contributor to crack growth. Therefore, one can argue that using the real parallel stress in equation 2.13, instead of the real perpendicular stress, would give more accurate fatigue life results. The difference is expected to be small since $\bar{\lambda}_{parallel\,stress}$ is so close to 1.

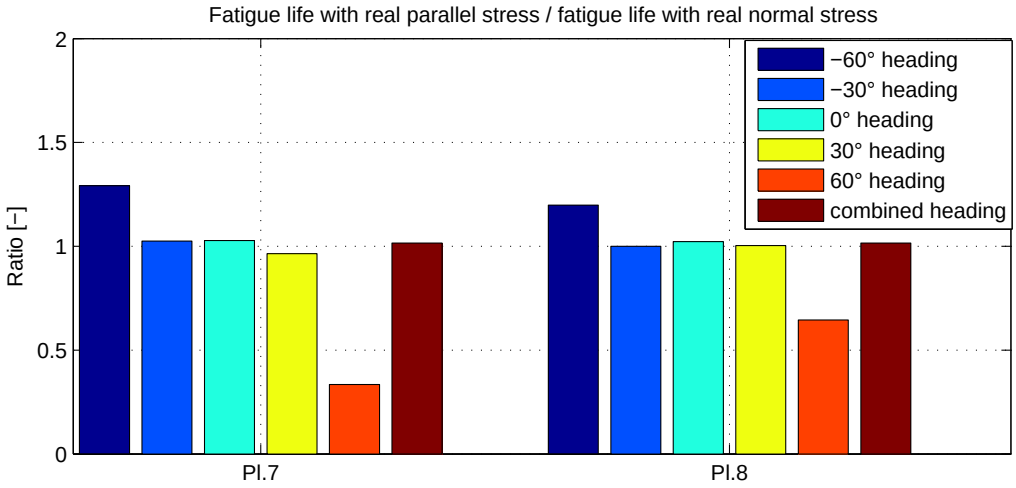


Figure 6.26: Ratio between time to failure when using the normal stress as the real component and when using the parallel stress as the real component

As can be seen from Figure 6.26 the overall difference for a combined heading is very small for both plates (less than 2%). The difference at -60°and 60°heading however, are unexpectedly high. Note the similarity between Figure 6.26 and 6.25. Using real shear stress component or real parallel stress component result in very similar differences compared to the original calculated fatigue life. This is an indication that there is a stronger linear relationship between the shear and parallel stress, than between the normal and parallel stress and between the normal and shear stress.

At Plate 8 $\bar{\lambda}_{parallel\,stress} = 0.97$ at 60°heading, but using the parallel stress as the real component, instead of the perpendicular stress, results in a much lower fatigue life estimate. Only 65% of the original value. This may suggest that $\bar{\lambda}$ is not as good as estimator of the accuracy of the linear simplification method, as previously thought. In some situations $\bar{\lambda}$ is above 0.95, but the simplified and real stress may still not be similar enough to use the method in fatigue calculations. The simplified and real parallel stress have been examined further at this plate and heading.

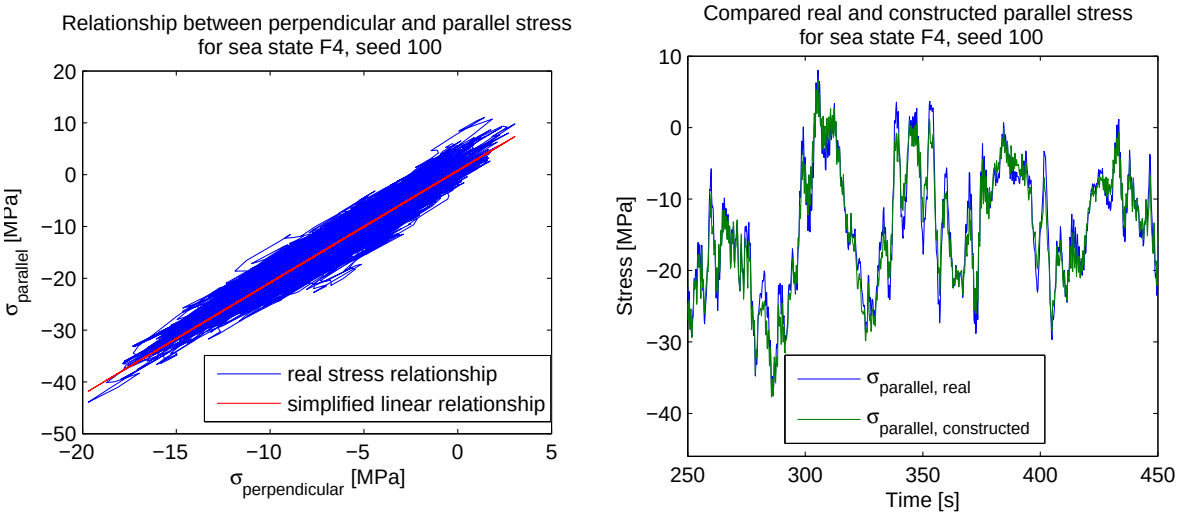


(a) $\sigma_{\perp} - \sigma_{\parallel}$ plane

(b) Real and constructed parallel stress

Figure 6.27: Comparison between real and constructed parallel stress at Plate 8 with 60°heading

Is seems that even tough the real and constructed parallel stress overall are quite similar, the constructed shear stress underestimate the amplitude of the largest peaks. These peaks need to be accurate in order to give reliable fatigue life results. From the figure one can clearly see the effect of slowly varying forces on the hot spot stress. $\bar{\lambda}$ is less suitable as estimator of the linear simplification method in these types of situations. Regardless, slowly varying hot spot stresses are only important for large headings that overall has a very minor effect on fatigue life. The difference in fatigue life prediction with a combined heading is still less than 2%. Therefore one can conclude that using the normal stress as real component, instead of the more important parallel stress, is acceptable for Plate 7 and 8.

# Chapter 7

# Results Submodel 2

The weld between the transition piece and the cylinder is a location that will experience stress concentration. The stress picture differ by each load case and it is hard to estimate exactly at what point along the weld, fatigue failure is most likely to occur. As a result of this 13 hot spots along the weld were analyzed, as indicated in Figure 7.2. The angle between the points is 15°. Due to structural symmetry around the x-z plane only the part of the weld with positive y-coordinates have been investigated.

A crack can start to grow from both the upper cylinder plate, marked in blue, and the lower plates that are parts of the transition piece, marked in pink, in Figure 7.1. Although it is not so easy to see from the figure, the geometry of the lower plates is rather complex. It consist of plates with a conical form and straight plates with a triangular form, together forming the transition piece. Both sides of the weld at each hot spot have been analyzed in regard to fatigue. Also, both sides of each plate have been analyzed. Unless specifically stated otherwise the figures and discussions in this section refer to the side of the plate with lowest estimated fatigue life from a combined heading, with real normal stress and simplified shear and parallel stress. With two exceptions this will be the outer surface. The two exceptions are at the lower plates in P4 and P10.

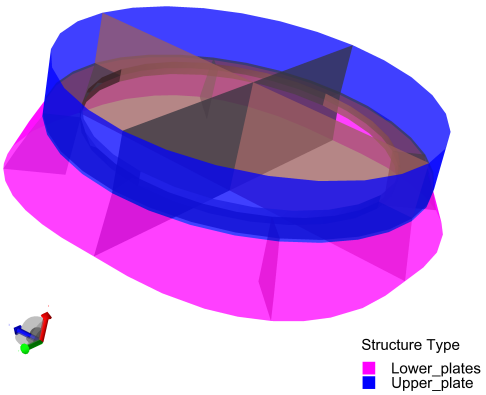


Figure 7.1: Hot spots investigated at cylinder-transition piece connection

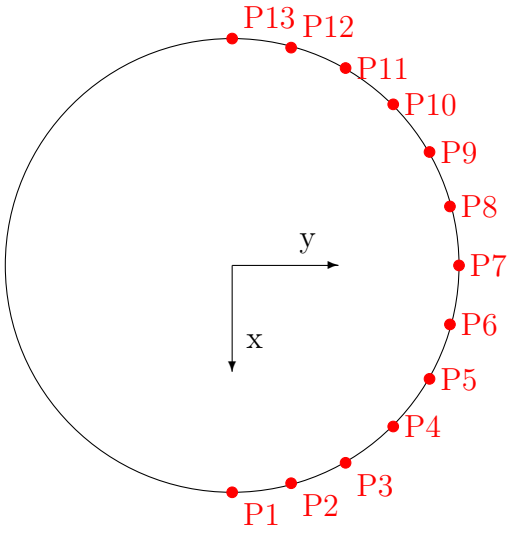


Figure 7.2: Hot spots investigated at cylinder transition piece connection

## 7.1 Hot spot stresses

The nondimenional hot spot stresses have been calculated the same way as the hot spot stresses in submodel 1. Because the bending stress gradients close to the hot spots are large the bending stress has also been reduced to 60% here. The simplified frame structure in Figure 6.2 has been used to check if the results are not differing completely from what could be expected. The effective nondimenional hot spot stresses are given in Figure 7.3 and 7.4 at the lower plates and the upper plate respectively. The hot spot stresses decomposed to bending and membrane parts are displayed in Figure 7.5-7.8. Note that at the figures only displaying the bending stress components the stress is not yet reduced to 60%. The nondimensional stresses are defined the same way as the stress is Submodel 1, but due to to the increase in number of areas analyzed, the stresses have been displayed differently to increase comparability. Now it is also easier to see how the hot spot stresses changes over the weld line.

Xtract have been used to extract the stresses at the read out points. When it is possible to calculate the nodal average of the stress this has been extracted and used in the calculation. At some points it is not possible to calculate the nodal average because vertical stiffeners also are connected to the read out nodes (P1, P4, P7, P10 and P13). In these situations the element stresses of a element with a local node at the read out point have been exacted. The element stresses at the local node, with same coordinates as the read out point, have been used in the calculations.

A simple mechanical analysis predicts that the perpendicular hot spot stress due to $F_x$ should be in compression from P1-P6 and in tension from P8-P13. It should be opposite for the perpendicular stress due to $F_z$ and $M_y$. $F_y$ and $M_x$ should result in perpendicular stresses in compression for all the areas. The effect of $M_z$ on the perpendicular stress is harder to predict based on simple mechanics. The normal stresses at the hot spots are in good accordance with what was expected.

Note how similar the membrane hot spot stresses are at the lower and upper plates. This is natural as the thickness of the plates is the same and there has to be a force equilibrium between the plates. This is not completely true when there are also vertical stiffeners behind the plates. That is why the stresses are less similar for these hot spots. At the hot spots with no vertical stiffener behind the plates the bending component of the parallel and normal stress are also very similar. The same can not be said for the bending component of the shear stress.

One very interesting thing one can see from the figures are how the vertical stiffeners affect bending stresses. The perpendicular stress will be reduced significantly because of the vertical plates, but the parallel stress will increase remarkably. Note how large the parallel bending stress are at P4 and P10. Inserting vertical stiffeners at these positions to reduce the overall stress level might have been a bad idea. It may seem like the reduction in normal stress does not outweigh the huge increase in parallel stress at these location, but it is too early to conclude this with certainty. Another thing worth noticing is that the bending stress at P4 and P10 is largest at the lower plate. This might be due to the fact that there is a ring stiffener located 5 cm above the weld line. This stiffener will reduce more of the hot spot stress at the plate above the intersection. Ideally the ring stiffener should be located at the weld line, but that causes welding complications.

In Figure 7.4 the effective parallel hot spot stress for P1 and P4 are actually quite small, despite the large parallel bending stresses at these hot spots. That is because it was found that fatigue life was shorter at the side of the plate where the bending and membrane parts are in opposite direction. The figures displaying effective hot spot stress are all for the worst side of the plate in regard to fatigue in a combined sea state, based on fatigue calculation with real perpendicular stress and simplified shear and parallel stress.

The effective hot spot stresses have been compared with the hot spot stresses found from the alternative method. Generally the stresses found from both methods are quite similar, but multiplying the stress at the 0.5t read out point with 1.12 is often more conservative.

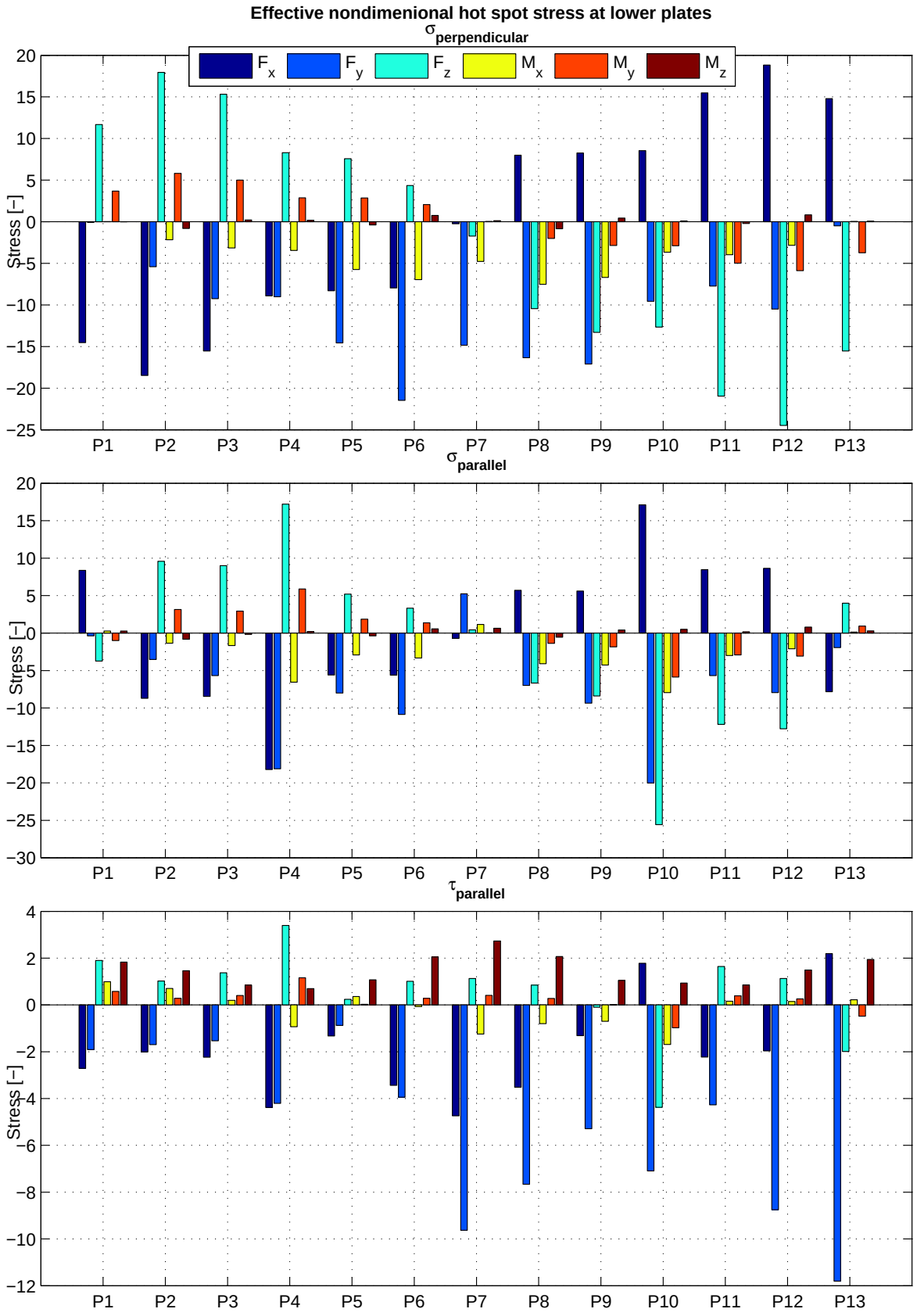


Figure 7.3: Effective nondimenional hot spot stresses at lower plates

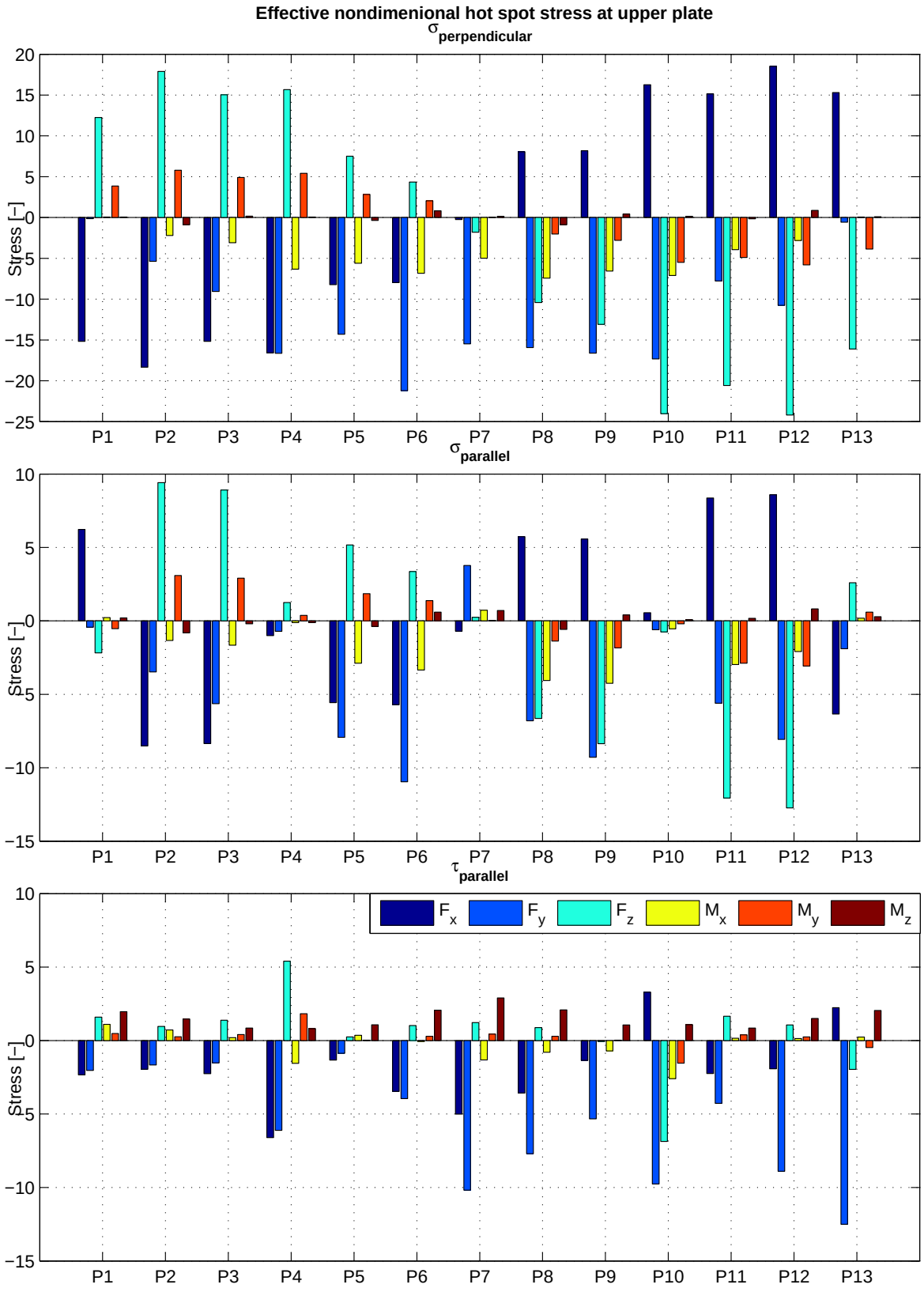


Figure 7.4: Effective nondimenional hot spot stresses at upper plate

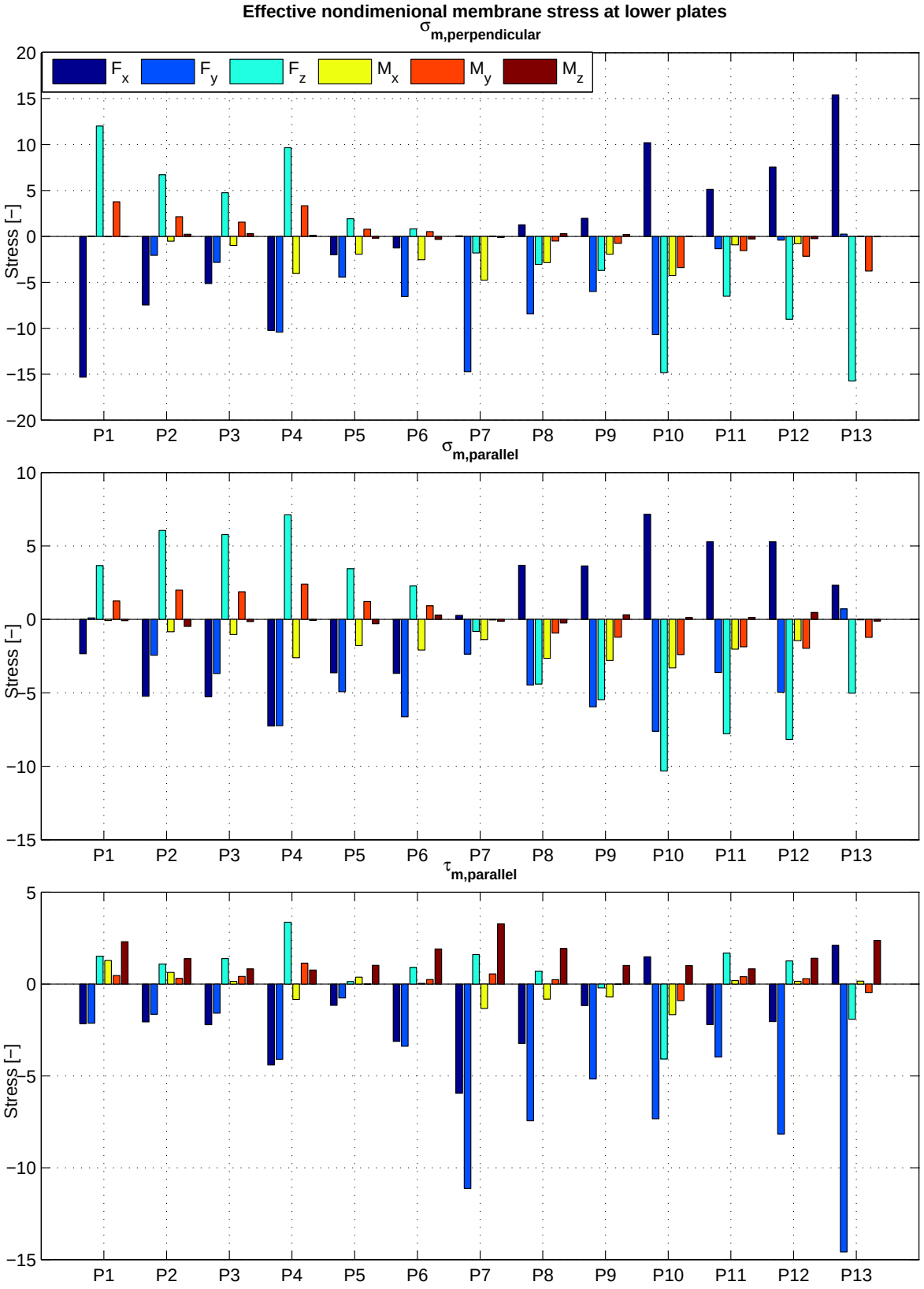


Figure 7.5: Nondimenional hot spot membrane stresses at lower plates

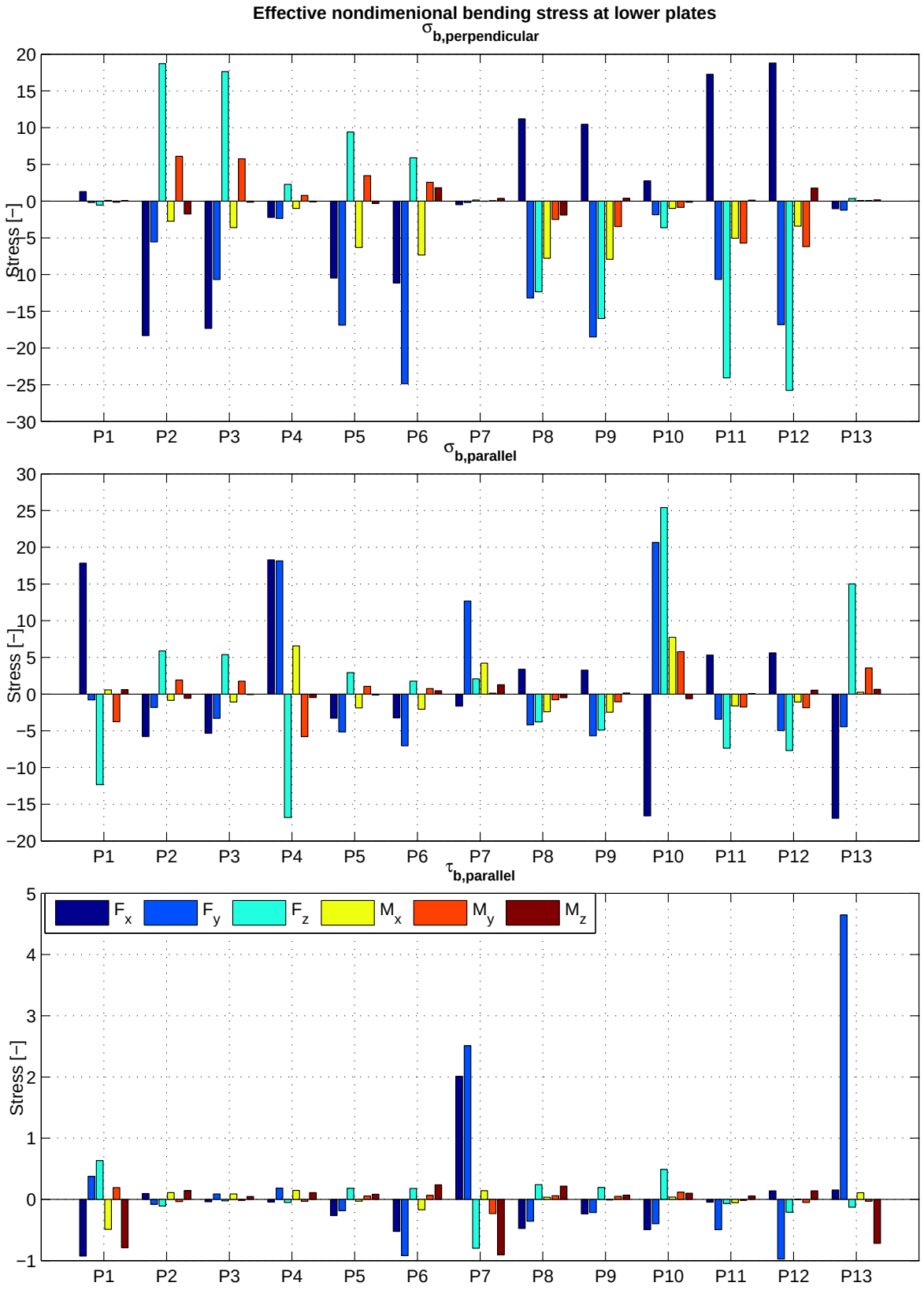


Figure 7.6: Nondimenional hot spot bending stresses at lower plates

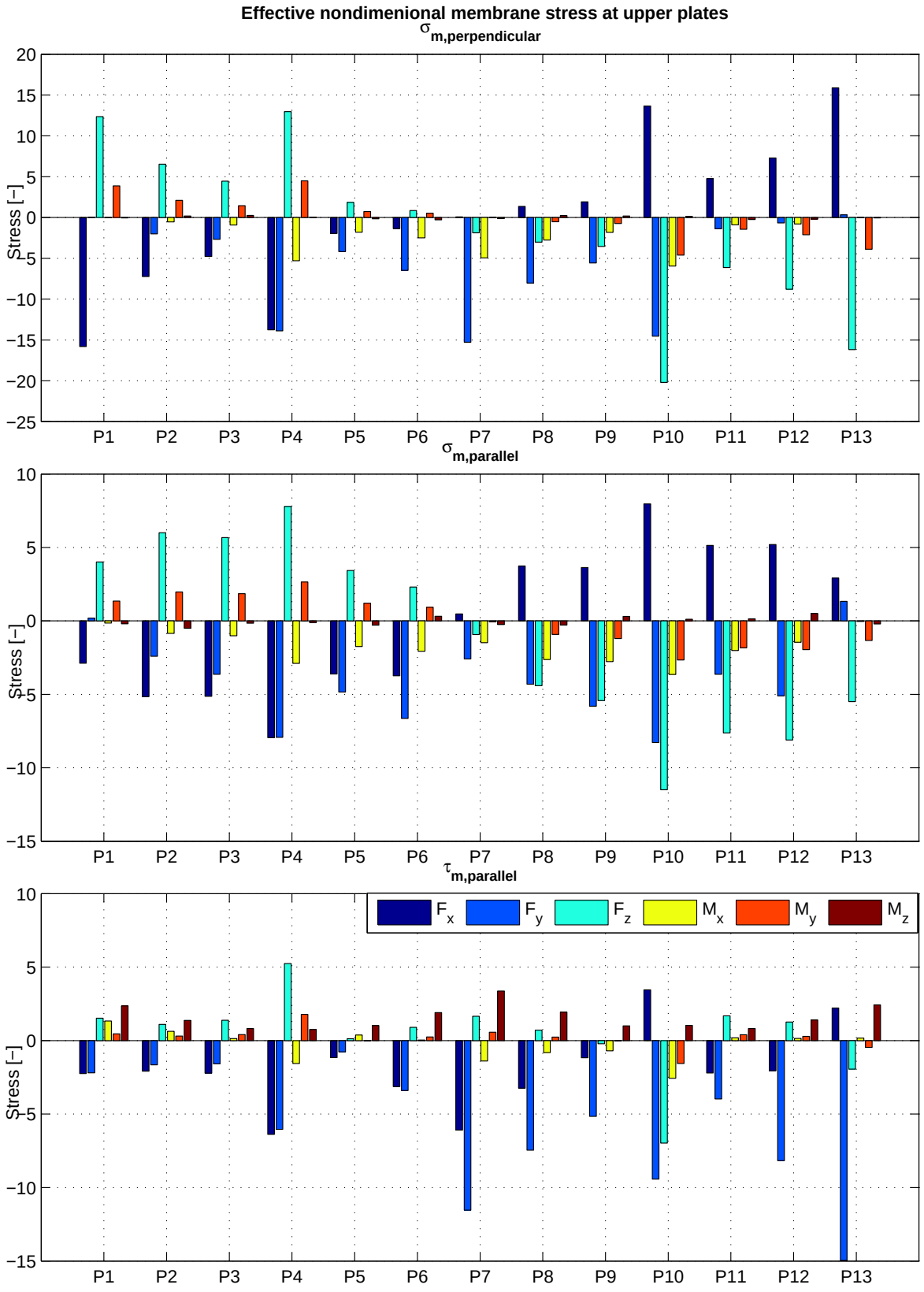


Figure 7.7: Nondimenional hot spot membrane stresses at upper plate

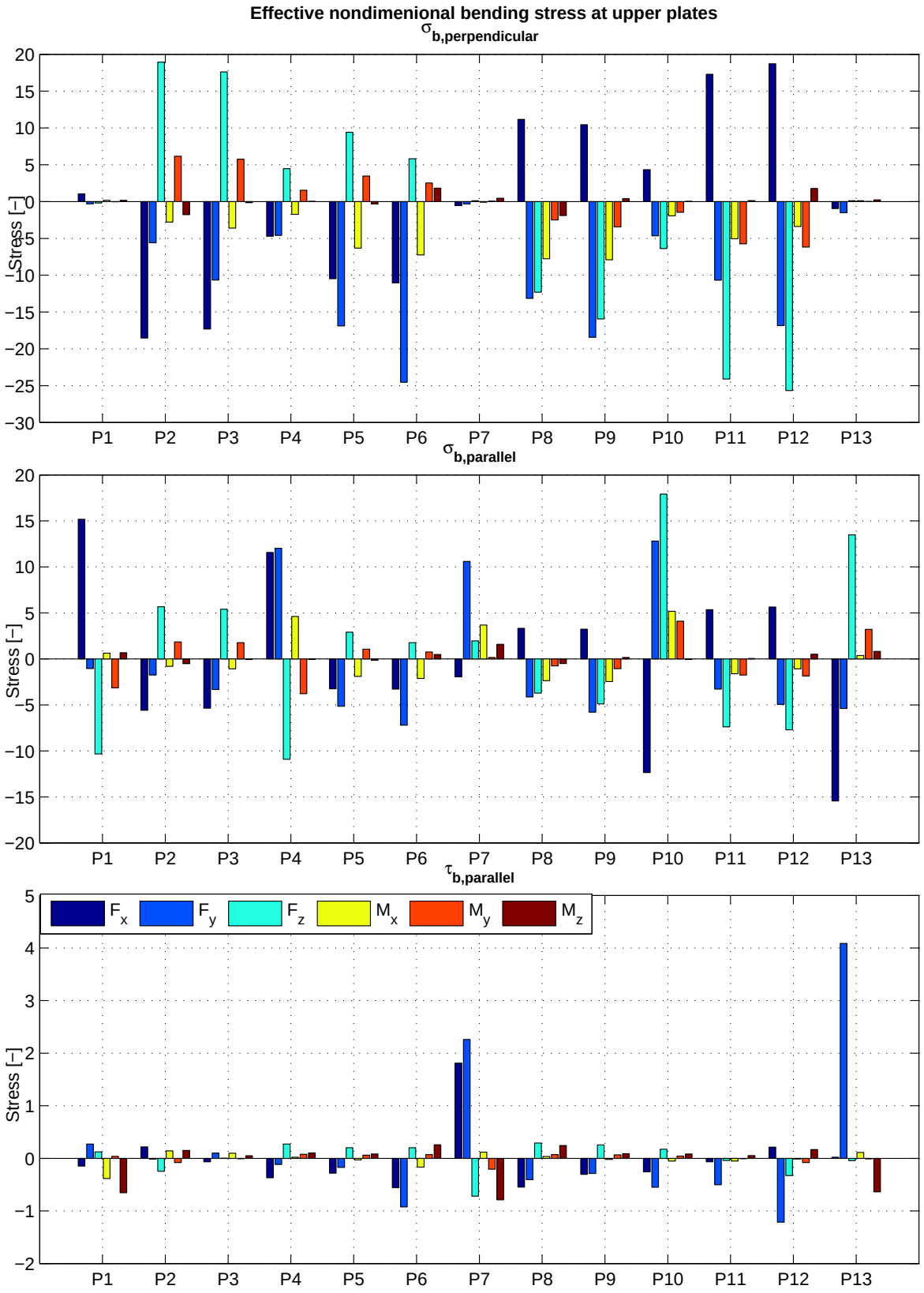


Figure 7.8: Nondimenional hot spot bending stresses at upper plate

## 7.2 Real stress variations

As the method for deriving the real hot spot stresses is the same as what is described previously it is not commented here. Figure 7.9 and 7.10 show how the weighted standard deviation average of the different stress component varies with different wave heading. The weighted standard deviation average for a combined heading is shown in Figure 7.11.

At the hot spot in Submodel 1 0° heading generally had the largest stress variations. What headings that will result in large stress variation differ much more at the hot spots in Submodel 2. At P1 and P13 0° heading gives largest stress variations because the points lie in the x-z plane. It seems like usually the normal stress will vary the most when the wave direction are parallel to the line that can be drawn from the hot spot to the center of the cylinder. The same tendency can also be seen with the parallel stress.

The largest stress variation occur at P4 and P10. At the inner surface of these points there will be large parallel stresses, while at the outer surface there will be large normal stresses. At these points there are also large shear stresses. Based on the stress variation one can predict that P4 and P10 will be the most critical points. Nonetheless, fatigue life have been calculated for all the points at both upper and lower side of the weld and for each side of the plates.

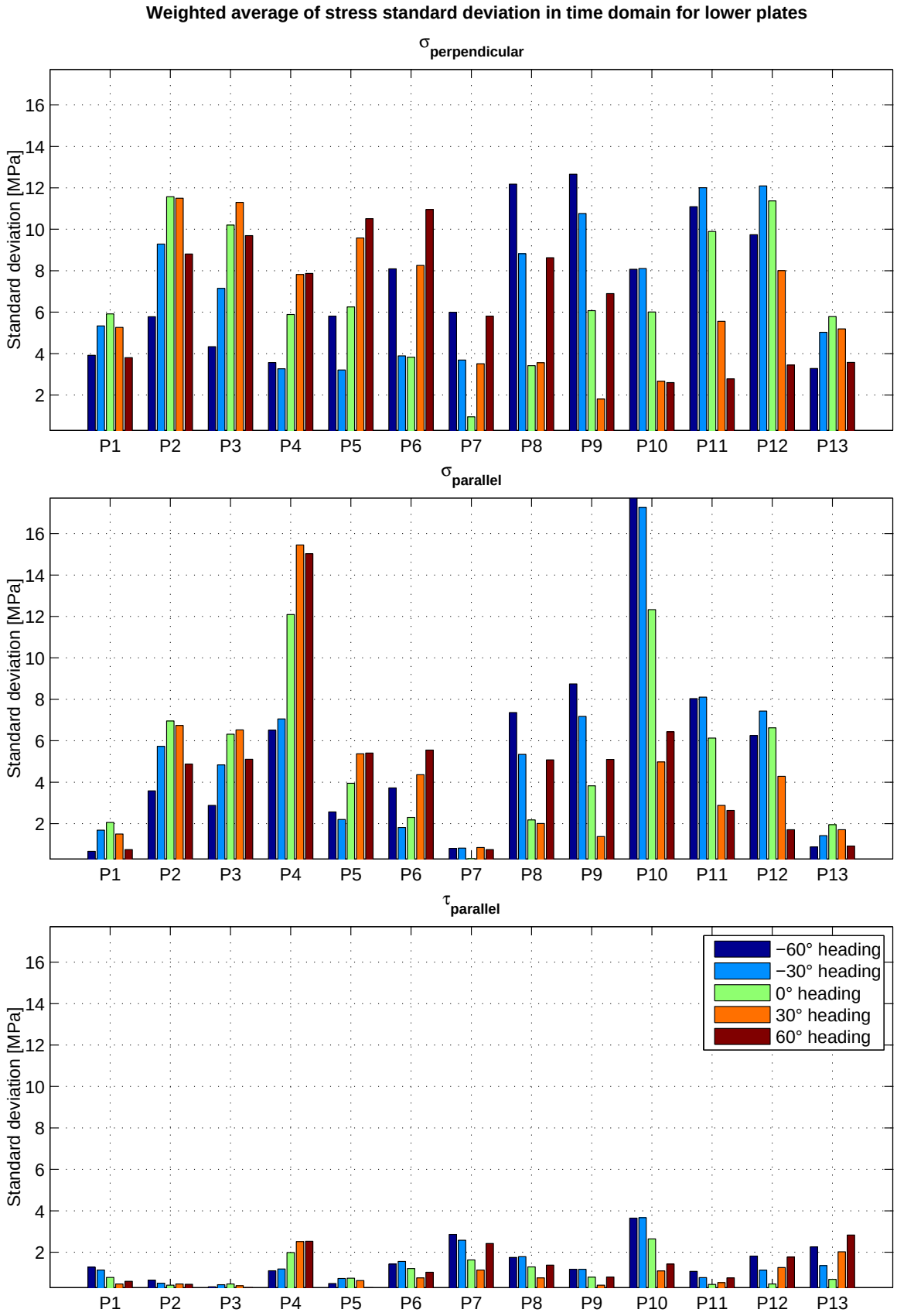


Figure 7.9: Weighted average of stress standard deviation in time domain for lower plates

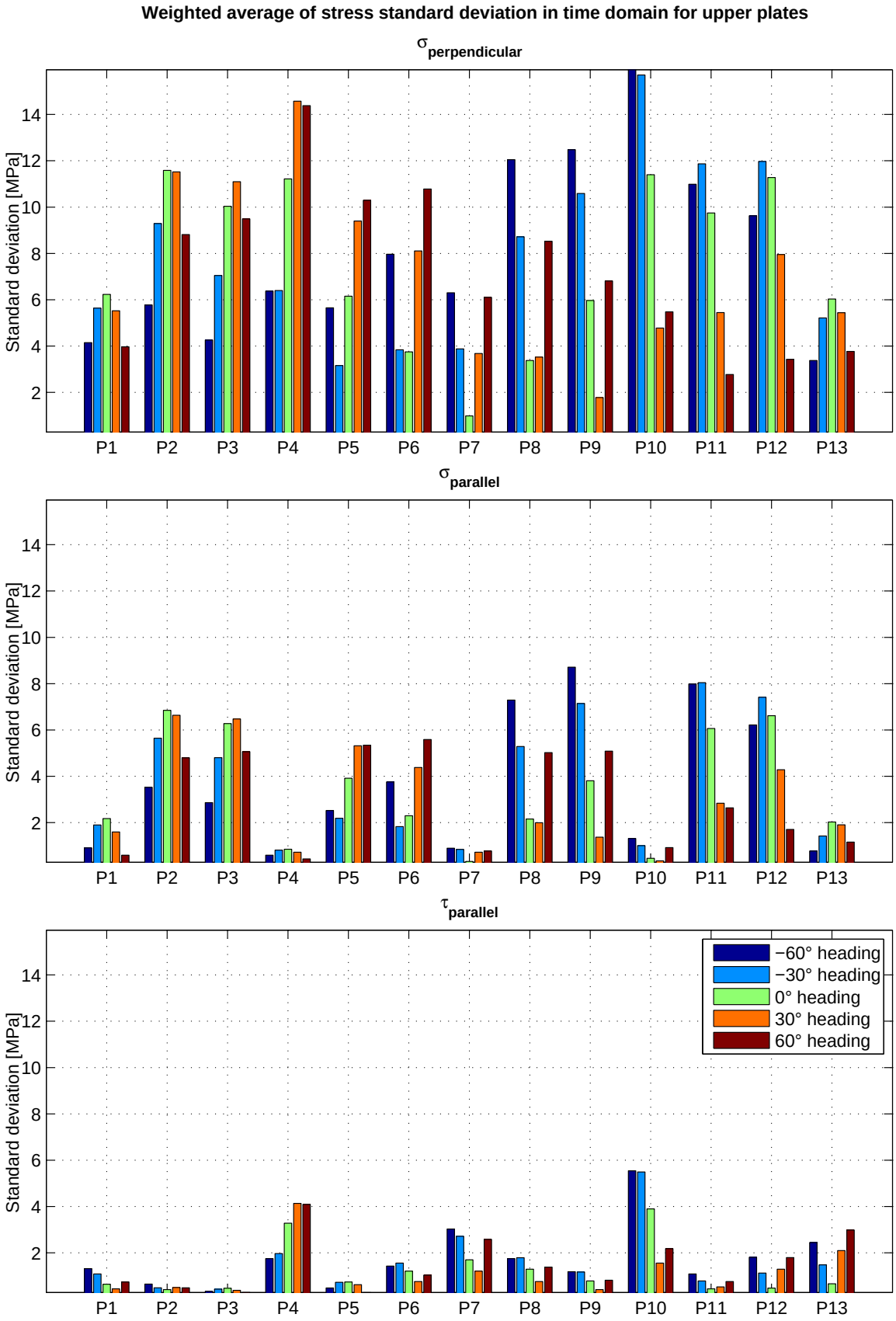


Figure 7.10: Weighted average of stress standard deviation in time domain for upper plates

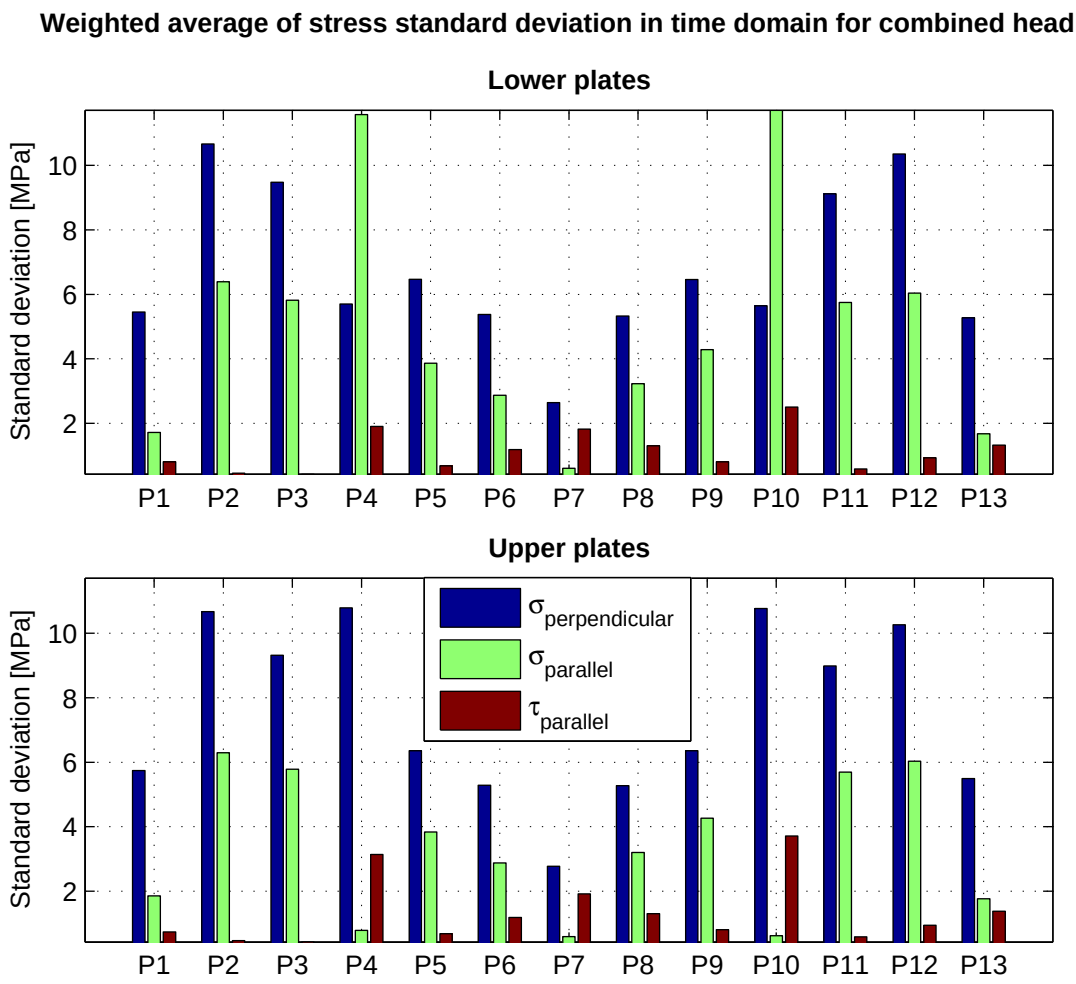


Figure 7.11: Weighted average of stress standard deviation in time domain for upper plates at combined heading

## 7.3 Stress simplifications

There will be a multiaxial stress state at all the hot spots analyzed. To attempt to include the effect of all three stress components ($\sigma_\perp$, $\sigma_\parallel$ and $\tau_\parallel$) the linear simplification method have been used. This method is only expected to give reasonably accurate results when there is a clear linear tendency between the stress components. In other words, writing a stress component as a linear function of another stress component should not give results far from reality. This is described in more detail previously in this report. For all hot spots $\sigma_\perp$ have been used as the real stress component, and $\sigma_\parallel$ and $\tau_\parallel$ have been simplified as linear functions of $\sigma_\perp$.

$\bar{\lambda}_{shear\ stress}$ and $\bar{\lambda}_{parallel\ stress}$ have been used as measurement of how accurate the linear simplification is. The values of $\bar{\lambda}$ for both upper and lower side of the weld at different headings are located in Figure 7.12. The defined limit $\bar{\lambda} = 0.95$ is marked with a red line. Values below this limit indicates that linearization will not give accurate results.

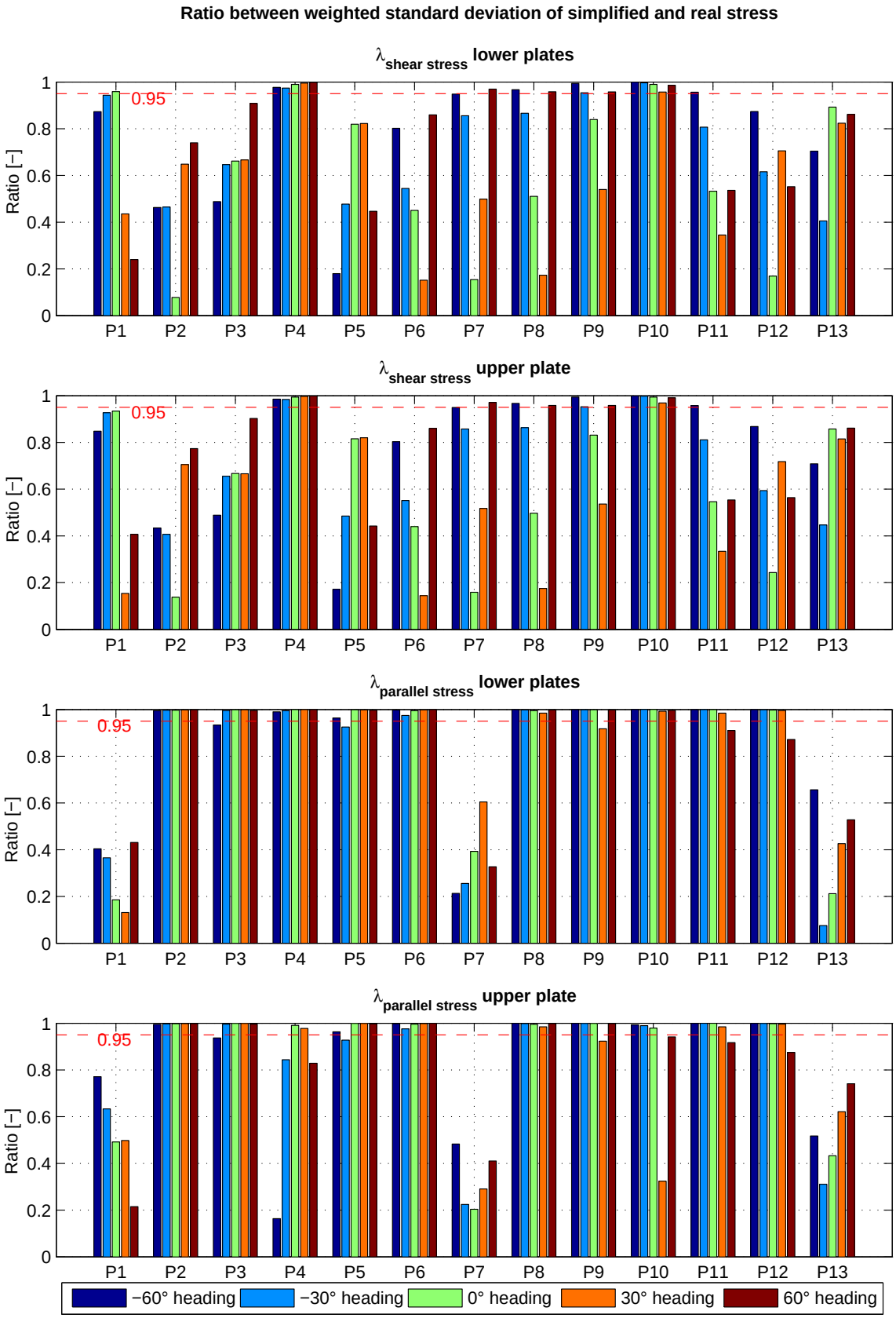


Figure 7.12: Ratio between weighted standard deviation of simplified and real stress

The correlation between the normal stress and parallel stress is generally very low. Only at P4 and P5 are the real and simplified shear stress similar enough that its effect on fatigue life are likely to be conserved for all headings. Here the shear stress variations are quite big and it can make a substantial difference in fatigue life calculation. At P7 the shear stress variations are very large compared to the normal stress. But the low correlation makes it impossible to include the effect of the shear stress properly with the linear simplification method when using the perpendicular stress as the real component. Nonetheless, this should not be the most critical point at the weld line, as the stress variations here are low compared to the other points.

Overall the correlation between the normal and parallel stress are higher, with some exceptions. At P1, P7, and P8 the correlation is very low. These are the points connected to vertical plates going from one side of the cylinder to the other. At these points the parallel stress should not be that important, at least not on the outer surface, because the stress variations are considerably low compared to the parallel stress.

At the lower side of the weld at P4 and P10, which are the only areas where parameters displayed are corresponding to the surface turning inwards, $\bar{\lambda}_{parallel\,stress}$ is approximately 1. The correlation is also very high at the surface turning outwards. The high correlation between the parallel and perpendicular stress are very important here, because the parallel stresses variations are so high compared to the normal stresses. They are likely to be the main cause of fatigue damage.

At the upper side of the weld at P4 and P10 the correlation between $\sigma_{\perp}$ and $\sigma_{\parallel}$ is not always high enough. Nonetheless, the parallel stress is very low compared to the normal stress and should be negligible in regard to fatigue at the outer surface. At the inner surface however (not displayed), the parallel stress variations are very high, but here $\bar{\lambda}_{parallel\,stress} \approx 1$ for all headings. Therefore, it should be possible to include the effect of the parallel stress properly in fatigue life calculations.

## 7.4 Fatigue damage

Fatigue damage have been calculated the same way as in Submodel 1. Effective stress ranges are calculated with equation 2.13, with $\alpha = 0.72$. The D-curve, from DNV-RP-C203, in the table of S-N curves to be used in seawater with cathodic protection, has been used to calculate the damage.

In Figure 7.13-7.15 the Miner damage has been divided between sea states and wave headings at the lower side of the weld for all hot spots analyzed. Only the damage at the lower side of the weld is displayed, as the damage distribution on the opposite side of the weld is approximately identical. The differences are a bit higher at P4 and P10, but still very limited.

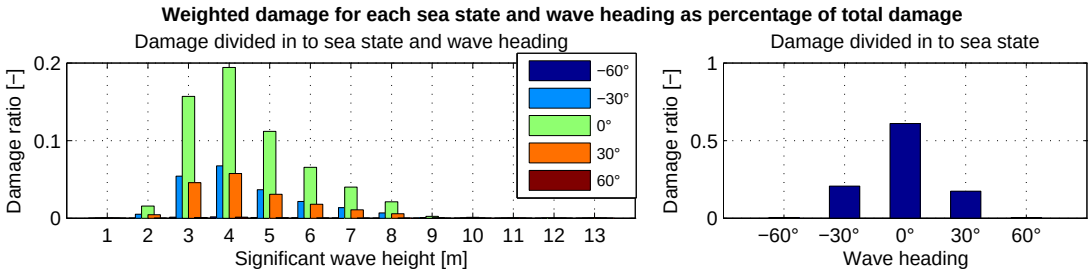


(a) P1 lower

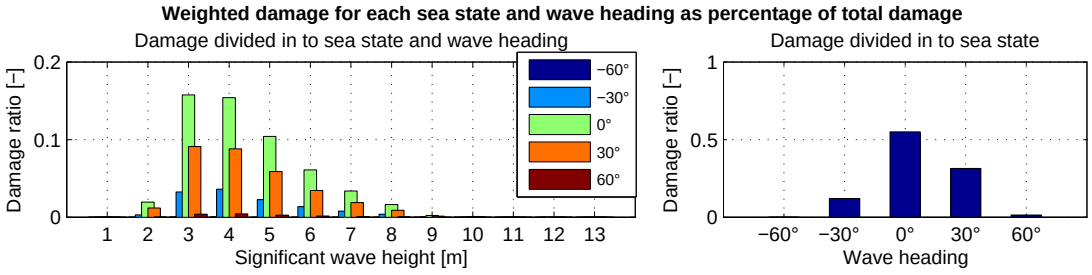


(b) P2 lower

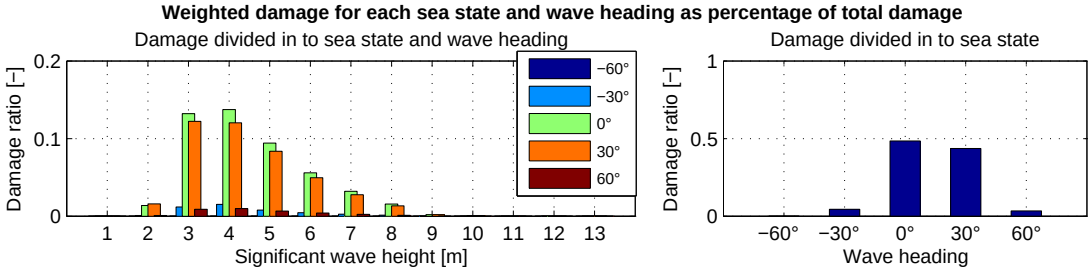


(c) P3 lower

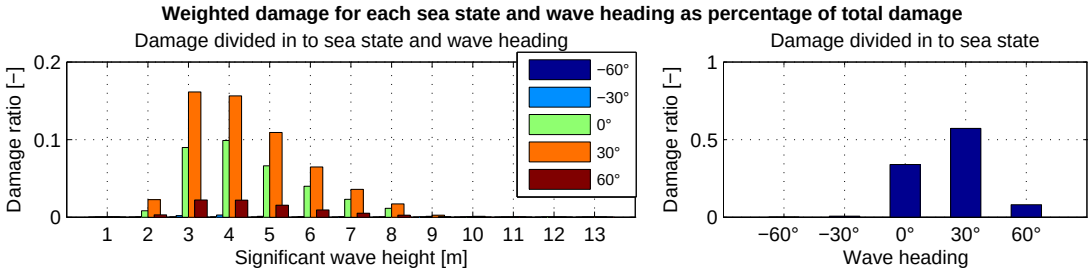


(d) P4 lower

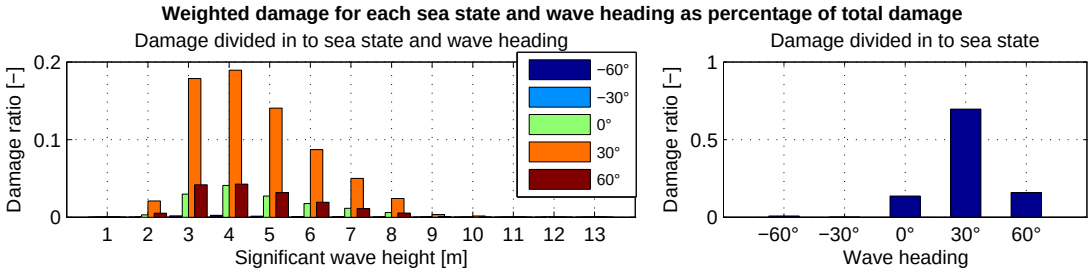


(e) P5 lower

Figure 7.13: Damage distribution between sea states and wave headings for lower plates at P1-P5

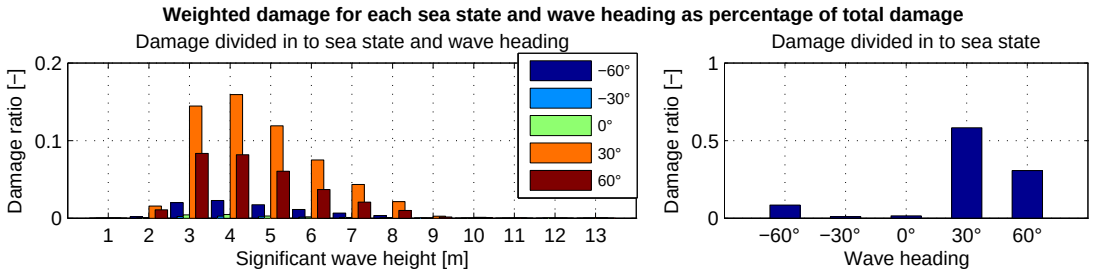


(a) P6 lower

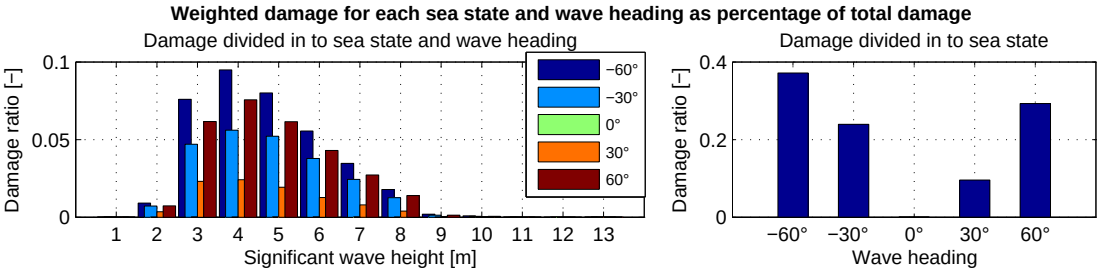


(b) P7 lower

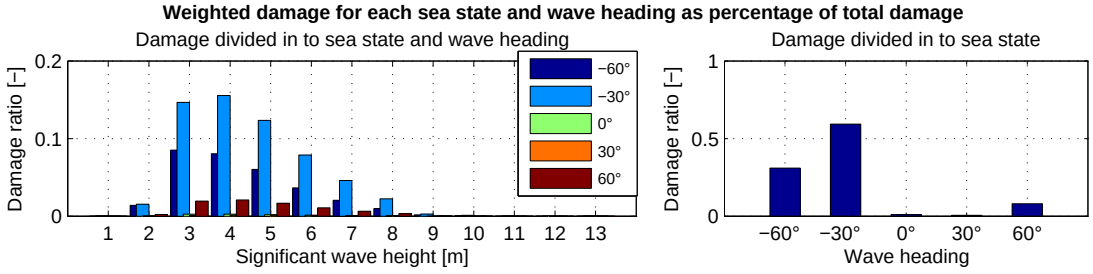


(c) P8 lower

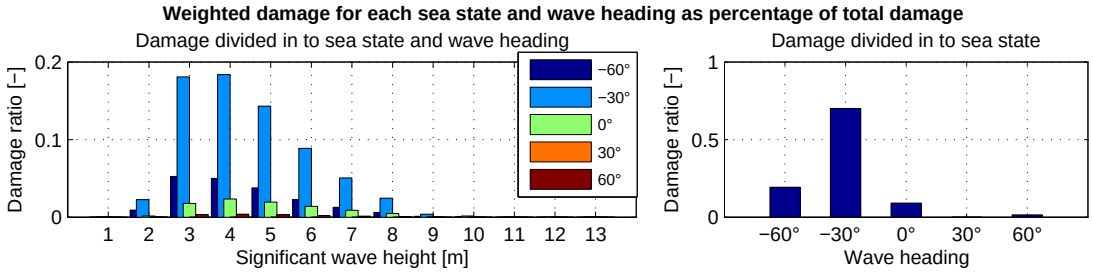


(d) P9 lower

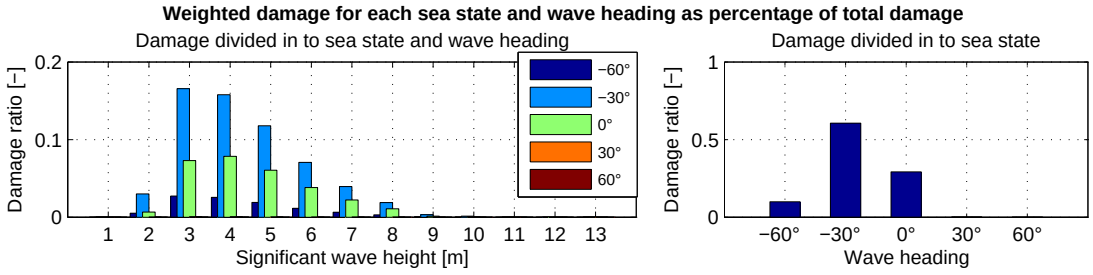


(e) P10 lower

Figure 7.14: Damage distribution between sea states and wave headings for lower plates at P6-P10

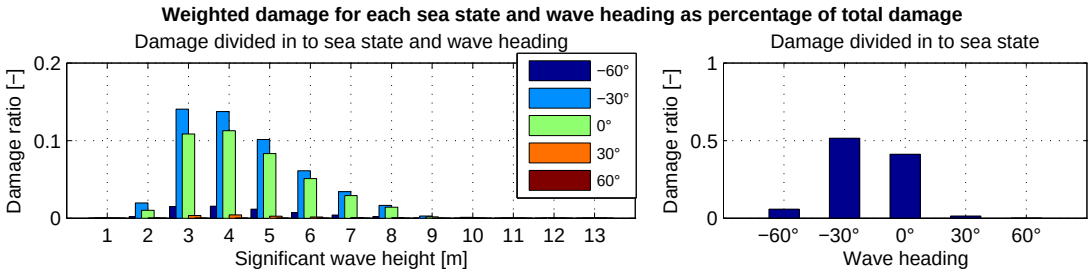


(a) P11 lower

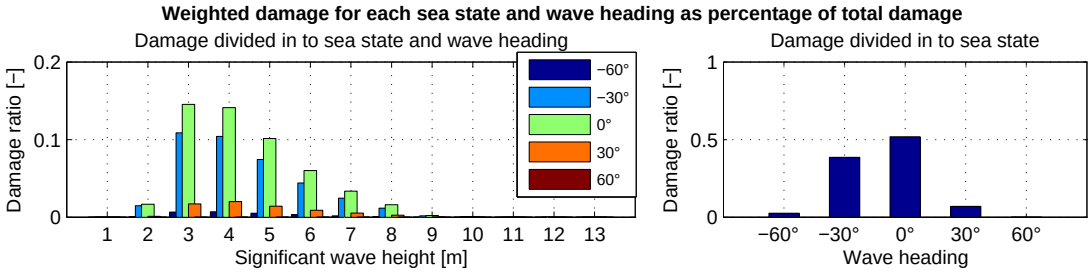


(b) P12 lower

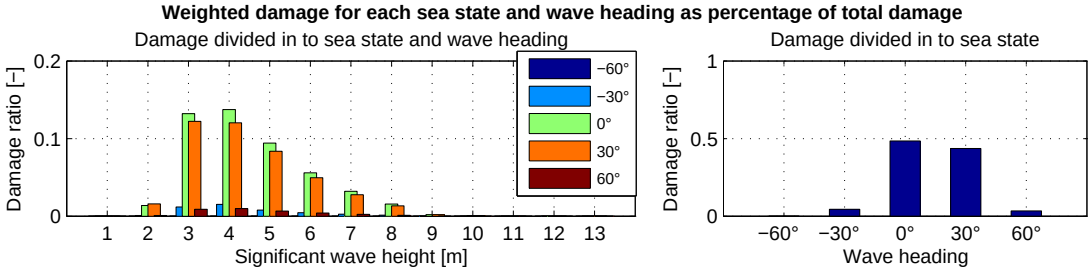


(c) P13 lower

Figure 7.15: Damage distribution between sea states and wave headings for lower plates at P11-P13

The damage divided by sea state is similar at all hot spots. Most of the damage will occur in sea states with a significant wave height approximately 4 meter. From Figure 7.15a-7.15c one can se that the cumulative damage added from sea states with a wave heading over 9 meters can easily be neglected. This is similar with the situation at the hot spot in Submodel 1.

What heading angle cause most cumulative damage differ considerably from hot spot to hot spot. As stated earlier the stress variations seemed to be highest when the wave direction were parallel with a line drawn from the hot spot to the middle of the cylinder. As it should, this is reflected in the fatigue damage distribution. Waves propagating perpendicular to the weld line tend to cause most fatigue damage.

This is not completely true for -60° and 60° heading. This heading is only the most important heading at P7, even tough -60° and 60° are more perpendicular to the weld line than -30° and 30° heading at P8 and P6. This can be explained because -60 and 60° heading have a very low probability. If the probability of the wave headings had been uniformly distributed the tendency should have been more clear.

Also worth noticing is that the 30° heading contribute much more to fatigue damage than -30° heading at P13, even tough the hot spot lies in the symmetry plane. This is not an indication of error in the calculation because the element stresses have been used in fatigue life calculations here, not the nodal average. The elements used does not lie perfectly on the symmetry line, only touches it.

## 7.5 Time to failure

Time to failure, using the real normal stress and simplified parallel and shear stress is presented in a logarithmic scale in Figure 7.16 and 7.17. The first figure show estimated fatigue life assuming a constant wave heading over the lifetime of the structure. The second figure is for a combined heading. Here fatigue life is shown using the stresses from both the inner and outer surface of the plate.

At every hot spot analyzed, the constant wave heading that will lead to failure first is always the heading normal to the weld line at this point. This is not unexpected given the damage distribution presented in the previous section.

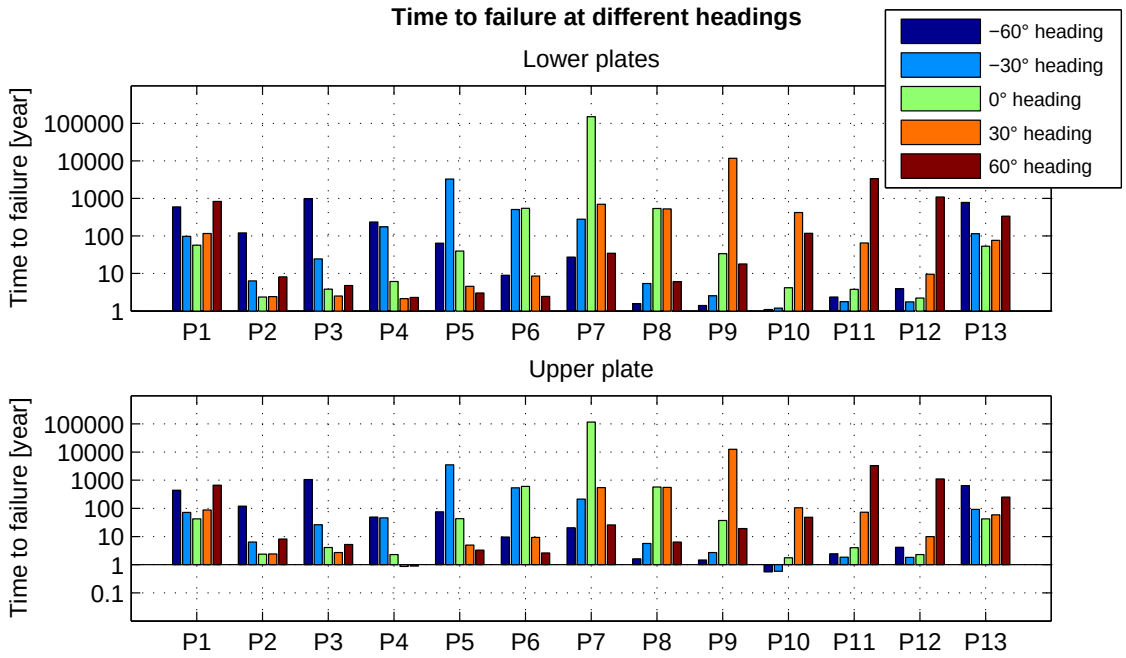


Figure 7.16: Time to failure for constant headings over the lifetime, with real normal stress combined with simplified shear and parallel stress, at both upper and lower side of the weld line

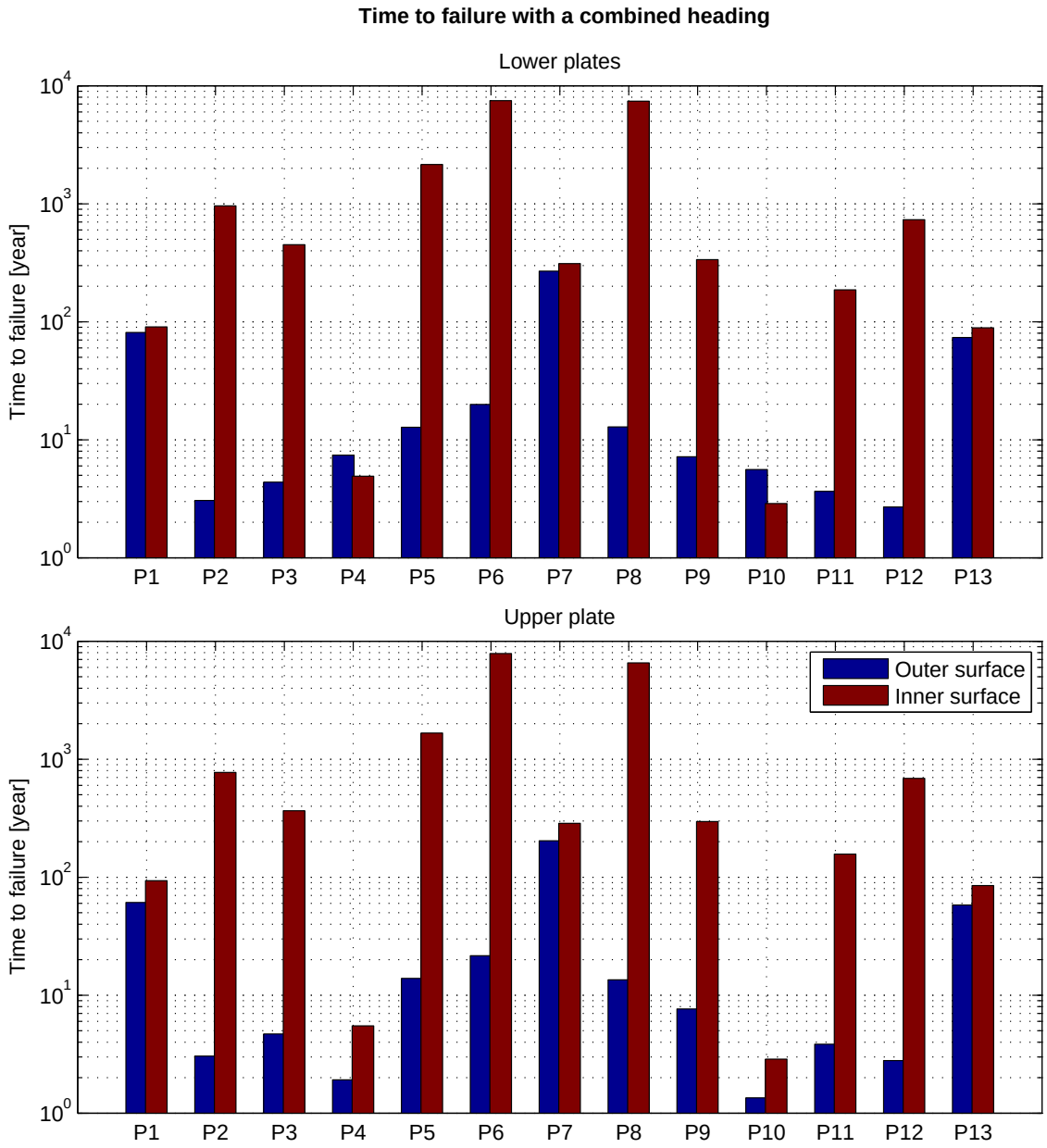


Figure 7.17: Time to failure for a combined heading, with real normal stress combined with simplified shear and parallel stress, at both upper and lower side of the weld line

P10 is the point with lowest estimated fatigue life for combined heading. Failure is expected after 1.4 years. This corresponds to a crack starting to grow from the outer surface of the plate above the weld line. P4 is the second worst point in regard to fatigue with 1.9 years fatigue life.

With two exceptions a crack is expected to form on the outer surface of the plates at the hot spots. For hot spots with no vertical stiffener behind the hull this is as expected, because the direction of the normal membrane stress will be the same as the normal bending stress. At P1, P7, and P13 the bending component of the dominating normal stress is very low for all cross sectional loading directions, so the fatigue life should be similar for

the outer and inner surface, which it is.

There is a special situation at P4 and P10. Both $\sigma_{\perp}$ and $\sigma_{\parallel}$ are large. At the outer surface $\sigma_{\perp,b}$ will be in the same direction as $\sigma_{\perp,m}$, but the large $\sigma_{\parallel,b}$ will be in the opposite direction as the approximately equally large $\sigma_{\parallel,m}$.Based on this it is hard to predict what side should be most exposed to fatigue damage. The values in Figure 7.17 suggest that the inner side is most exposed at the lower side of the weld line, and that the outer surface is most exposed at the upper side of the weld line.

It is very important to note that the estimated fatigue life is not necessarily is correct. The linear simplification method, with real perpendicular stress and simplified shear and parallel stress, have been used consistently to predict fatigue life, but this method will not necessarily produce accurate results when there is no clear linear tendency between the different stress components. At most hot spots one can predict that the results should be accurate because the normal stress is so much larger than the shear and parallel stress at both surfaces. This is not the case at P4 and P10, and to a lower extent also at P1 and P13. Because P4 and P10 have the largest stress variations, and also the lowest predicted fatigue life, these points have been investigated further.

To show the effect of including simplified shear and parallel stress, the ratio between fatigue life when using only the normal stress component and when also using simplified shear and parallel stress have been calculated. Figure 7.18 show the ratio for all hot spots and wave headings. The ratio for a combined heading is given in Table 7.1. The effect of including simplified shear and parallel stress is very limited at most hot spots. At the points where there is no vertical stiffener behind the hull, the increase in fatigue life when only using normal stress is never higher than 1%. There are several reasons for this. First, the simplified parallel stress variations will always be so low that the effective stress ranges will be defined by the term in equation 2.13 consisting of normal and shear stress ranges. Also the shear stress variations at these points are very low, and even the very limited effect they should have cannot be included properly by the linear simplification method. $\bar{\lambda}_{shear\ stress}$ is generally much lower than 0.95 at these points.

If the simplified stress at the lower side at P4 and P10 is not included, this will lead to 6 and 8 times longer fatigue life, respectively. This is because the parallel stress variations are much higher than the normal stress variations here. $\bar{\lambda}_{parallel\ stress}$ is also very high. so the parallel should be included properly in fatigue calculations. At the upper side of the weld at these points there will be a 12% and 18% increase in fatigue life if one only used the normal stress. The increase is not caused by the parallel stress, but the shear stress. The shear stress is relatively high at these points and has an almost completely linear relation with the normal stress.

Table 7.1: Ratio between fatigue life for a combined heading when using only normal stress and when also using simplified shear and parallel stress

| | P1 | P2 | P3 | P4 | P5 | P6 | P7 | P8 | P9 | P10 | P11 | P12 | P13 |
|---|---|---|---|---|---|---|---|---|---|---|---|---|---|
| L. | 1.04 | 1.00 | 1.00 | 6.46 | 1.01 | 1.01 | 1.54 | 1.05 | 1.02 | 8.30 | 1.00 | 1.00 | 1.09 |
| U. | 1.03 | 1.00 | 1.00 | 1.12 | 1.00 | 1.01 | 1.56 | 1.05 | 1.02 | 1.18 | 1.00 | 1.01 | 1.08 |

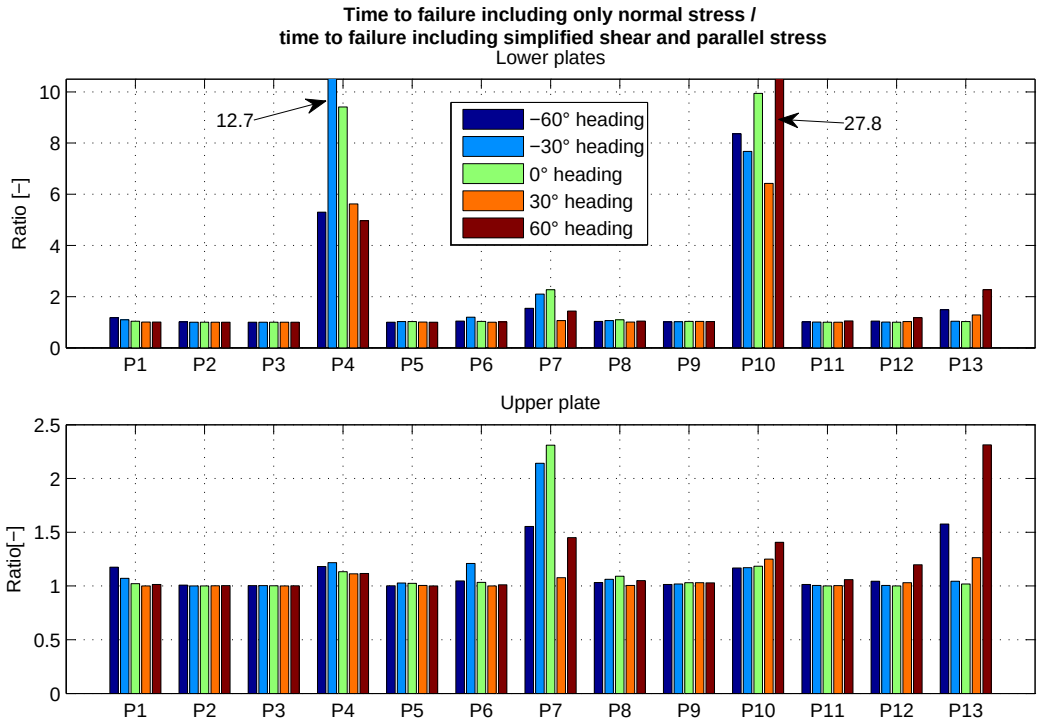


Figure 7.18: Ratio between time to failure when including only normal stress and when including simplified shear and parallel stress

To get another measurement of the accuracy of the linear simplification method, fatigue life has also been calculated using the shear stress as the real stress component. The ratio between fatigue life when using real shear stress and when using real normal stress is presented in logarithmic scale in Figure 7.19. This data corresponds very well with the $\bar{\lambda}_{shear\,stress}$ values presented in Figure 7.12. Fatigue life predictions differ tremendously at most hot spots when using real shear stress instead of normal stress. This is proof that the linear simplification method can not capture the actual effect of the shear stress at these points.

At P4 and P10, where the shear stress variations are highest, the difference in fatigue life is much lower. It is not easy to see the exact values from the logarithmic plot. Therefore the values are also presented in Table 7.2. At P4 and P5 the difference in fatigue life for a combined heading is always under or equal 5% at both the upper and lower side of the weld line. This is in good accordance with the $\bar{\lambda}_{shear\,stress}$ values at these points, which is very close to 1. This confirms that the linear simplification method is able to capture the actual effect of the shear stress in regard to fatigue. This is important because these are the most critical points, and because the shear stress variations here are too large to be neglected. Not including the shear stress will lead to 12% and 18% increase in estimated time to failure at the upper side of the weld line.

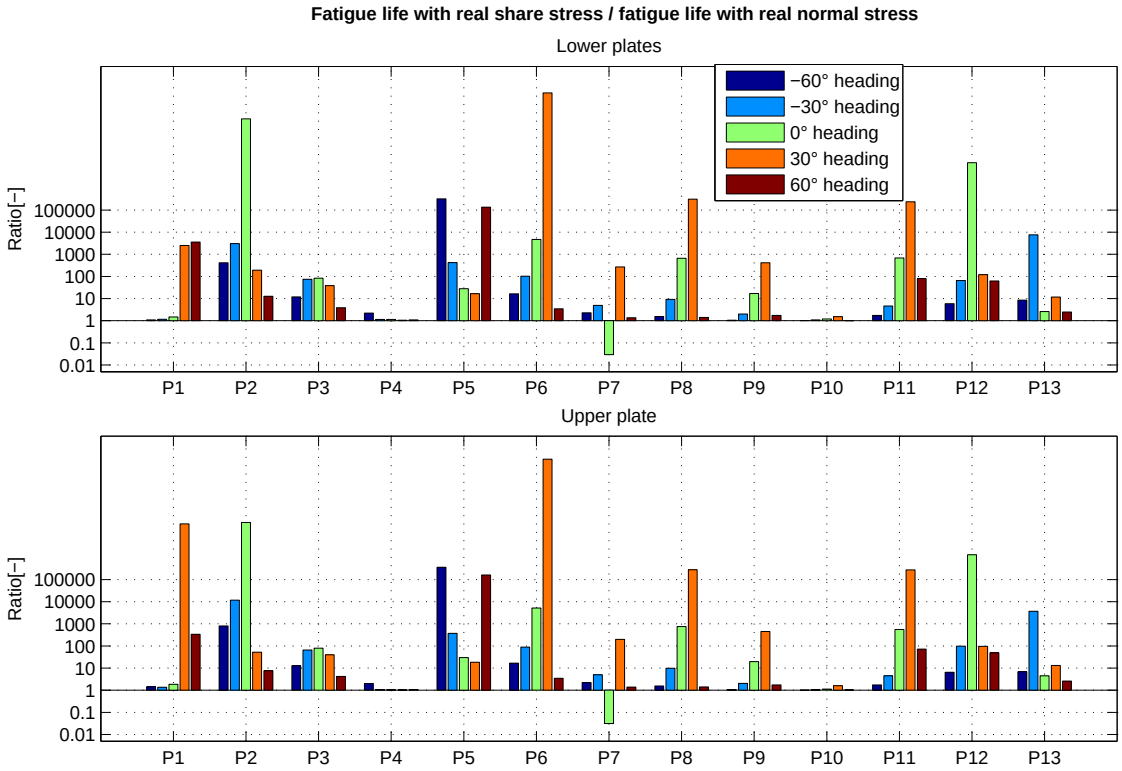


Figure 7.19: Ratio between fatigue life with real shear and real normal stress

Table 7.2: Ratio between fatigue life with real shear and real normal stress at P4 and P10

| | | **Wave heading** | | | | | |
|---|---|---|---|---|---|---|---|
| | | -60° | -30° | 0° | 30° | 60° | Combined |
| **P4** | Lower | 1.41 | 1.06 | 1.06 | 1.03 | 1.04 | 1.04 |
| | Upper | 1.35 | 1.03 | 1.03 | 1.02 | 1.03 | 1.02 |
| **P10** | Lower | 1.01 | 1.04 | 1.08 | 1.20 | 1.00 | 1.05 |
| | Upper | 1.00 | 1.02 | 1.05 | 1.23 | 1.01 | 1.03 |

Based on fatigue life estimation using $\sigma_{\perp}$ as the real stress component at P4 and P10, the outer surface is most critical at the upper side of the weld and the inner surface is most critical at the lower side of the weld. As stated earlier this is not necessarily correct. The plates will have large parallel stresses at the inner surface of the plates. If these stresses have not been included correctly in fatigue life calculations, one can not be certain the inner surface is also the most critical at the upper side of the weld line. One can neither be sure that the fatigue life predictions at the lower side of the weld line are correct.

The ratio between the weighted average of the real and constructed parallel stress strandard deviations ($\bar{\lambda}_{parallel\,stress}$), at the inner surface at P4 and P10, indicates that the parallel stress is properly accounted for in fatigue calculations. $\bar{\lambda}_{parallel\,stress} > 0.99$ at all headings for both the upper and lower side of the weld line. At the side of the plates turning outwards, there does not need to be a very high correlation between $\sigma_{\perp}$ and $\sigma_{\parallel}$,

because the parallel stress variations are much lower than the perpendicular stress variations. Be that as it may, $\bar{\lambda}_{parallel\,stress} > 0.95$ at all headings that contribute significantly to fatigue damage. There is one exception at P4 at the upper side of the weld line at 60 ° heading where $\bar{\lambda}_{parallel\,stress} = 0.83$.

Table 7.3: $\bar{\lambda}_{parallel\,stress}$ at outer surface of P4 and P10

| | | **Wave heading** | | | | |
|---|---|---|---|---|---|---|
| | | -60° | -30° | 0° | 30° | 60° |
| **P4** | Lower | 0.98 | 0.93 | 1.00 | 1.00 | 1.00 |
| | Upper | 0.16 | 0.84 | 0.99 | 0.98 | 0.83 |
| **P10** | Lower | 1.00 | 1.00 | 1.00 | 0.98 | 0.95 |
| | Upper | 0.99 | 0.99 | 0.98 | 0.32 | 0.94 |

Table 7.4: $\bar{\lambda}_{parallel\,stress}$ at inner surface of P4 and P10

| | | **Wave heading** | | | | |
|---|---|---|---|---|---|---|
| | | -60° | -30° | 0° | 30° | 60° |
| **P4** | Lower | 0.99 | 1.00 | 1.00 | 1.00 | 1.00 |
| | Upper | 1.00 | 1.00 | 1.00 | 1.00 | 1.00 |
| **P10** | Lower | 1.00 | 1.00 | 1.00 | 0.99 | 1.00 |
| | Upper | 1.00 | 1.00 | 1.00 | 1.00 | 1.00 |

For P4 and P10 fatigue life has also been calculated by using the parallel stress as the real component to compare it with the $\bar{\lambda}_{parallel\,stress}$ values in Table 7.3 and 7.4. The values are presented in Figure 7.20. At the surface turning inwards the differences in fatigue life are very small. For a combined heading the difference is always less than 3%. This confirms that the effect of the parallel stress has been included properly in fatigue life calculations.

Except for P4 at the upper side of the weld line, the differences for a combined heading on the outer surface equals the differences on the inner side. At the upper side of the weld line at P4 there is a 18% increase in fatigue life if the parallel stress is used as the real component. However, at the outer surface the parallel stress variations are so low compared to the normal stress that fatigue damage caused by it should be negligible. It is still interesting to see the connection between $\bar{\lambda}_{parallel\,stress}$ and the ratio between fatigue life using real parallel and normal stress. $\bar{\lambda}_{parallel\,stress}$ is only 0.83 at this point at 60° wave heading. This heading is only estimated to cause around 10% of the total damage, so it can't be the only reason fatigue life is 18% higher. For a constant heading equal 30°, which will cause around 55% of the damage in a combined heading condition, the increase in fatigue life is 16 %, despite the fact that $\bar{\lambda}_{parallel\,stress} = 0.98$ at this heading. The reason is that the peaks of the constructed normal stress will usually be a bit lower than the real stress, even tough the correlation between the parallel and normal stress is very high.

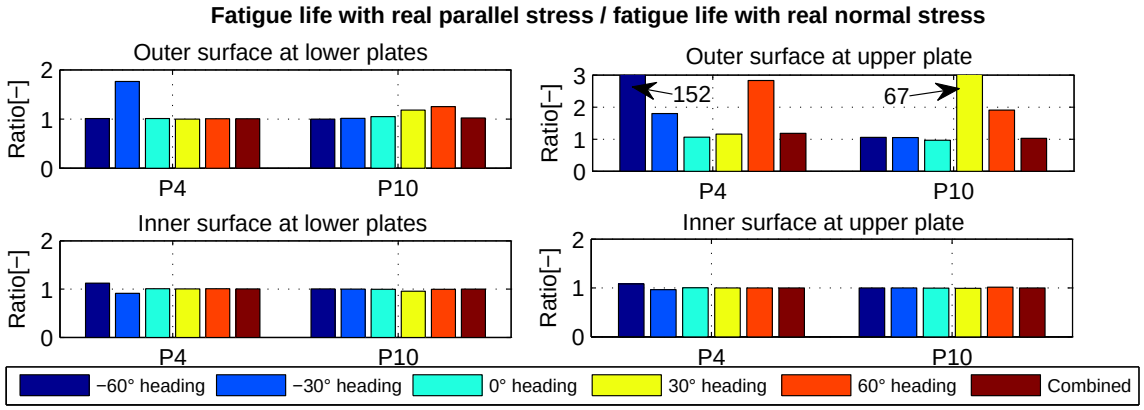


Figure 7.20: Ratio between fatigue life with real parallel and real normal stress

From the values of $\bar{\lambda}$ and the ratio between fatigue life using different real stress components one can conclude the following. The plate surfaces at P4 and P10 predicted to be most critical, by using the normal stress as the real component in fatigue calculations, should be the most critical plates in reality. The lowest estimated fatigue life, occurring at P10, is a good estimate. Both shear and parallel stress are included correctly in calculations. This is also true for P4 which is the second most critical point. Even though the shear and parallel stress have not been included correctly at all the other hot spots, the real fatigue life at these areas should not be lower than the estimated fatigue life at P10.

# Chapter 8

# Conclusion

This thesis has dealt with fatigue associated challenges related to a column-pontoon connection in a semi-submersible floating wind turbine developed at CeSOS, NTNU [16]. Stress concentration study and fatigue analysis were carried out at the intersection between the midpoint at the upper hull of the pontoon and a transition piece linking the column with the pontoon (Submodel 1). The same was done at 13 points along the weld between the hull of the transition piece and the hull of the column (Submodel 2). Fatigue life has been predicted based on short term global response analysis for various sea states and wave headings.

There will be a multiaxial stress state at the different hot spots. A simplified method for including the fatigue damage contribution from all the different stress components ($\tau_{\parallel}$, $\sigma_{\parallel}$ and $\sigma_{\perp}$) is proposed. The method has large limitations, but is intended to be used when there is a close to linear relationship between the different stress components. This method has been used when predicting fatigue life at all hot spots and the results have been evaluated.

Some structural changes have been made on the structure in order to improve fatigue performance, especially in the area of Submodel 1, where stress concentration originally were extremely high.

## 8.1 Submodel 1

At the connection between the pontoon and transition piece there are multiple plates intersecting at one point. The most critical side of the hot spot here is the plate being part of the rectangular pontoon hull. The plate surface turning inwards is most critical. Estimated fatigue life for a combined wave heading is 10 years. 0° wave heading is the most critical for this location. Around 62% of the accumulated damage is a result of waves in this direction.

At the most critical point the normal stress has by far the highest variations. For a combined heading the weighted average of the normal stress standard deviation (8 MPa) is 4 times larger than the parallel shear stress and 8 times larger than the parallel stress. Fatigue life calculations using only the normal stress component result in 11% longer fatigue life prediction. This is compared to using the real normal stress and a simplified shear

and parallel stress to calculate effective stress ranges, in accordance with the proposed method described in 2.9.

The simplified linear shear stress is not a good representation of the real shear stress at all wave headings, suggesting that estimated fatigue life is a bit too high. On the other hand, the shear stress is only likely to increase crack growth rate when the normal stress is in tension, something equation 2.13 does not account for. At critical point the perpendicular stress will mostly be in compression, suggesting the shear stress damage contribution is too high.

## 8.2 Submodel 2

At the weld line between the column and transition piece there are various points with estimated fatigue life less than 10 years. The most critical hot spot is P10, located 45° from the point on the weld line closest to where the loads are applied. The upper side of the weld corresponding to the cylindrical column plate is most critical. The plate surface turning outwards is most exposed to fatigue damage. Estimated fatigue life for a combined heading is 1.9 years. -30° wave heading is most critical and is the cause of around 60% of the accumulated damage.

At the most critical point the normal stress variations will dominate. The weighted average of the normal stress standard deviation is 11 MPa, around 2.5 times larger than the shear stress. The parallel stress is negligible. Neglecting the shear stress result in 18% increase in estimated time to failure. The simplified shear stress is a very good representation of the real shear stress at all wave headings. Therefore, using the linear simplification method to include the effect the shear stress have on fatigue, should produce very accurate results.

## 8.3 Linear Simplification Method

The accuracy of the method proposed for including fatigue damage contribution from secondary stress components depend on the point on structure analyzed and the wave heading. In some situations the linear correlation between the different stress components is low, making the simplified stress too inaccurate to capture the real fatigue damage contribution. In other situations the method produce results which is believed to be very accurate.

Even if the simplified stresses are not accurate, using them in fatigue calculation would still be more conservative than neglecting the two secondary stress components completely. Neither will it be too conservative. The effective stress ranges when the linear correlation between the stresses are 0 will converge towards the stress ranges found when only evaluating the chosen real stress component.

As the accuracy of the method differ, some uncertainty is associated with predicted fatigue life at some of the points analyzed. That being said, the points found to be most critical should also be the most critical in reality.

# Chapter 9

# Recommendations for Further Work and Sources of Error

- The column-pontoon connection design changes conducted in the work with this thesis is not enough to achieve acceptable fatigue life. More changes are needed to increase fatigue life. This can be archived by increasing the plate thickness in stress concentration areas or by improving the design of local structural parts.
- In the FE-model used there are various hot spots that have not been investigated. It is essential that that these areas also will be analyzed.
- In the work with this thesis some assumptions have been made in order to calculate fatigue damage. The validity of this assumptions need to be assessed. Especially the choice of S-N curve and the choice of $\alpha$ parameter should be assessed in order to calculate effective stress ranges.
- Cross sectional loading results based on global response analysis from 0°, 30° and 60° wave heading have been used in this report. Cross sectional loading from -30° and -60° wave headings have been constructed by assuming load symmetry around the x-z-plane. This is not entirely correct. More accurate loads from wave heading in these directions may be needed in a later phase of design studies. Loads from additional wave headings may also be needed.
- The fatigue life analysis with a combined wave heading in this report corresponds to the column-pontoon connection where 0° wave heading is dominating. There are 2 other similar connections in the semi-submersible that will have different wave heading probability density functions. These connections also need to be analyzed.
- At the weld line between the transition piece hull and column hull the most critical hot spots, according to the fatigue analysis conducted in this report, are the ones with an added stiffener connected to it on the inside of the hull. This indicates that inserting vertical stiffeners in the transition piece may have been counterproductive. This should be investigated further.
- The economic aspect of the design changes made on the structure has not been analyzed thoroughly. A cost increase analysis should be considered.

- The kneeplate inserted between the transition piece and pontoon may be exposed to hydrodynamic forces too large to be neglected. This should be investigated.
- The consequence of failure at the various points analyzed has not been studied in this work, and the fatigue design factor is set to 1. If a more comprehensive fatigue analysis is to be conducted in the future the consequence of failure needs to be addressed.
- The points interpolation points at Plate 3 in Submodel 1 is not completely accurate. The plate is 20 mm thick, but read out points 12.5 mm and 37.5 mm from the weld have been used. Therefore one can expect that the hot spot stresses here are a bit higher, and fatigue life a bit lower, than what is presented in this report. If the plate thickness is increased to 25 mm the values presented will become conservative.

# Bibliography


[1] Anderson, T.L. (2005). *Fracture Mechanics: Fundamentals and Application, Third Edition*. CRC Press, Taylor & Francis Group.

[2] Ariduru, Secil (2004). *Fatigue Life Calculation by Rainflow Cycle Counting method*. The Graduate School of Natural and Applied Sciences of Middle East Technical University.
`http://wind.nrel.gov/designcodes/papers/fatlifecalcbyrfcyclecountingmeth_ariduru.pdf`

[3] Bai, Young (2003). *Marine Structural Design*. Elsevier

[4] Berge, Stig (2006). *Fatigue and Fracture Design of Marine Structures, Volume 1, Fracture Design of Welded Structures*. NTNU, Department of marine technology.

[5] Berge, Stig (2006). *Fatigue and Fracture Design of Marine Structures, Volume 2, Fatigue Design of Welded Structures*. NTNU, Department of marine technology.

[6] Dong, Pingsha, Wei, Zhigang and Hong, Jeong K (2010). *A path-dependent cycle counting method for variable-amplitude multi-axialø loading* . International Journal of Fatigue 32.

[7] DNV (2010). *Classification Notes No.30.7 Fatigue Assessment of Ship Structures*. Det Norske Veritas.

[8] DNV (2013). *SESAM User Manual GeniE Vol. 1 (Valid from program version 6.6)*. Det Norske Veritas Software, Norway

[9] DNV (2013). *SESAM User Manual GeniE Vol. 3 (Valid from program version 6.6)*. Det Norske Veritas Software, Norway.

[10] DNV (2013). *SESAM User Manual Xtract (Valid from program version 4.1)*. Det Norske Veritas Software, Norway.

[11] DNV (2013) *Use of Probabilistic Methods for Planning of Inspection for Fatigue Cracks in Offshore Structures*. Joint Industry Project report.

[12] DNV-RP-C203. *Fatigue Design of Offshore Steel Structures 2011*, Det Norske Veritas AS, 2011.

[13] Geva, Alon (2012). *subplotplus() - Enhanced layout MATLAB subplot function.*
`http://www.mathworks.com/matlabcentral/fileexchange/34594-subplotplus---enhanced-layout-matlab-subplot-function`

[14] Irvine, Tom (2011). *Rainflow cycle counting in fatigue analysis, revision A*
`http://citeseerx.ist.psu.edu/viewdoc/download?doi=10.1.1.366.1680&rep=rep1&type=pdf`, visited 14.05.2014.

[15] Leira, Bernt J (2011). *Kompendium Marine Konstruksjoner Grunnkurs*, NTNU, Department of marine technology.

[16] Luan, C., Gao, Z., and Moan, T. *Conceptual designs of a 5-MW and a 10-MW semi-submersible wind turbine with emphasis on the design procedure.* Journal of Offshore Mechanics and Arctic Engineering (submitted, 2014).

[17] Luan, Chenyu. chenyu.luan@ntnu.no. Questions fatigue life. 02.06.2014

[18] Marin, Traian Ionutyt (2013). *Design and stress Analysis of the Column-Pontoon Connection in a Semi-Submersible Floating Wind Turbine.* Pre-project Thesis, Department of Marine Technology, NTNU.

[19] Moan, Torgeir (2003). *Finite Element Modelling and Analysis of Marine Structures.* NTNU, Department of marine technology.

[20] Moan, Torgeir (2013). *Lecture notes in TMR4305/4505 Advanced Structural Analysis analysis: TMR4305.Week.36-37.Plates.Shells.web.2013.pdf*

[21] N. Pungo, M. Ciavarella, P Cornetti, A. Carpinteri (2006). *A generalized Paris' law for fatigue crack growth.* Journal of the Mechanics and Physics of Solids.

[22] Nicolay, S (2011). *Controllable tight subplot* .
`http://www.mathworks.com/matlabcentral/fileexchange/30884-controllable-tight-subplot`

[23] NORSOK standard N-001 (2012 ). *Structural Design, eddition 8, September 2012*, Standards Norway.

[24] Næss, Arvid and Moan, Torgeir (2012). *Stochastic Dynamics of Marine Structures.* Cambridge University Press.

[25] S. Butterfield, W. Musial, and J. Jonkman (2007). *Engineering Challenges for Floating Offshore Wind Turbines.* Conference paper.

[26] Schwarz, Douglas (2010). *Fast and Robust Curve Intersections.*
`http://www.mathworks.com/matlabcentral/fileexchange/11837-fast-and-robust-curve-intersections`

[27] Socie, Darrell F. and Marquis, Gary B. (2000). *Multiaxial Fatigue.* Society of Automotive Engineers, Inc.

[28] WAFO-group (2000). *WAFO - A Matlab Toolbox for Analysis of Random Waves and Loads - A Tutorial* Math. Stat., Center for Math. Sci., Lund Univ., Lund, Sweden.
`http://www.maths.lth.se/matstat/wafo`

[29] Wei, Zhigang and Forte, Thomas P. (2010). *Multi-Axial Fatigue Life Assessment of Wind Turbine Structural Components*. Proceedings of the ASME 2010 4th International Conference on Energy Sustainability. Phoenix, Arizona, USA.

# Apendix A: Comments

Matlab scripts, and all input and result files were uploaded at DAIM.

GeniE .xml concept model files of global model, Submodel 1 and Submodel 2 were also uploaded at DAIM.

See readme file for more information.